metals

Review

The Challenges and Advances in Recycling/Re-Using Powder for Metal 3D Printing: A Comprehensive Review

Alex Lanzutti [1,*] and Elia Marin [1,2,3,4,*]

[1] Department Polytechnic of Engineering and Architecture, University of Udine, 33100 Udine, Italy
[2] Biomaterials Engineering Laboratory, Kyoto Institute of Technology, Sakyo-ku, Matsugasaki, Kyoto 606-8585, Japan
[3] Materials Innovation Laboratory, Kyoto Institute of Technology, Sakyo-ku, Matsugasaki, Kyoto 606-8585, Japan
[4] Biomedical Research Center, Kyoto Institute of Technology, Sakyo-ku, Matsugasaki, Kyoto 606-8585, Japan
* Correspondence: alex.lanzutti@uniud.it (A.L.); elia-marin@kit.ac.jp (E.M.)

Abstract: This review explores the critical role of powder quality in metal 3D printing and the importance of effective powder recycling strategies. It covers various metal 3D printing technologies, in particular Selective Laser Melting, Electron Beam Melting, Direct Energy Deposition, and Binder Jetting, and analyzes the impact of powder characteristics on the final part properties. This review highlights key challenges associated with powder recycling, including maintaining consistent particle size and shape, managing contamination, and mitigating degradation effects from repeated use, such as wear, fragmentation, and oxidation. Furthermore, it explores various recycling techniques, such as sieving, blending, plasma spheroidization, and powder conditioning, emphasizing their role in restoring powder quality and enabling reuse.

Keywords: metal 3D printing; powder recycling; additive manufacturing; sustainability; powder degradation; L-PBF; EB-PBF; binder jetting; DED

check for updates

Citation: Lanzutti, A.; Marin, E. The Challenges and Advances in Recycling/Re-Using Powder for Metal 3D Printing: A Comprehensive Review. *Metals* **2024**, *14*, 886. https://doi.org/10.3390/met14080886

Academic Editor: Wenming Jiang

Received: 5 July 2024
Revised: 31 July 2024
Accepted: 1 August 2024
Published: 2 August 2024

1. Introduction

Metal 3D printing, also commonly referred to as additive manufacturing (AM), encompasses various technologies that build parts layer-by-layer, based on a CAD-3D model, using metallic powders. The origins of 3D printing can be traced back to the 1980s with the development of stereolithography (SLA), which used UV lasers to cure photopolymer resins [1]. The technology quickly evolved, and in the 1990s, the first patents for metal additive manufacturing were filed [2], leading to the development of techniques such as selective laser sintering (SLS) [3].

Today, metal 3D printing is used in a wide range of industries, including aerospace [4], automotive [5], medical [6], and tooling [7], offering unprecedented design freedom and manufacturing flexibility.

These technologies can be broadly categorized into two main groups: those that use a bonding agent to bind the powder and those that melt the material directly using a heat source. Each category faces unique industrial challenges and has distinct advantages and applications (Figure 1).

Binder Jetting [8] involves spreading a thin layer of metal powder onto a build platform, followed by the deposition of a liquid binding agent using an inkjet print head. The binder selectively binds the powder particles together to form a solid layer. This process is repeated layer-by-layer until the entire part is built. Post-processing steps such as curing, debinding, and sintering are required to remove the binder and densify the part.

Binder Jetting is particularly suitable for producing complex geometries, metal prototypes, and small-to-medium batch production. Commonly used materials include stainless steel [9,10], titanium [11], and other alloys [12–15]. Despite its advantages, Binder Jetting faces industrial challenges such as the need for extensive post-processing to achieve final mechanical properties and managing and recycling unused binder and powder.

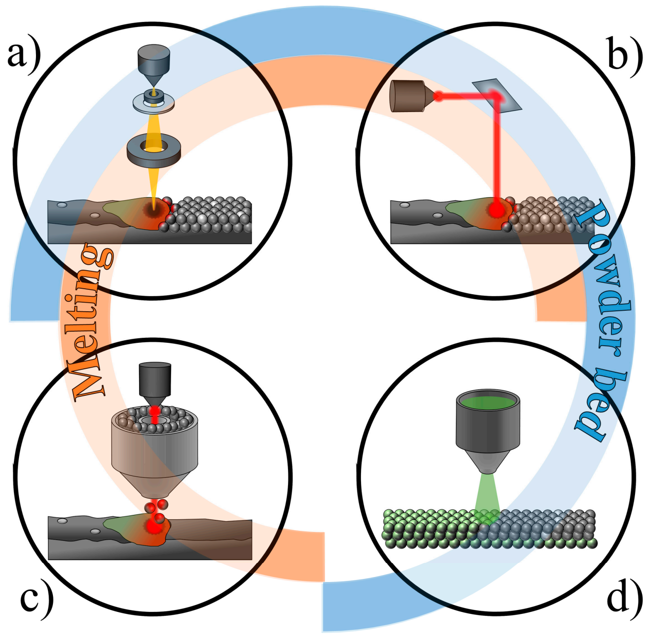

Figure 1. Overview of the main 3D printing techniques using powders as feedstock: EB-PBF (**a**), L-PBF (**b**), L-DMD (**c**), and Binder Jetting (**d**).

Selective Laser Melting (SLM or L-PBF, Laser Powder Bed Fusion) [16] utilizes a high-powered laser to selectively melt and fuse metal powder particles together. A thin layer of powder is spread over the build platform, and the laser traces the cross-sectional geometry of the part, melting the powder. The platform then lowers, and a new layer of powder is spread, repeating the process layer-by-layer. L-PBF is capable of producing fully dense, high-strength metal parts, but it requires support structures to counteract warping due to thermal stresses.

Initially, due to technological limitations in laser power, this process was referred to as selective laser sintering (SLS) [17]. Unlike L-PBF, SLS could only achieve sintering, where the metal powder particles are fused together but not fully melted. However, advancements in laser technology have enabled SLM to achieve complete melting of the metal powder, resulting in stronger and more homogeneous parts [18]. Despite the dominance of L-PBF in industries requiring fully dense metal parts, SLS still survives in applications where part density and mechanical properties are not critical, such as in prototyping [19].

L-PBF is widely used in aerospace [20], medical implants [21], automotive components [22], and tooling [23]. Commonly used materials include aluminum alloys [24], titanium [25], stainless steel [26], magnesium [27], nickel [28] and cobalt–chrome [29]. The primary industrial challenges for L-PBF include high thermal gradients that can cause residual stresses and distortions, as well as the need for sophisticated powder handling and recycling to maintain powder quality.

Electron Beam Melting (EBM or EB-PBF, Electron Beam Powder Bed Fusion) [30] uses an electron beam to melt metal powder in a vacuum environment, reducing oxidation and contamination. A layer of powder is spread, and the electron beam selectively melts the powder. EB-PBF offers higher build rates compared to L-PBF due to the electron beam's high energy density, but it requires vacuum conditions, which limit the size of the build chamber.

EB-PBF is commonly used in aerospace [31] and medical implants [32], particularly orthopedic implants [33]. Materials such as titanium and its alloys [34] and cobalt–chrome [35] are frequently used. Industrial challenges for EB-PBF include the complexity and cost associated with vacuum requirements and managing powder in a vacuum environment.

Direct Energy Deposition (DED) [36] uses focused thermal energy (laser, electron beam, or plasma arc) to fuse metal powder or wire feedstock as it is deposited. The material is directly fed into the heat source, where it is melted and deposited onto the substrate or previously built layers. DED is also suitable for repairing existing components and adding material to existing parts, and it can produce large parts with complex geometries.

DED is utilized in aerospace [37], defense [38], and repair applications [39], with materials such as titanium [40], stainless steel [41], Inconel [42], and other high-performance alloys [36]. The industrial challenges for DED include maintaining consistent powder flow and quality, managing residual stresses, and achieving fine feature resolution.

All technologies require effective strategies for powder management [43], including recycling and maintaining powder quality standards over time. Direct melting technologies (L-PBF, EB-PBF, and DED) face challenges with residual stresses, necessitating robust thermal management and support strategies. Additionally, Binder Jetting requires extensive post-processing to achieve desired properties and must deal with the issue of residual binder in recycled powders, which can compromise the quality of new builds and requires thorough cleaning and reprocessing [15].

The quality of metal powder used in 3D printing plays a critical role in determining the final properties of printed parts. High-quality powder ensures optimal flowability, which in turn increases the quality of the 3D printing process and the mechanical properties of the final product. Several factors influence powder quality, including particle size and shape, density, roughness, chemical composition, and the presence of impurities [44,45]. Understanding and controlling these factors is essential for achieving consistent and reliable results in metal additive manufacturing.

Uniform particle size distribution is vital for achieving a smooth and consistent powder layer during the 3D printing process [46,47]. In technologies such as Selective Laser Melting and Electron Beam Melting, keeping a consistent layer thickness is crucial to obtain an even melting and solidification of each layer [48]. Powders with a narrow particle size distribution tend to flow better, which improves the packing density and reduces the likelihood of defects such as porosity and incomplete fusion.

Inconsistent particle size can lead to variations in packing density, affecting thermal conductivity and laser absorption during the melting process. This can result in defects such as balling, where un-melted powder forms spherical particles, or lack of fusion between layers. Ensuring a consistent particle size distribution helps in maintaining the integrity of the printed part and achieving desired mechanical properties [49–51].

The shape of the powder particles significantly impacts the flowability and packing density of the powder bed [52]. Spherical particles are generally preferred in metal 3D printing due to their superior flowability and packing characteristics compared to irregularly shaped particles. Spherical particles reduce friction and allow for a more uniform powder layer, which is essential for high-quality builds [53,54]. The method used to produce the powder affects its shape. Gas atomization, a common method for producing metal powders, tends to produce highly spherical particles, while other methods like water atomization may give more irregular results.

The chemical composition of the powder must be carefully controlled to ensure that it meets the specifications required for the intended application. Impurities or variations in the alloy composition can affect the mechanical properties, corrosion resistance, and overall performance of the printed parts [55]. For example, the presence of oxygen or other contaminants can lead to the formation of oxides, which can weaken the material [56,57]. Maintaining a consistent chemical composition across different batches of powder is essential for achieving repeatable results.

Powder contamination can occur during production, handling, or recycling processes [43,58]. Common contaminants include moisture, oils, metal residues from the distribution system, and other foreign particles, which can adversely affect the flowability, melting behavior, and mechanical properties. Ensuring a clean production environment and using appropriate storage and handling procedures are crucial for maintaining powder purity, in particular considering that, because of their high surface-area-to-volume ratio, particles are more reactive and can easily absorb high amounts of humidity [59].

Contaminants can lead to defects in the printed parts, such as inclusions or voids, which can compromise the mechanical properties and structural integrity of the parts [60,61]. For critical applications, such as aerospace and medical implants, maintaining a high powder purity is essential to meet stringent performance and safety standards.

Recent studies have emphasized the importance of monitoring changes in powder characteristics during recycling. Techniques such as scanning electron microscopy (SEM), X-ray diffraction (XRD), and particle size analysis are used to assess changes in particle morphology, size distribution, and phase composition [62]. These analyses help in understanding degradation mechanisms and ensuring that recycled powders maintain their performance characteristics.

Research has shown that repeated recycling can lead to changes in powder properties, such as increased particle size and altered shape due to agglomeration and oxidation. For instance, titanium alloys [63–66] and nickel-based superalloys [67–69] are prone to oxidation, which can affect their flowability and mechanical properties. Studies have investigated the effects of these changes on the final part quality, highlighting the need for strict quality control measures.

Sieving is commonly used to remove oversized particles and contaminants from recycled powder [70]. Blending recycled powder with virgin powder is another technique to restore the desired properties. Recent advances have focused on optimizing these processes to maintain a consistent quality of recycled powder. For example, dynamic sieving methods [71] have been developed to improve efficiency and accuracy in separating usable powder from debris.

Plasma spheroidization [72] is an advanced technique that reshapes irregular particles into spherical ones using thermal plasma. This process improves the flowability and packing density of recycled powders, making them suitable for reuse in 3D printing. Research has demonstrated that plasma-spheroidized powders can achieve a comparable performance to virgin powders, thus extending their usable life.

Studies have investigated the mechanical properties of parts printed with recycled powders, focusing on tensile strength, hardness, and fatigue resistance. Results indicate that, with proper recycling and quality control, parts produced from recycled powders can achieve mechanical properties comparable to those made from virgin powders [62]. However, the extent of property retention depends on the material and the number of recycling cycles [62].

Research has shown that adjusting process parameters, such as laser power, scanning speed, and layer thickness, can mitigate the effects of powder degradation [73]. Optimizing these parameters for recycled powders helps in achieving consistent part quality and performance. For example, increasing the laser power can compensate for the reduced absorption efficiency of oxidized powders.

Recycling powders significantly reduces the material costs associated with metal 3D printing. By extending the usable life of powders, manufacturers can lower their production costs and improve the economic viability of additive manufacturing [73]. Research has quantified these cost savings, demonstrating that effective recycling can lead to substantial reductions in overall production expenses [74].

Recycling metal powders contributes to sustainability by reducing waste and minimizing the environmental impact of metal extraction and processing. Studies have highlighted the environmental benefits of powder recycling, including reduced energy consumption and lower carbon emissions [75]. These findings support the adoption of recycling practices in industrial applications to promote greener manufacturing processes.

In conducting this review, we gathered and analyzed a wide range of recent studies and publications on the topic of powder recycling in metal 3D printing. Our approach involved an extensive literature search using databases such as Google Scholar, PubMed, and IEEE Xplore to identify peer-reviewed articles, conference papers, and industry reports published within the last ten years. We focused on research that addressed the key aspects of powder quality, recycling techniques, and their impact on mechanical properties and sustainability.

By synthesizing findings from various sources, including experimental studies, theoretical analyses, and case studies, we aimed to provide a comprehensive overview of the current state of knowledge in this field. Additionally, we consulted expert reviews and conducted meta-analyses to identify emerging trends and gaps in the literature, ensuring that our review not only highlights recent advances but also points to future research directions.

2. Overview of Metal 3D Printing

2.1. Metal Powders Used in 3D Printing

The most commonly used metals and alloys in 3D printing include titanium alloys, stainless steels, aluminum alloys, nickel-based superalloys, and cobalt–chrome alloys. In particular, the economic convenience of the use of metal powders in 3D printing is the ability to use, with minimal adaptations, a wide range of high-cost materials to obtain complex shapes that would be impossible to produce by conventional manufacturing methods [76–80]. The primary 3D printing methods for metals are Electron Beam Melting, Directed Energy Deposition, Selective Laser Melting, and Binder Jetting. Each of these methods utilizes metal powders with specific characteristics tailored to the process requirements in order to obtain the optimum performances in terms of the mechanical properties or degradation resistance of material.

Titanium alloys, particularly Ti-6Al-4V [32,81], are favored for their high strength-to-weight ratio, corrosion resistance, and biocompatibility. These properties make them ideal for aerospace, automotive, and biomedical applications. Other titanium alloys used in 3D printing include Ti-6Al-2Sn-4Zr-2Mo [82] and Ti-5Al-2.5Sn [83]. Additionally, commercially pure grade 2 [34] titanium is also used, especially in applications requiring excellent corrosion resistance and moderate strength.

Stainless steels, such as 316L [84] and 17-4PH [85], offer excellent corrosion resistance, mechanical properties, and cost-effectiveness. They are widely used in the manufacturing of tools, medical devices, and structural components. Other commonly used stainless steels include 304L [86], 15-5PH [87], and 410 [88].

Aluminum alloys, such as $AlSi_{10}Mg$ [89], are valued for their light weight, good thermal conductivity, and mechanical properties. They are commonly used in the aerospace and automotive industries. Other popular aluminum alloys in 3D printing include AlMg1SiCu [90], AlSi12 [91], and AlSi7Mg [92].

Nickel-based superalloys like Inconel 718 [93] and Inconel 625 [94] are known for their high-temperature strength and resistance to oxidation and corrosion. These alloys are essential in the aerospace, power generation, and chemical processing industries. Additional nickel-based superalloys used in 3D printing include Hastelloy X [95], Ni-Cu alloys [96], and Rene 41 [97].

Cobalt–chrome alloys, such as CoCrMo [98], exhibit excellent wear and corrosion resistance and are used extensively in dental and orthopedic implants, as well as in aerospace components. Other cobalt–chrome alloys used include CoCrW [99] and CoCrNiMo [100].

Copper alloys [101,102] are widely used, mainly for their excellent physical properties also at high temperatures. There are several fields where they are used, including as components of steel-making plants, components of nuclear plants, and so on. In the 3D printing field, there are many Cu-based alloys that are specifically designed in order to be produced by laser processes by conditioning their reflectance [103,104].

A list of metal alloys that have found application in 3D printing is presented in Table 1.

Table 1. List of the most common alloys used in 3D printing, with relevant literature references.

Base Metal	Alloy	Ref.	Technique
Titanium	Ti-6Al-4V	[105–108]	L-PBF
		[109–112]	EB-PBF
		[37,113–115]	DED
		[116–119]	BJ
	Ti-6Al-2Sn-4Zr-2Mo	[120–123]	L-PBF
		[122,124–126]	EB-PBF
	Ti-6Al-2Sn-4Zr-6Mo	[82,127–129]	L-PBF
	Ti-5Al-2.5Sn	[130–133]	L-PBF
	Ti-5Al-2Sn-2Zr-4Mo-4Cr	[134]	L-PBF
	Ti-xCu	[135]	L-PBF
	Ti-xCu-yFe	[136]	L-PBF
	Ti-8.5Cu	[137]	L-PBF
	Ti-xMo	[138–140]	L-PBF
		[141,142]	EB-PBF
		[143–145]	DED
	Ti-3Al-8V-6Cr-4Mo-4Zr	[146]	L-PBF
		[147]	DED
	Ti-5Al-5Mo-5V-3Cr-1Zr	[148–150]	L-PBF
	Ti-5Al-5V-5Mo-3Cr	[148]	L-PBF
	Ti-6Al-7Nb	[151–154]	L-PBF
	Ti-15Mo-3Nb-3Al-0.2Si	[155–157]	L-PBF
	Ti-5Al-2.5Sn	[130,131,133,158]	L-PBF
	Ti-36Nb-2Ta-3Zr-0.35O	[159]	EB-PBF
	Ti-35Nb-7Zr-5Ta	[160]	EB-PBF
	Ti-4Al-5Co-0.25Si	[161]	DED
	CP	[162–165]	L-PBF
		[166–168]	EB-PBF
		[169,170]	DED
		[11,171,172]	BJ
Steel	316	[173–175]	L-PBF
		[176,177]	EB-PBF
		[178]	DED
	316L	[26,179–181]	L-PBF
		[179,182]	EB-PBF
		[183–186]	DED
		[187–190]	BJ
	303	[191–194]	DED
	17-4PH	[85,195–197]	L-PBF
		[198,199]	DED
		[200–202]	BJ

Table 1. *Cont.*

Base Metal	Alloy	Ref.	Technique
Steel	304	[203,204]	L-PBF
		[205]	EB-PBF
		[202,206,207]	DED
	304L	[86,208–210]	L-PBF
		[211]	EB-PBF
	15-5PH	[87,212–214]	L-PBF
		[215–217]	DED
	410	[88]	L-PBF
	310S	[218]	L-PBF
	321	[219]	L-PBF
		[220,221]	EB-PBF
	420	[222–225]	L-PBF
		[226]	DED
	430	[227]	L-PBF
	4140	[228,229]	L-PBF
	2205	[230]	L-PBF
	2507	[231]	L-PBF
	904L	[232]	L-PBF
Aluminum	AlSi10Mg	[89,233–235]	L-PBF
		[236–238]	DED
		[12]	BJ
	AlMg1SiCu	[90]	L-PBF
	AlSi12	[91,239–241]	L-PBF
		[242]	DED
	AlSi7Mg	[92]	L-PBF
		[243]	BJ
	AlSi10Mg	[244]	DED
	2024	[245,246]	L-PBF
	2011	[247]	L-PBF
	2219	[248]	L-PBF
	3003	[249]	L-PBF
	3104	[250,251]	DED
	4020	[252]	L-PBF
	4047	[253]	L-PBF
	5005	[254]	L-PBF
	5052	[254]	L-PBF
	5083	[252]	L-PBF
	5183	[255]	L-PBF
	5087	[256,257]	L-PBF
	5754	[256]	L-PBF
		[258]	DED

Table 1. *Cont.*

Base Metal	Alloy	Ref.	Technique
Aluminum	6061	[259–262]	L-PBF
		[263]	DED
		[264]	BJ
	6063	[265–267]	L-PBF
	6082	[268]	L-PBF
	7075	[269–272]	L-PBF
		[273]	DED
	7050	[253,274]	L-PBF
		[275]	DED
Nickel	Monel 400	[96,276]	L-PBF
		[277]	DED
	Monel K-500	[278]	L-PBF
		[279]	DED
	Inconel 600	[280]	L-PBF
		[281,282]	DED
	Inconel 625	[94,283,284]	L-PBF
		[285]	EB-PBF
		[42,281,286,287]	DED
		[288–290]	BJ
	Inconel 718	[93,291–293]	L-PBF
		[294–296]	EB-PBF
		[42,297,298]	DED
		[299,300]	BJ
	Inconel 825	[301]	L-PBF
	Hastelloy C-22	[302]	L-PBF
		[303,304]	DED
	Invar 36	[305–308]	L-PBF
		[309]	EB-PBF
		[310–312]	BJ
	Nitinol	[313–316]	L-PBF
		[317–319]	EB-PBF
		[320–322]	DED
	Waspaloy	[323–326]	L-PBF
		[327]	DED
Cobalt	CoCrMo	[328–331]	L-PBF
		[332–335]	EB-PBF
		[336]	DED
		[337,338]	BJ
	CoCrW	[99,339–341]	L-PBF
	CoCrNiMo	[100]	L-PBF
		[342]	DED

Table 1. *Cont.*

Base Metal	Alloy	Ref.	Technique
Cobalt	Stellite 6	[343]	L-PBF
		[343,344]	DED
		[345,346]	BJ
	Stellite 21	[347]	L-PBF
		[348]	DED
	Stellite 12	[349]	L-PBF
	Haynes 188	[350–352]	L-PBF
	Haynes 230	[353,354]	L-PBF
	Haynes 233	[355]	L-PBF
	Haynes 282	[356–358]	L-PBF
		[359,360]	EB-PBF
	Mar-M509	[361–363]	L-PBF
		[364]	EB-PBF
Copper	CP	[365–367]	L-PBF
		[368–370]	EB-PBF
		[371–373]	BJ
	Cu-xCr-yZr	[374–377]	L-PBF
		[378,379]	EB-PBF
		[380–382]	DED
	Cu-xCr-yZn	[383,384]	L-PBF
	Cu-xCr	[385–387]	L-PBF
		[388]	EB-PBF
	Cu-xCr-yNb	[389–392]	L-PBF
		[393]	DED
	Cu-xSn	[394–396]	L-PBF
		[397]	DED
		[398]	BJ
	Cu-xNi-ySn	[399–401]	L-PBF

The quality and performance of metal 3D printing are highly dependent on the properties of the metal powders used (Figure 2). These properties include morphological characteristics such as particle shape, size, distribution, and roughness, as well as chemical composition and other physical properties. Most requirements are universal, meaning that they apply to all 3D printing techniques. In particular, the following properties are considered:

Flowability [70]: good flowability is essential for achieving smooth powder spreading and layer consistency, which are critical for the quality and precision of the printed components. Flowability depends on the powder morphological characteristics, such as shape, texture, size, and distribution, on the chemical composition, in particular concerning the surface oxides, and is also influenced by environmental conditions such as moisture content.

Shape [402]: spherical particles are generally preferred across all 3D printing techniques due to their high flowability and packing density, which contribute to consistent layer formation and uniform melting.

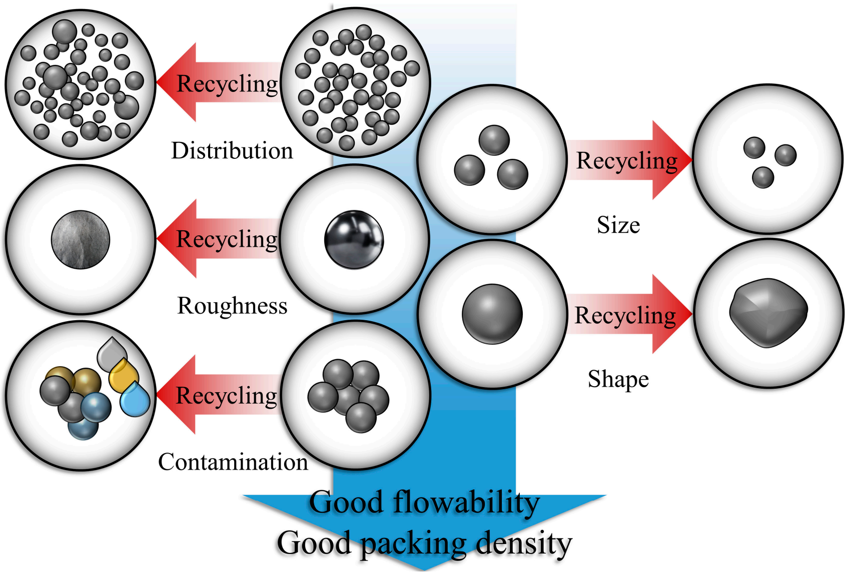

Figure 2. Five major powder characteristics that affect flowability and that are altered in recycled powders: powder distribution, powder average size, surface roughness, particle shape, and presence of contaminants.

Particle size and distribution [403]: requirements about particle size and distribution tend to vary depending on the technique used. For EB-PBF, powders usually have a particle size range of 45–110 µm. A narrow size distribution ensures uniform layer deposition and efficient melting. DED is more forgiving, with a typical particle size range of 50–150 µm, followed by EB-PBF (45–110 µm), then Binder Jetting (20–100 µm), and finally L-PBF (15–45 µm). Apart from DED, which has higher deposition rates but lower resolution compared to the other techniques, the typical powder size range is strictly correlated with the usual layer thickness during printing.

Density [47]: powder density reflects the quality of the powder and the presence of internal voids can usually negatively affect the flowability of the powder due to powder fragmentation during coating and recoating in the powder bed fusion process. Another important parameter to consider is that the powders should have a certain degree of compaction. The packing density indicates how the powders can fill a volume with a low number of voids. This property then reflects the amount of defect associated with the printed component. In fact, the powders, within their PSD, present certain coarse particles that mainly fill the volume and certain fine particles to fill the space between the other particles.

Chemical composition [404]: the chemical composition of powder is crucial to obtain a printed material with certain precise requirements in terms of chemical composition that then have an influence on the 3D-printed part. The chemical composition of the printed component may vary during the printing process due to the evaporation of some elements.

Other physical properties [405]: the physical properties of the powders are crucial for the correct formation of the melt pool according to the chosen process parameters. In fact, melting in the 3D printing process is strongly controlled by the heat transfer process from the energy imparted by the energy source (laser or electron beam). The presence of trace elements in powders or of thin films on the surface can reduce the heat transfer process and thus modify the solidification mechanism of the molten metal. Another important property is related to the optical properties of the powders, which influence the energy adsorption of the printed material. Laser-based 3D printing processes of copper alloys, for example, are complicated by the material's high reflectivity [103].

2.2. Powder Production Methods

As we previously discussed, the use of high-quality metallic powders is fundamental to the success of metal 3D printing. Various methods are employed to produce powders with specific characteristics, and they prevalently fall within three main groups (Figure 3):

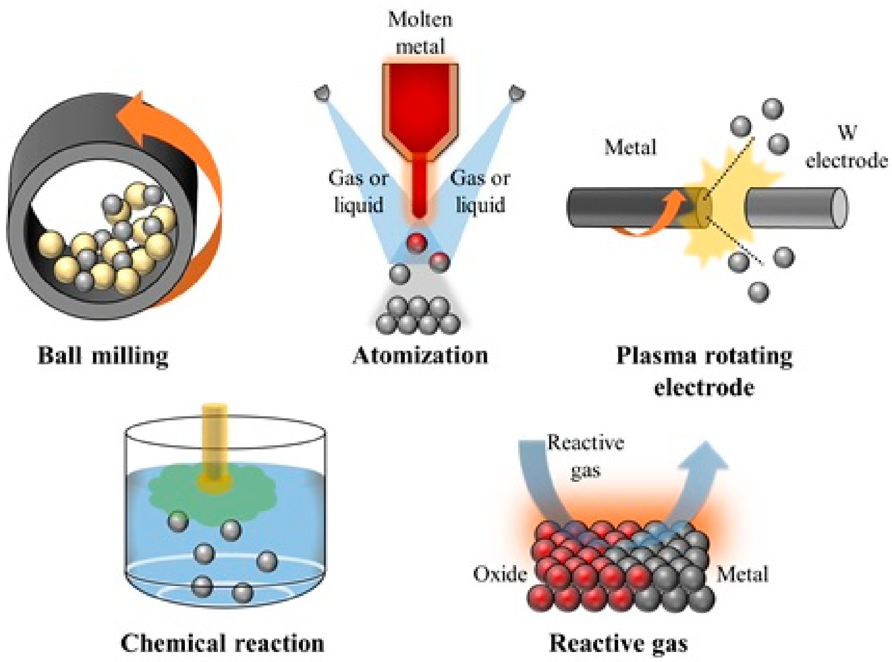

Figure 3. Scheme of the most common powder production processes.

Mechanical methods [406]: ball milling is a mechanical process that involves the grinding of metal powders in a rotating cylindrical chamber with hardened steel or tungsten carbide balls. This method is particularly useful for producing fine and uniform powders from brittle materials. Ball milling is cost-effective, allows for the production of very fine powders, and can be used for a wide range of metals and alloys. The powders produced by ball milling typically have an irregular shape. The mechanical forces involved in the grinding process cause the particles to fracture in a random manner, leading to a non-spherical, angular morphology. This irregular shape can affect the flowability of the powder, making it less ideal for certain 3D printing applications that require a smooth and consistent powder flow [407]. It is also a time-consuming process, and the powder produced can be contaminated by the milling media and the chamber [408].

Atomization methods [404]: atomization is one of the most common methods for producing high-quality metal powders. It involves the disintegration of molten metal into fine droplets, which solidify into powder particles. There are three main types of atomization methods, gas [409], water [410], and plasma [411]. Gas atomization uses a high-pressure gas stream to break up molten metal into fine droplets, resulting in spherical particles with high flowability and packing density, ideal for 3D printing applications. Water atomization uses high-pressure water jets instead of gas to disintegrate molten metal. The particles produced by water atomization are generally irregular and can have a rough surface texture, which may affect flowability and packing density. It is more cost-effective than gas atomization, but it can introduce impurities and lead to the formation of oxides. Plasma atomization uses a plasma torch both to melt metal wire and to disintegrate it into fine droplets. The particles produced by plasma atomization are highly spherical and have excellent purity and consistency, but the technique is more expensive due to the higher energy requirements.

An advanced and interesting process for the production of metal powders is the rotating plasma electrode technique [412–414]. The process consists of a rotating sacrificial electrode installed in a vacuum chamber. The heat source is provided by a counter electrode, usually made of tungsten, which generates a plasma under controlled conditions that is responsible for melting the electrode. The rotation causes the molten particles to be centrifugally expelled, producing small drops of liquid metal which solidify and fall into the collector. This process is a valid method used to produce metal alloys that are reactive to gases. The number of internal defects is usually low compared to conventional processes.

Chemical methods: chemical methods are a group of time-consuming techniques that involve the reduction or decomposition of metal compounds to produce fine powders. These methods can produce highly pure powders with controlled particle sizes and shapes. In chemical reduction [415], metal oxides are mixed with a reducing agent and heated in a controlled environment, where the oxide is reduced to metal powder. The morphology of the powders produced can vary but generally includes a mix of irregular and semi-spherical particles, depending on the reduction conditions. Electrolytic deposition [416] involves the reduction of metal ions from a solution on a cathode to form a powder. This process typically produces dendritic or spongy particles that may require further processing to achieve a desired shape and size. Other chemical methods involve the precipitation of metal from a solution [417], often followed by thermal decomposition. They can produce fine powders with varied shapes, ranging from spherical to irregular, depending on the precipitation conditions.

Each process has its advantages and disadvantages. Mechanical methods like ball milling are suitable for brittle materials but produce irregularly shaped powders. Atomization methods (gas, water, and plasma) are favored for producing high-quality spherical powders, though they vary in cost and particle morphology. Chemical methods provide high-purity powders with controlled characteristics, making them suitable for specific applications.

3. Powder Degradation Mechanisms

The powders used in the 3D printing process can degrade due to the interaction of the powders with the printing environment and in particular with the energy source (laser and electron beam), the molten metal, the chemical compound in the printing chamber, and the contact with mechanical components present in the printing chamber (re-coater) [73,418] (Figure 4). Degradation mainly occurs due to thermal effects, chemical effects, and/or mechanical effects. Collectively, these degradation processes can alter the above properties and therefore the performance of the powder when reused for other printing cycles. By detailing the source of degradation, a careful analysis of the printing process should be carried out, particularly for powder bed fusion processes [419].

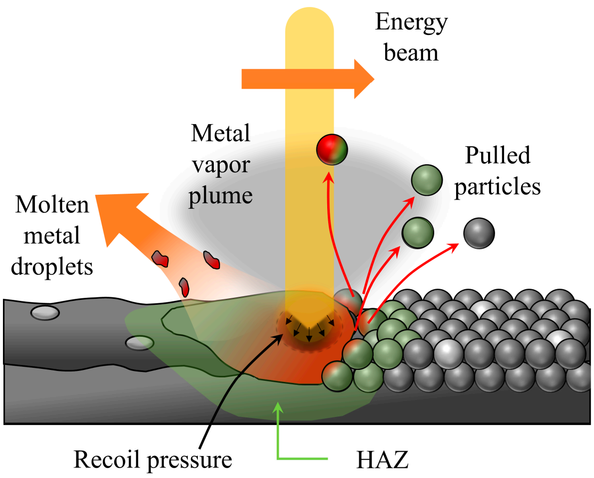

Figure 4. Simplified diagram of the effects of the interaction between a high-energy beam and metallic powders. The green region represents the heat-affected zone (HAZ), while red is used for the melted material.

Some mechanisms of powder degradation are common across all the different 3D printing techniques, particularly those involving mechanical damages such as wear, fragmentation, and deformation. However, there are specific mechanisms that are unique to certain techniques or require particular conditions. For instance, processes such as dealloying, sintering, and oxidation necessitate an intense source of heat, which is absent in the printing phase of Binder Jetting.

Within beam-based techniques, Electron Beam Melting operates in a more controlled atmosphere, which significantly reduces the risk of oxidation compared to other methods. The various techniques also differ in their susceptibility to contamination. Binder Jetting is more prone to contamination due to binder residuals on the powder, while the EB-PBF controlled atmosphere also reduces the contamination risks. Directed Energy Deposition (DED) techniques face variable contamination risks depending on the location and size of the equipment, particularly if used for on-site builds, which can increase the likelihood of contamination.

The review of powder degradation mechanisms is mainly based on the alloys listed in Table 1.

The first source of powder degradation is the interaction of the powder with the molten pool [420–423]. In fact, the pool can be a source of molten metal projection due to the flow of molten metal and the resulting spread of molten droplets to the surrounding part. This metal projection can produce the following: metal jets, droplet spatter, and powder spatter. In the case of droplet spatter, molten metal droplets are spread from the molten pool to form a powder-like solidified material that rarely resembles the original powder in shape, dimension, or chemical composition. More or less the same observation is made for metal jets, but in this case the molten metal is usually overheated with respect to the previous droplets. In the case of powder spatter, the molten metal drops usually fall on the surrounding powder, causing morphological changes in the particulate.

Another important source of degradation is related to the movement of powders during the printing process; in this case, the particles can be moved from the original process site due to fluodynamic interaction with the molten pool or with the printing environment. In this case, the affected powders can interact with the molten bath, heating particles surrounding the molten pool, or with the energy source. In both cases, the powder can be altered and thus degraded from its original properties.

An overview of the eight main powder degradation mechanisms is presented in Figure 5.

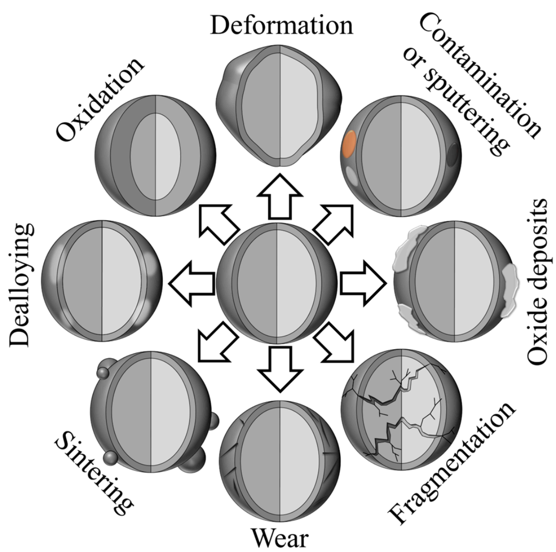

Figure 5. Simplified models for the eight main mechanisms of degradation occurring on recycled powders: deformation, contamination, oxide deposits, fragmentation, wear, sintering, dealloying, and oxidation.

3.1. Thermal Effects

Thermal degradation mechanisms in metal 3D printing are primarily associated with the extreme temperatures involved in the printing process, including pre-heating, heating during melting and solidification, and subsequent thermal cycling during the build and post-processing stages; this is not to forget the powder/beam interaction.

By analyzing the effect of thermal degradation due to the interaction of the energy beam with powders (Figure 4), one can see that the effects are mainly related to the presence of molten metal drops that undergo a very fast solidification when expelled from the energy source [424,425]. In this case, there are multiple phenomena affecting powder composition and size/geometry. Indeed, a molten metal drop can be directly ejected from the molten pool and in this case there is an independent solidification that can produce, as a function of the overheating temperature reached by the metal, either a new crystal or a phase change. In stainless steels, for example, when powders are overheated the microstructure can transform from austenite to ferrite [426]. Usually, the phase transformation occurs when there is a strong beam interaction with the molten metal drop. Other effects due to the melting process can be related to slag projection, which can produce a new single-oxide powder [427].

Another important thermal degradation mechanism is related to the presence of low-melting-point elements that can evaporate/sublimate [428]. In some cases, such as with Ti alloys or aluminum alloys, low-melting-point elements can vaporize during the powder/beam interaction, producing element depletion in the printed component [429]. Part of the produced vapor re-condenses when the elements are driven out of the energy source and are cooled. The re-condensed particles usually present a non-conformal morphology (not-spherical shape) and a chemical composition not in agreement with the chemical composition of the not-affected powders.

Another significant thermal degradation mechanism is powder oxidation, wherein exposure to elevated temperatures in environments with certain partial pressures of oxygen (even when small) can lead to the formation of oxide layers on the surface of metal powders [430,431]. These oxide layers can negatively impact powder flowability, heat transfer, and the mechanical properties of printed parts. In this case, some materials are more prone to O adsorption, for example Ti alloys, than other materials (e.g., Ni-based alloys). The amount of O adsorption depends on many factors, for example powder age/reuse cycles, material chemical affinity, and atmosphere control in the printing chamber. The effect of gaseous element adsorption is to reduce the impact on both the physical properties of the powders as well as the solidification behavior of the molten metal. As a consequence, the modification of the chemical composition of the powders can lead to a change in powder behavior during the printing process or during the solidification of the molten pool, which then has an influence on the microstructure of the printed material. The chemical composition change, and in particular the adsorption of gaseous elements, usually has an impact on both the inclusion content of the printed material and also on the defect amount of the printed material (pores). It is also possible that a splat of metal oxides (slags) can coat the surrounding powders.

An important thermal effect is related to the fact that the powders can interact with the molten metal by producing a heat-affected zone (HAZ) on the surrounding powders [432,433]. These effects can produce a partial melting or a melting at a low temperature of the powders, usually producing elongated powders in a non-spherical shape. These particles usually have an effect on the flowability and also on the apparent density of the powders. If the powder is not molten but heated at temperatures below the melting temperature of the metal, some microstructural changes in the powder can occur.

Partial sintering can also be considered a thermal degradation mechanism in metal 3D printing [434]. Partial sintering occurs when metal powders are subjected to temperatures below their melting points but high enough to induce partial bonding and consolidation of powder particles. This phenomenon can occur during the preheating and initial stages of the printing process, where the temperature of the powder bed is elevated to facilitate subsequent fusion and solidification, or simply in the regions surrounding the molten metal, where the temperature progressively decreases with the distance. While controlled partial sintering can be actually used to improve powder flowability, packing density, and layer adhesion, excessive or uncontrolled partial sintering can lead to issues such as poor powder flowability, increased porosity, reduced surface roughness, and dimensional inaccuracies in printed parts [434–436]. Therefore, it is essential to carefully control and optimize the thermal conditions to minimize the negative effects of partial sintering and ensure the quality and integrity of printed parts. An indirect thermal-effect-related phenomena is the formation of particles coated with metal spatters that can produce an external overlayer of metal which can modify the geometry and the microstructure of the powder.

3.2. Mechanical Effects

Mechanical degradation mechanisms in metal 3D printing encompass a broad range of physical forces and stresses experienced by metal powders throughout the printing process. These mechanisms include powder handling, spreading, compaction, and fusion, as well as frictional interactions between the powder and various components of the printing system.

One common mechanical degradation mechanism is powder attrition, wherein repeated handling and mechanical agitation during powder storage, transportation, and processing can cause abrasion and fragmentation of powder particles [437,438]. This can lead to changes in particle size distribution, morphology, and surface roughness, affecting powder flowability and packing density. Additionally, frictional forces between the powder and components such as powder distribution systems, re-coaters, and metal blades can further contribute to powder degradation by causing wear and erosion of both the powder particles and the machine components themselves. These frictional interactions can result in the generation of fine particles, powder contamination, and increased levels of airborne debris, all of which can impact the quality and consistency of printed parts.

Furthermore, mechanical degradation can occur during the printing process itself, particularly in techniques involving powder bed fusion, where powders are subjected to mechanical compaction, layer-by-layer deposition, and energy inputs from lasers or electron beams [439–441]. The mechanical forces exerted on the powder bed during these processes can induce powder densification, deformation, and consolidation, affecting the microstructure and properties of printed parts. Moreover, inadequate powder handling practices, such as improper powder storage conditions or excessive vibrations during printing, can exacerbate mechanical degradation mechanisms, leading to defects and inconsistencies in printed parts. Another important parameter that can influence mechanical degradation is related to the presence of internal voids/porosities that enhance the powder degradation by means of mechanical failure of the powder. In addition, the microstructural alteration of the powders due to heat transfer can decrease the mechanical properties of the powder particles and thus the mechanical resistance of the powder.

3.3. Chemical Effects

Chemical degradation mechanisms in metal 3D printing are interactions between metal powders and various chemical agents present in the printing environment. These mechanisms include reactions with reactive gases, moisture, contaminants, low-melting-point element evaporation/sublimation, and the binder used in certain printing processes.

One chemical degradation mechanism in metal 3D printing is powder contamination [58,70,442–444], wherein metal powders can become contaminated by airborne particles, residual processing materials, or surface contaminants introduced during handling and storage. Contaminants such as oils, greases, dust, and other airborne pollutants can adhere to powder surfaces, leading to defects in printed parts and affecting their properties.

Another important chemical phenomenon that can occur, as previously discussed under the “thermal effects” sub-chapter, is the sublimation of low-melting-point elements during the 3D printing process, which also results in alterations in the chemical composition [428]. In particular, evaporation [445–448] can deplete the powders of alloying elements that change the properties of the printed component, if the powders are used to produce a component. Usually, the evaporated elements precipitate in the powder bed due to the possible condensation when the volatile elements are cooled in the cold areas of the printing chambers. Ti, Zn, Mg, and Al alloys are most sensitive to this phenomenon.

Another significant consideration for powder recycling in metal 3D printing involves the removal of residual binder from the printed parts. In Binder Jetting processes, where metal powders are selectively bonded together using a liquid binder, small amounts of residual binder may remain within the printed parts after the printing process is complete [449]. This residual binder can interfere with subsequent printing runs and affect the properties of recycled powders.

To address this, special attention must be given to the removal of residual binder during the powder recycling process [450]. Various techniques, such as solvent extraction, thermal treatments, and chemical baths, can be employed to effectively remove the binder from the printed parts. Solvent extraction involves immersing the printed parts in a solvent that dissolves the binder, leaving behind clean metal powders. Thermal treatments, such as sintering or pyrolysis, can also be used to burn off the binder at elevated temperatures, leaving behind pure metal powders. Additionally, chemical baths containing specific reagents can be used to chemically dissolve the binder without affecting the metal powders.

3.4. Impact on Powder Properties

All types of degradation processes, such as contamination, thermal decomposition, and partial sintering, can lead to significant changes in the properties of metal powders used in 3D printing.

The most important powder technological properties, such as flowability, packing density [49,50], and energy adsorption, are a function of the powder size distribution, the morphology of the powders, and the presence of contaminants. The powder size distribution has the greatest influence on packing density [451]. Indeed, recycled powders usually have, for materials that have not experienced element sublimation, a broader distribution that moves towards coarser particles [73] (Figure 6). In this case, the packing density is usually reduced and, as a result, the thermal energy is transferred to the powders via fewer contact points during the printing process.

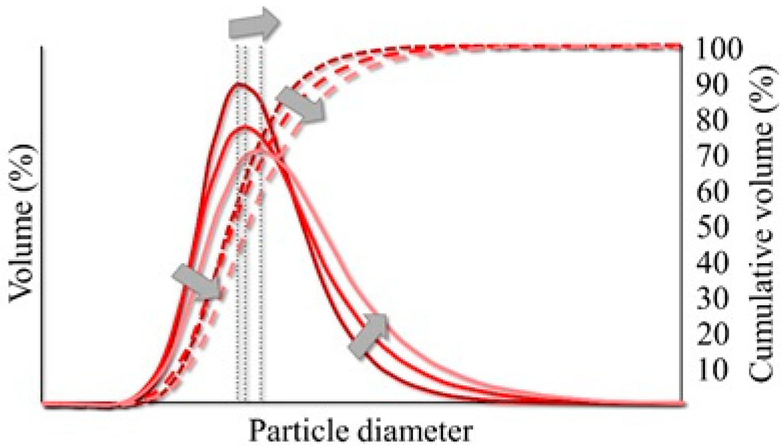

Figure 6. Qualitative comparison of recycled powder size distribution as a function of number of cycles. The arrows indicate the increase in reuse cycles. A brighter color indicates a more recycled powder.

On the other hand, in materials with a high propensity for alloy depletion, the distribution becomes broader and the average particle size can also be reduced at a high number of re-using cycles [73]. In this case, the powders during the printing process adsorb high amounts of energy. These effects are also related to the powder morphology; indeed, a not-spherical powder grain has an influence on the PSD and thus on the aforementioned properties.

In addition, the flowability is reduced due to the fact that the not-spherical powders do not flow well during the re-coater action [452,453]. The effect of the powder impurities, instead, is to alter the physical properties of the powders, in particular by altering the heat transfer properties or the melting point of the powder itself. By increasing the impurity amount, which usually is observed during the recycling cycle increase, a decrease in thermal conductivity and an increase in the melting point is observed. In particular, the oxides that are present on the external surface reduce the heat conductivity of the powders, while the internal impurities usually change the physical properties of the molten pool and thus the solidified microstructures. These property changes can then have an influence on the printed component as described in the next paragraph. Generally speaking, the property that is mainly influenced by the decay of the powders due to reuse is flowability.

4. Effect of Recycled Powders on 3D-Printed Components

As discussed in the previous paragraph, reused powders have different properties compared to the virgin powder due to the interaction of these powders with the energy beam and the surrounding environment. In particular, it has been discussed how the reused powder influences the packing density, flowability, and physical properties, which in turn affects the outcome of the printing process itself.

A simplified schematic of the seven main categories of printing defects that can be caused by recycled powders is presented in Figure 7.

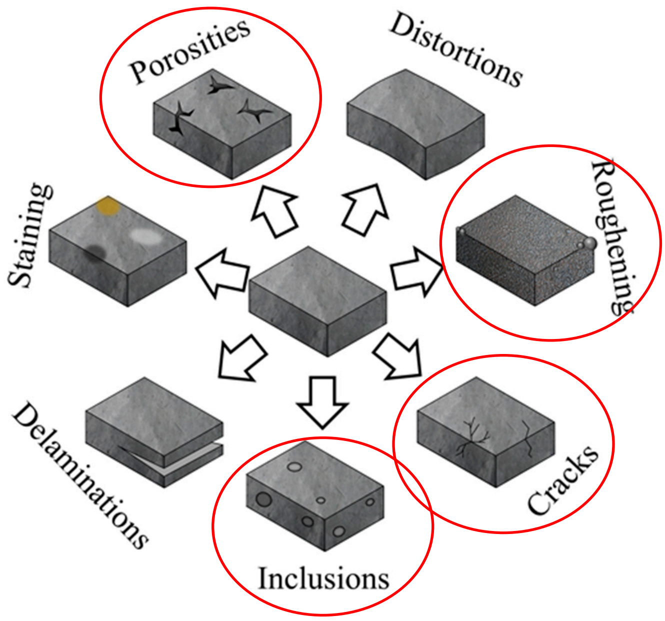

Figure 7. Seven categories of defects that can be observed on 3D-printed components and can sometimes be caused by the use of recycled powders (circled ones): distortions, roughening, cracks, inclusions, delamination, staining, and porosities. The circled images correspond to the effects most observed due to powder recycling.

The presence of defects in the powders can result in internal defects, surface roughness, microstructure, mechanical properties, and degradation (corrosion) resistance. Usually, the strategy of using reused powders is to continuously screen the powders after each printing job until the powders are finished, or to add a quantity of used powders to new powders. Details of the powder reuse strategy will be discussed in a separate paragraph. The overview of the impact of powder reuse on 3D printed components is based on the most common metal alloys used in additive manufacturing processes, which are listed in Table 1.

In terms of internal defects, many authors have observed an increase in void density and dimension in printed components produced with recycled powders [62,454]. This has been observed by CT scan measurements and also by light microscopy observations. In particular, the effect of using recycled powders is to increase the number and size of discontinuities. The morphology is also changed to more elongated voids, similar to the absence of fusion discontinuities. The increase in the number of elongated voids is probably related to the reduced flowability of the powders, which increases the tendency of the material to produce a lack of fusion, while the increase in the number of voids in general could be attributed to the variation in packing density compared to virgin powders. Regarding the chemical composition of the printed material with the reused powders, an increase in the oxygen content in the printed part has been observed for materials sensitive to O adsorption. This usually leads to the formation of non-metallic inclusions [62], usually of nanometric size, or to O enrichment in the metal matrix [455]. The surface texture is also affected by the use of recycled powders. In fact, a reduction in surface quality has been observed and this is usually attributed to the presence of non-spherical powders, impurities in the powders, and reduced flowability. All printed surfaces are affected by a reduction in surface quality [443,456]. By detailing the discussion of the most common alloys used for the 3D printing process, a general increase in defect amount and size is observed in austenitic stainless steel [457] and Ti alloys. On the other hand, the inclusion content is strongly influenced by the O content of the powders and usually the dimension of these particles is in the sub-nanometric range. It seems that these particles are responsible for the mechanical property increase due to the fact that they act as precipitates. A general increase in both O and inclusion content has been observed in all the most used alloys systems (Ni, Ti, stainless steel, and Al).

Regarding the effect of recycled powders on microstructure, many studies have been carried out on the effect of using both pure recycled powders and recycled powders mixed with virgin powders [443,457–459]. In the latter case, no microstructural differences have been observed when using virgin or virgin/blended recycled powders [460]. However, some differences have been observed in components printed with recycled powders. In this case, the microstructure is refined and the content of some secondary phases is observed. In particular, the grain refinement can be attributed to both the presence of a higher amount of oxides and a change in the melting/cooling properties of the molten metal. This was observed in Ni [461], Ti, and stainless steels [462]. The refinement was detected through EBSD analysis and the elongated columnar grains are usually thinner in components produced with recycled powders. In Ti alloys, on the other hand, a decrease in the beta phase was observed, probably due to the increase in the O content, which is an alpha stabilizer phase [459,463]. This element probably inhibited the formation of the beta phase. Some studies on stainless steels have also shown that the presence of powders with an undesirable phase (delta ferrite phase) promotes the formation of these phases in the printed material [62]. To avoid this, the authors suggested magnetic separation of delta ferrite powders from the batch.

Obviously, the effect of powder reuse has an impact on the mechanical properties, as 3D-printed parts with reused powders show a higher number of defects, sometimes microstructural changes and altered chemistry [458]. In terms of hardness tests, no significant differences were observed between components printed with reused powders and those printed with recycled powders [62]. The differences are all within the experimental error for all the most common alloys systems. It is likely that the hardness is strongly linked to the tensile strength of material, which is slightly affected by re-using the powders. In this case, the measurement method seems not to be sensitive for detecting the small variations in the printed material. Indeed, tensile properties are slightly affected by the reuse process. In general, an increase in tensile strength (TS) is observed, accompanied by a decrease in ductility, especially in materials that tend to adsorb trace elements (O) from the printing environment. This behavior was observed in Ti and Al [464,465] alloys. On the other hand, Ni [461] and stainless steel did not show any appreciable variation of TS and YS (Yield

Strength). A general decrease in ductility has been observed in all the most common metal systems and this is related to both an increase in inclusion content and increase in porosity size and distribution.

On the other hand, the fatigue properties are affected by the use of recycled powders [466,467]. It has been observed that the fatigue limit usually decreases as a function of the number of recycling cycles. This is due to the fact that the components printed with reused powders have a higher number of internal defects, which are also coarser with respect to the components printed with virgin powders. Some studies have been carried out by analyzing the statistical distribution of failures for samples tested at the same stress level. The results showed that the specimens produced with reused powders had failures that were anticipated with respect to the specimens produced with virgin powders. A different behavior was observed in 17-4 PH steel [468], where the fatigue resistance increased as a function of reuse cycles and this was related to the reduction in agglomerates in powders.

Although the effect of reused powders on the corrosion properties of printed alloys has not been deeply investigated, some studies performed on Al alloys [459] have evidenced that the specimens made with reused powders have a higher activity compared to the same specimens made with new powders. This effect is related to the lower internal quality of the material produced by 3D printing processes.

A qualitative summary of the effect of recycled powder use on the microstructural and mechanical properties of 3D-printed parts is shown in Figure 8.

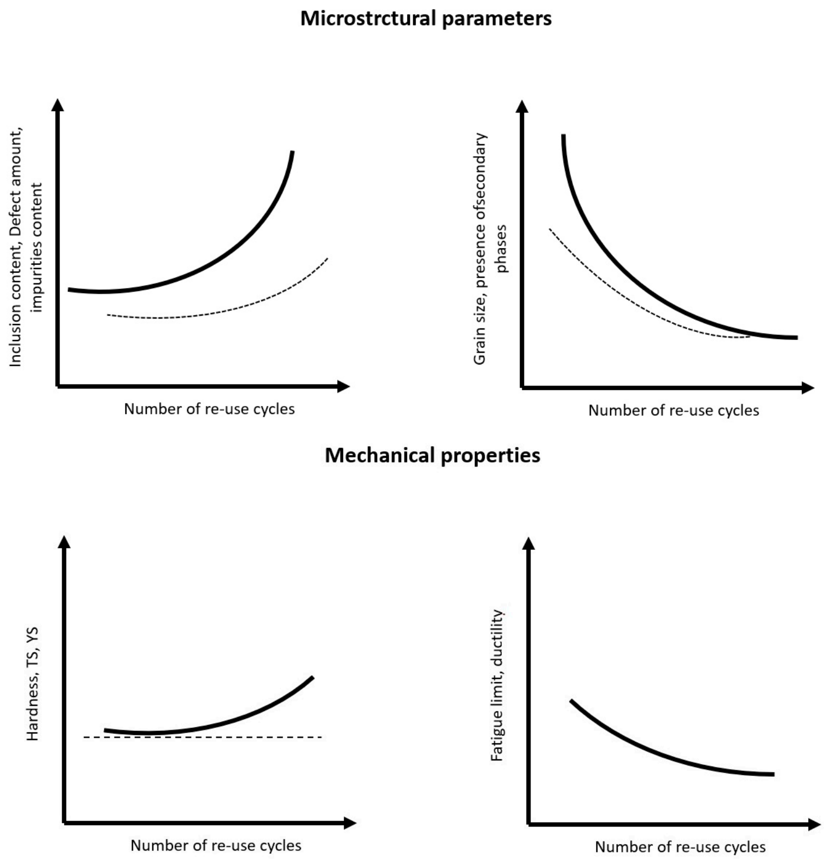

Figure 8. Qualitative summary of property variation as a function of recycling cycles. Continuous line corresponds to metals more sensitive to impurity pick up, while dotted lines correspond to metals less prone to impurity pick up.

5. Powder Reuse Strategies

Powder reuse strategies are some methods set up to optimize the reuse of powders in order to obtain a 3D part with an acceptable quality by wasting the least amount of powder [73]. Each strategy has its own advantages and disadvantages depending on how the method is set up. For industrial production, one of the most important parameters is the traceability of the powder batch, also considering that the strategy should be as simple as possible and at the same time have the minimum waste of powder. The most used strategies in both industry and academia are as follows: the single-batch method, the collective aging method and the replenishment method.

Researchers often recycle powders when a batch becomes depleted (insufficient for another component) in the single-batch method [469]. This approach is valued for its simplicity (requiring only continuous post-printing sieving) and high traceability. However, despite ongoing process improvements, it still generates significant powder waste [470].

More complex recycling processes, like the "collective ageing method", can reduce the amount of wasted powder [471,472]. This method consists of aging many different batches separately, and then mixing them with powders of the same ageing time. This method is more suitable for high-productivity plants, but traceability is sacrificed. Another important disadvantage is the need to manage many batches and large quantities of stored powder [473,474].

The replenishment method can be considered a hybrid process [73,405,469]. After each printing process, the powders are first replenished with new powders up to a certain number of printing cycles. After these cycles, the replenished powders are a mixture of virgin powders and reused powders with low working cycles (lower than the original powders). The main disadvantage of this process is its complexity, as the powders have to be managed in terms of continuous replenishment with both reused and virgin powders, and it requires accurate management of the reused powders that are then used to replenish the print batch. Traceability is lost after the first print batch, similar to the replenishment method. A major advantage of this strategy is the significant reduction in powder waste.

The above strategies are some of the most common ones found in industrial and academic fields, where 3D printing is constantly evolving as far as recycling strategies are concerned.

6. Advances in Powder Recycling Techniques

As powder recycling has become an essential aspect of metal 3D printing, enabling the reuse of excess or spent powders and reducing material waste and production costs, various recycling techniques have been developed. These recycling methods range from simple mechanical approaches to more advanced technologies like plasma and laser post-treatments.

6.1. Mechanical Recycling Methods

Mechanical recycling methods are the simple and cost-effective way to eliminate large particles and contaminants. There are two main mechanical powder recycling methods available:

Sieving [475,476], which involves passing used metal powders through a mesh screen to separate particles of different sizes. It is the most common method used in additive manufacturing, often combined with other techniques to further improve the outcome.

Centrifugal separation [477], which uses centrifugal force to separate powders based on their density, but is less effective in removing fine contaminants. Despite being the industrial standard in many production fields, centrifugal separators are not usually applied in current 3D printing systems, as they are more effective on larger volumes.

Mechanical recycling methods can damage the particles because of wear and mechanical stress, resulting in changes in morphology and contaminations from the sieving equipment.

6.2. Thermal Recycling Methods

Thermal recycling processes are more focused on the chemical composition of the powders, in particular trapped gases and impurities. There are two main thermal recycling methods that are found industrial applications:

Vacuum degassing [478,479]: this involves heating the used powder in a vacuum to remove absorbed gases and contaminants, but is energy-intensive and can alter the properties of the powders.

Re-sintering [480,481]: this involves heating the used powder to fuse small particles together, removing contaminants and improving powder properties. This technology is rarely used in additive manufacturing, and is still in its infancy for metal powder recycling.

Conventional remelting can also be considered a thermal recycling method [469]. In this case, the end-of-life powders are used as scrap for further melting. It is important to point out that the end-of-life powders usually do not fulfil the requirements in terms of chemical composition due to both the presence of impurities above the acceptability level and the lack of elements in their chemical composition. To solve this quality problem, an addition of fresh metal with appropriate composition is added and, to reduce the gas in metal issues, a vacuum process is performed.

6.3. Chemical Recycling Methods

Acid etching [482,483] can be utilized to improve the rheological properties, decrease the laser reflectance, and reduce the oxide layer on metallic powders, in particular for metals like aluminum or copper. This technology can be used either on virgin or recycled powders.

Electrochemical etching, like acid etching, can improve the surface properties of metallic powders, in particular for materials that are resistant to conventional acid treatments [484].

6.4. Emerging Technologies and Future Perspectives

Additive manufacturing has been an environmentally friendly process since its inception [485]. In fact, its peculiarity of producing components by adding material instead of subtracting material has considerably revolutionized the approach in the industrial field by increasing the sustainability of the production process. However, it has to be taken into account that this process also generates small amounts of waste, mainly consisting of end-of-life powders, i.e., powders that do not meet the quality requirements to be used. As previously indicated in this work, powder reuse strategies should be better implemented to reduce the complexity of powder management and automation; in high-productivity plants, this can be a solution to simplify the management issues and thus reduce the human factor. In process and powder management, care should also be taken in powder handling to avoid contamination, which can reduce powder quality and thus the reuse life of the powder. Re-use strategies should also be optimized to increase powder re-use life.

Scrapped powders can be conditioned during the production process to avoid remelting. In this case, a huge energy saving can be expected and the life of the powders can be extended by reducing the amount of scrapped powders. This strategy can also be applied before the end of the life of the powders, with the main aim of prolonging the time until they are scrapped. The emerging technologies may be suitable for this purpose in the near future [485].

Plasma cleaning [486] involves using a high-temperature ionized gas (plasma) to remove contaminants like moisture and trapped gases from the powder particles, or to etch surface oxide layers. Apart from cleaning, plasma can also be used for powder spheroidization.

Plasma spheroidization [72,487] is a relatively novel technique that utilizes thermal plasma to reshape irregular powder particles into near-perfect spheres. This significantly improves the flowability and packing density of recycled powders, making them more suitable for reuse in 3D printing processes. Research has shown that plasma-spheroidized powders can achieve comparable performance to virgin powders, extending their usable life and minimizing waste.

7. Conclusions

Powder recycling offers a technological solution for reducing costs and environmental impact in metal 3D printing technologies. However, achieving high-quality parts from recycled powders presents significant challenges. Recycled powders undergo modifications in their chemical composition, morphology, microstructure, and size distribution compared to virgin powders. These changes can negatively impact the flowability and density of the powder, which in turn affect the surface quality and mechanical properties of the printed parts. A decrease in surface quality and an increase in internal defects are commonly observed, particularly affecting ductility and dynamic mechanical properties.

Despite these limitations, several strategies hold promise for improving the quality of parts printed from recycled powders. Pre-treatment techniques like plasma or laser cleaning can remove contaminants and improve powder morphology, leading to better printability. Optimizing the 3D printing process parameters for recycled powders can also compensate for some of the potential flowability or density issues, but blending controlled amounts of virgin powder with recycled powder is so far more effective in improving the overall quality of the feedstock.

Traceability is also a crucial issue for ensuring consistent quality and managing potential safety concerns associated with recycled powders. A robust system should be implemented to track the origin, processing history, and properties of the powder throughout its life cycle. Furthermore, minimizing powder waste during the printing process is essential to maximize the efficiency and sustainability of powder recycling in 3D printing.

Looking ahead, further research is needed to fully unlock the potential of metal powder recycling. Advanced powder characterization techniques can help predict the printability and quality of recycled powders, allowing for tailored pre-treatment strategies for different metal powders and contaminants. Exploring novel powder blending strategies can optimize the properties of the feedstock. Finally, developing closed-loop powder recycling systems that minimize waste generation would significantly enhance the sustainability of this approach.

Metal powder recycling has the potential to become a reliable and environmentally friendly method for producing high-quality metal parts via 3D printing, once these challenges are finally solved.

Author Contributions: Conceptualization, A.L. and E.M.; methodology, A.L. and E.M.; validation, A.L. and E.M.; formal analysis, A.L. and E.M.; investigation, A.L. and E.M.; resources, A.L. and E.M.; data curation, A.L. and E.M.; writing—original draft preparation, A.L. and E.M.; writing—review and editing, A.L. and E.M.; visualization, A.L. and E.M.; supervision, A.L. and E.M.; project administration, A.L. and E.M.; funding acquisition, A.L. and E.M. All authors have read and agreed to the published version of the manuscript.

Funding: This research received no external funding.

Conflicts of Interest: The authors declare no conflicts of interest.

References

1. Savvides, L.A. History of 3D Printing: Three Waves of Development. In *3D Printing Cultures, Politics and Hackerspaces*; Emerald Publishing Limited: Leeds, UK, 2021; pp. 29–51. Available online: https://www.emerald.com/insight/content/doi/10.1108/978-1-80071-665-020211005/full/html (accessed on 31 May 2024).
2. Kumar, S.P.; Elangovan, S.; Mohanraj, R.; Ramakrishna, J.R. Review on the evolution and technology of State-of-the-Art metal additive manufacturing processes. *Mater. Today Proc.* **2021**, *46*, 7907–7920. [CrossRef]
3. Kumar, S. Selective laser sintering: A qualitative and objective approach. *JOM* **2003**, *55*, 43–47. [CrossRef]
4. Joshi, S.C.; Sheikh, A.A. 3D printing in aerospace and its long-term sustainability. *Virtual Phys. Prototyp.* **2015**, *10*, 175–185. [CrossRef]
5. Lecklider, T. 3D printing drives automotive innovation. *Eval. Eng.* **2017**, *56*, 16–20.
6. Aimar, A.; Palermo, A.; Innocenti, B. The role of 3D printing in medical applications: A state of the art. *J. Healthc. Eng.* **2019**, *2019*, 5340616. [CrossRef] [PubMed]
7. Jandyal, A.; Chaturvedi, I.; Wazir, I.; Raina, A.; Haq, M.I.U. 3D printing—A review of processes, materials and applications in industry 4.0. *Sustain. Oper. Comput.* **2022**, *3*, 33–42. [CrossRef]

8. Mostafaei, A.; Elliott, A.M.; Barnes, J.E.; Li, F.; Tan, W.; Cramer, C.L.; Nandwana, P.; Chmielus, M. Binder jet 3D printing—Process parameters, materials, properties, modeling, and challenges. *Prog. Mater. Sci.* **2021**, *119*, 100707. [CrossRef]
9. Do, T.; Kwon, P.; Shin, C.S. Process development toward full-density stainless steel parts with binder jetting printing. *Int. J. Mach. Tools Manuf.* **2017**, *121*, 50–60. [CrossRef]
10. Mao, Y.; Li, J.; Li, W.; Cai, D.; Wei, Q. Binder jetting additive manufacturing of 316L stainless-steel green parts with high strength and low binder content: Binder preparation and process optimization. *J. Mater. Process. Technol.* **2021**, *291*, 117020. [CrossRef]
11. Wheat, E.; Vlasea, M.; Hinebaugh, J.; Metcalfe, C. Sinter structure analysis of titanium structures fabricated via binder jetting additive manufacturing. *Mater. Des.* **2018**, *156*, 167–183. [CrossRef]
12. Im, S.; Ghasri-Khouzani, M.; Muhammad, W.; Batmaz, R.; Esmati, K.; Chakraborty, A.; Natarajan, A.; Martin, É. Evaluation of Different Sintering Agents for Binder Jetting of Aluminum Alloy. *J. Mater. Eng. Perform.* **2023**, *32*, 9550–9560. [CrossRef]
13. Karlsson, D.; Lindwall, G.; Lundbäck, A.; Amnebrink, M.; Boström, M.; Riekehr, L.; Schuisky, M.; Sahlberg, M.; Jansson, U. Binder jetting of the AlCoCrFeNi alloy. *Addit. Manuf.* **2019**, *27*, 72–79. [CrossRef]
14. Hong, D.; Chou, D.-T.; Velikokhatnyi, O.I.; Roy, A.; Lee, B.; Swink, I.; Issaev, I.; Kuhn, H.A.; Kumta, P.N. Binder-jetting 3D printing and alloy development of new biodegradable Fe-Mn-Ca/Mg alloys. *Acta Biomater.* **2016**, *45*, 375–386. [CrossRef] [PubMed]
15. Ziaee, M.; Crane, N.B. Binder jetting: A review of process, materials, and methods. *Addit. Manuf.* **2019**, *28*, 781–801. [CrossRef]
16. Yap, C.Y.; Chua, C.K.; Dong, Z.L.; Liu, Z.H.; Zhang, D.Q.; Loh, L.E.; Sing, S.L. Review of selective laser melting: Materials and applications. *Appl. Phys. Rev.* **2015**, *2*, 041101. [CrossRef]
17. Singh, S.; Sharma, V.S.; Sachdeva, A. Progress in selective laser sintering using metallic powders: A review. *Mater. Sci. Technol.* **2016**, *32*, 760–772. [CrossRef]
18. Olakanmi, E.O.; Cochrane, R.F.; Dalgarno, K.W. A review on selective laser sintering/melting (SLS/SLM) of aluminium alloy powders: Processing, microstructure, and properties. *Prog. Mater. Sci.* **2015**, *74*, 401–477. [CrossRef]
19. Kumar, M.B.; Sathiya, P.; Varatharajulu, M. Selective laser sintering. In *Advances in Additive Manufacturing Processes*; Natarajan, J., Cheepu, M., Yang, C.-H., Eds.; China Bentham Books: Beijing, China, 2021; p. 28.
20. Blakey-Milner, B.; Gradl, P.; Snedden, G.; Brooks, M.; Pitot, J.; Lopez, E.; Leary, M.; Berto, F.; Du Plessis, A. Metal additive manufacturing in aerospace: A review. *Mater. Des.* **2021**, *209*, 110008. [CrossRef]
21. Fe-Perdomo, I.L.; Ramos-Grez, J.A.; Beruvides, G.; Mujica, R.A. Selective laser melting: Lessons from medical devices industry and other applications. *Rapid Prototyp. J.* **2021**, *27*, 1801–1830. [CrossRef]
22. Vasco, J.C. Additive manufacturing for the automotive industry. In *Additive Manufacturing*; Elsevier: Amsterdam, The Netherlands, 2021; pp. 505–530. Available online: https://www.sciencedirect.com/science/article/pii/B9780128184110000100 (accessed on 31 May 2024).
23. Chantzis, D.; Liu, X.; Politis, D.J.; El Fakir, O.; Chua, T.Y.; Shi, Z.; Wang, L. Review on additive manufacturing of tooling for hot stamping. *Int. J. Adv. Manuf. Technol.* **2020**, *109*, 87–107. [CrossRef]
24. Wang, Z.; Ummethala, R.; Singh, N.; Tang, S.; Suryanarayana, C.; Eckert, J.; Prashanth, K.G. Selective laser melting of aluminum and its alloys. *Materials* **2020**, *13*, 4564. [CrossRef] [PubMed]
25. Rahulan, N.; Sharma, S.S.; Rakesh, N.; Sambhu, R. A short review on mechanical properties of SLM titanium alloys based on recent research works. *Mater. Today Proc.* **2022**, *56*, A7–A12. [CrossRef]
26. Röttger, A.; Boes, J.; Theisen, W.; Thiele, M.; Esen, C.; Edelmann, A.; Hellmann, R. Microstructure and mechanical properties of 316L austenitic stainless steel processed by different SLM devices. *Int. J. Adv. Manuf. Technol.* **2020**, *108*, 769–783. [CrossRef]
27. Zhang, W.; Wang, L.; Feng, Z.; Chen, Y. Research progress on selective laser melting (SLM) of magnesium alloys: A review. *Optik* **2020**, *207*, 163842. [CrossRef]
28. Korkmaz, M.E.; Gupta, M.K.; Waqar, S.; Kuntoğlu, M.; Krolczyk, G.M.; Maruda, R.W.; Pimenov, D.Y. A short review on thermal treatments of Titanium & Nickel based alloys processed by selective laser melting. *J. Mater. Res. Technol.* **2022**, *16*, 1090–1101.
29. Hong, J.H.; Yeoh, F.Y. Mechanical properties and corrosion resistance of cobalt-chrome alloy fabricated using additive manufacturing. *Mater. Today Proc.* **2020**, *29*, 196–201. [CrossRef]
30. Negi, S.; Nambolan, A.A.; Kapil, S.; Joshi, P.S.; Karunakaran, K.P.; Bhargava, P. Review on electron beam based additive manufacturing. *Rapid Prototyp. J.* **2020**, *26*, 485–498. [CrossRef]
31. Monteiro, H.; Carmona-Aparicio, G.; Lei, I.; Despeisse, M. Energy and material efficiency strategies enabled by metal additive manufacturing—A review for the aeronautic and aerospace sectors. *Energy Rep.* **2022**, *8*, 298–305. [CrossRef]
32. Marin, E.; Fusi, S.; Pressacco, M.; Paussa, L.; Fedrizzi, L. Characterization of cellular solids in Ti6Al4V for orthopaedic implant applications: Trabecular titanium. *J. Mech. Behav. Biomed. Mater.* **2010**, *3*, 373–381. [CrossRef]
33. Marin, E. Forged to heal: The role of metallic cellular solids in bone tissue engineering. *Mater. Today Bio* **2023**, *23*, 100777. [CrossRef]
34. Marin, E.; Pressacco, M.; Fusi, S.; Lanzutti, A.; Turchet, S.; Fedrizzi, L. Characterization of grade 2 commercially pure Trabecular Titanium structures. *Mater. Sci. Eng. C* **2013**, *33*, 2648–2656. [CrossRef] [PubMed]
35. Gaytan, S.M.; Murr, L.E.; Ramirez, D.A.; Machado, B.I.; Martinez, E.; Hernandez, D.H.; Martinez, J.L.; Medina, F.; Wicker, R.B. A TEM study of cobalt-base alloy prototypes fabricated by EBM. *Mater. Sci. Appl.* **2011**, *2*, 355. [CrossRef]
36. Svetlizky, D.; Das, M.; Zheng, B.; Vyatskikh, A.L.; Bose, S.; Bandyopadhyay, A.; Schoenung, J.M.; Lavernia, E.J.; Eliaz, N. Directed energy deposition (DED) additive manufacturing: Physical characteristics, defects, challenges and applications. *Mater. Today* **2021**, *49*, 271–295. [CrossRef]

37. Liu, Z.; He, B.; Lyu, T.; Zou, Y. A Review on Additive Manufacturing of Titanium Alloys for Aerospace Applications: Directed Energy Deposition and Beyond Ti-6Al-4V. *JOM* **2021**, *73*, 1804–1818. [CrossRef]
38. Busachi, A.; Erkoyuncu, J.; Colegrove, P.; Martina, F.; Watts, C.; Drake, R. A review of Additive Manufacturing technology and Cost Estimation techniques for the defence sector. *CIRP J. Manuf. Sci. Technol.* **2017**, *19*, 117–128. [CrossRef]
39. Saboori, A.; Aversa, A.; Marchese, G.; Biamino, S.; Lombardi, M.; Fino, P. Application of directed energy deposition-based additive manufacturing in repair. *Appl. Sci.* **2019**, *9*, 3316. [CrossRef]
40. Saboori, A.; Gallo, D.; Biamino, S.; Fino, P.; Lombardi, M. An overview of additive manufacturing of titanium components by directed energy deposition: Microstructure and mechanical properties. *Appl. Sci.* **2017**, *7*, 883. [CrossRef]
41. Smith, T.R.; Sugar, J.D.; San Marchi, C.; Schoenung, J.M. Strengthening mechanisms in directed energy deposited austenitic stainless steel. *Acta Mater.* **2019**, *164*, 728–740. [CrossRef]
42. Kumar, S.P.; Elangovan, S.; Mohanraj, R.; Ramakrishna, J.R. A review on properties of Inconel 625 and Inconel 718 fabricated using direct energy deposition. *Mater. Today Proc.* **2021**, *46*, 7892–7906. [CrossRef]
43. Wu, H.-C.; Chen, T.-C.T. Quality control issues in 3D-printing manufacturing: A review. *Rapid Prototyp. J.* **2018**, *24*, 607–614. [CrossRef]
44. Chua, C.K.; Wong, C.H.; Yeong, W.Y. *Standards, Quality Control, and Measurement Sciences in 3D Printing and Additive Manufacturing*; Academic Press: Cambridge, MA, USA, 2017. Available online: https://books.google.com/books?hl=en&lr=&id=PfTtDQAAQBAJ&oi=fnd&pg=PP1&dq=3D+printing+metals+powder+quality&ots=Kr8EN_Ff-P&sig=NtqLVrM_O3NMe91yxZUSFuNSDn4 (accessed on 31 May 2024).
45. Lyckfeldt, O. Powder Characterisation: Powder rheology of steel powders for additive manufacturing. In Proceedings of the European Congress and Exhibition on Powder Metallurgy, Gothenburg, Sweden, 15–18 September 2013; European PM Conference Proceedings; The European Powder Metallurgy Association: Chantilly, Frane, 2013; p. 1. Available online: https://search.proquest.com/openview/e37e3a7bcef846f9eae895b6931bf2fa/1?pq-origsite=gscholar&cbl=596295 (accessed on 31 May 2024).
46. Yang, H.; Li, S.; Li, Z.; Ji, F. Experimental and numerical study on the packing densification of metal powder with gaussian distribution. *Metals* **2020**, *10*, 1401. [CrossRef]
47. Hajnys, J.; Pagac, M.; Mesicek, J.; Petru, J.; Spalek, F. Research of 316L Metallic Powder for Use in SLM 3D Printing. *Adv. Mater. Sci.* **2020**, *20*, 5–15. [CrossRef]
48. Wei, C.; Li, L.; Zhang, X.; Chueh, Y.-H. 3D printing of multiple metallic materials via modified selective laser melting. *CIRP Ann.* **2018**, *67*, 245–248. [CrossRef]
49. Abu-Lebdeh, T.; Damptey, R.; Lamberti, V.; Hamoush, S. Powder Packing Density and Its Impact on SLM-Based Additive Manufacturing. In *TMS 2019 148th Annual Meeting & Exhibition Supplemental Proceedings*; The Minerals, Metals & Materials Series; Springer International Publishing: Cham, Switzerland, 2019; pp. 355–367, ISBN 978-3-030-05860-9. Available online: https://link.springer.com/chapter/10.1007/978-3-030-05861-6_33 (accessed on 31 May 2024).
50. Lee, Y.S.; Nandwana, P.; Zhang, W. Dynamic simulation of powder packing structure for powder bed additive manufacturing. *Int. J. Adv. Manuf. Technol.* **2018**, *96*, 1507–1520. [CrossRef]
51. Bai, Y.; Wagner, G.; Williams, C.B. Effect of particle size distribution on powder packing and sintering in binder jetting additive manufacturing of metals. *J. Manuf. Sci. Eng.* **2017**, *139*, 081019. [CrossRef]
52. Popovich, A.; Sufiiarov, V. Metal powder additive manufacturing. In New Trends in 3D Printing. IntechOpen: London, UK, 2016. Available online: https://books.google.com/books?hl=en&lr=&id=fm-QDwAAQBAJ&oi=fnd&pg=PA215&dq=3D+printing+powder+shape+metals&ots=xzgQvpzo1X&sig=zi9hFurVgnILcUYm2IvY0l71UM4 (accessed on 31 May 2024).
53. Spierings, A.B.; Voegtlin, M.; Bauer, T.; Wegener, K. Powder flowability characterisation methodology for powder-bed-based metal additive manufacturing. *Prog. Addit. Manuf.* **2016**, *1*, 9–20. [CrossRef]
54. Vock, S.; Klöden, B.; Kirchner, A.; Weißgärber, T.; Kieback, B. Powders for powder bed fusion: A review. *Prog. Addit. Manuf.* **2019**, *4*, 383–397. [CrossRef]
55. Sutton, A.T.; Kriewall, C.S.; Leu, M.-C.; Newkirk, J.W. Powders for additive manufacturing processes: Characterization techniques and effects on part properties. In Proceedings of the 26th Annual International Solid Freeform Fabrication Symposium—An Additive Manufacturing Conference, Austin, TX, USA, 8–10 August 2016. Available online: https://scholarsmine.mst.edu/mec_aereng_facwork/3694/ (accessed on 31 May 2024).
56. Tan, X.P.; Tan, Y.J.; Chow, C.S.L.; Tor, S.B.; Yeong, W.Y. Metallic powder-bed based 3D printing of cellular scaffolds for orthopaedic implants: A state-of-the-art review on manufacturing, topological design, mechanical properties and biocompatibility. *Mater. Sci. Eng. C* **2017**, *76*, 1328–1343. [CrossRef] [PubMed]
57. Deng, P.; Karadge, M.; Rebak, R.B.; Gupta, V.K.; Prorok, B.C.; Lou, X. The origin and formation of oxygen inclusions in austenitic stainless steels manufactured by laser powder bed fusion. *Addit. Manuf.* **2020**, *35*, 101334. [CrossRef]
58. Brandão, A.D.; Gerard, R.; Gumpinger, J.; Beretta, S.; Makaya, A.; Pambaguian, L.; Ghidini, T. Challenges in additive manufacturing of space parts: Powder feedstock cross-contamination and its impact on end products. *Materials* **2017**, *10*, 522. [CrossRef]
59. Vluttert, N. The Absorption of Moisture by Metal Powder in a Humid Environment and the Effects on Its Composition. Bachelor's Thesis, University of Twente, Enschede, The Netherlands, 2016. Available online: http://essay.utwente.nl/71620/ (accessed on 3 July 2024).

60. Mukherjee, T.; Elmer, J.W.; Wei, H.L.; Lienert, T.J.; Zhang, W.; Kou, S.; DebRoy, T. Control of grain structure, phases, and defects in additive manufacturing of high-performance metallic components. *Prog. Mater. Sci.* **2023**, *138*, 101153. [CrossRef]
61. Qu, M.; Guo, Q.; Escano, L.I.; Nabaa, A.; Hojjatzadeh, S.M.H.; Young, Z.A.; Chen, L. Controlling process instability for defect lean metal additive manufacturing. *Nat. Commun.* **2022**, *13*, 1079. [CrossRef] [PubMed]
62. Lanzutti, A.; Sordetti, F.; Montanari, R.; Varone, A.; Marin, E.; Andreatta, F.; Maschio, S.; Furlani, E.; Magnan, M.; Vaglio, E. Effect of powder recycling on inclusion content and distribution in AISI 316L produced by L-PBF technique. *J. Mater. Res. Technol.* **2023**, *23*, 3638–3650. [CrossRef]
63. Soltani-Tehrani, A.; Isaac, J.P.; Tippur, H.V.; Silva, D.F.; Shao, S.; Shamsaei, N. Ti-6Al-4V powder reuse in laser powder bed fusion (L-PBF): The effect on porosity, microstructure, and mechanical behavior. *Int. J. Fatigue* **2023**, *167*, 107343. [CrossRef]
64. Ghods, S.; Schur, R.; Schultz, E.; Pahuja, R.; Montelione, A.; Wisdom, C.; Arola, D.; Ramulu, M. Powder reuse and its contribution to porosity in additive manufacturing of Ti6Al4V. *Materialia* **2021**, *15*, 100992. [CrossRef]
65. Chen, G.; Zhao, S.Y.; Tan, P.; Wang, J.; Xiang, C.S.; Tang, H.P. A comparative study of Ti-6Al-4V powders for additive manufacturing by gas atomization, plasma rotating electrode process and plasma atomization. *Powder Technol.* **2018**, *333*, 38–46. [CrossRef]
66. Denti, L.; Sola, A.; Defanti, S.; Sciancalepore, C.; Bondioli, F. Effect of powder recycling in laser-based powder bed fusion of Ti-6Al-4V. *Manuf. Technol.* **2019**, *19*, 190–196. [CrossRef]
67. Gruber, K.; Smolina, I.; Kasprowicz, M.; Kurzynowski, T. Evaluation of Inconel 718 Metallic Powder to Optimize the Reuse of Powder and to Improve the Performance and Sustainability of the Laser Powder Bed Fusion (LPBF) Process. *Materials* **2021**, *14*, 1538. [CrossRef]
68. Zhang, P.; Jiang, M.; Luan, B. Influence of Inconel 625 alloy powder reusing on feedstock characteristics and mechanical properties of deposited parts. *J. Mater. Res. Technol.* **2024**, *29*, 3782–3794. [CrossRef]
69. Rock, C.; Ledford, C.; Garcia-Avila, M.; West, H. The Influence of Powder Reuse on the Properties of Nickel Super Alloy ATI 718^{TM} in Laser Powder Bed Fusion Additive Manufacturing. *Metall. Mater. Trans. B* **2021**, *52*, 676–688. [CrossRef]
70. Radchenko, O.K.; Gogaev, K.O. Requirements for Metal and Alloy Powders for 3D Printing (Review). *Powder Metall. Met. Ceram.* **2022**, *61*, 135–154. [CrossRef]
71. Chen, H.; Wei, Q.; Zhang, Y.; Chen, F.; Shi, Y.; Yan, W. Powder-spreading mechanisms in powder-bed-based additive manufacturing: Experiments and computational modeling. *Acta Mater.* **2019**, *179*, 158–171. [CrossRef]
72. Ji, L.; Wang, C.; Wu, W.; Tan, C.; Wang, G.; Duan, X.-M. Spheroidization by Plasma Processing and Characterization of Stainless Steel Powder for 3D Printing. *Powder Metall. Met. Ceram.* **2017**, *48*, 4831–4841. [CrossRef]
73. Powell, D.; Rennie, A.E.; Geekie, L.; Burns, N. Understanding powder degradation in metal additive manufacturing to allow the upcycling of recycled powders. *J. Clean. Prod.* **2020**, *268*, 122077. [CrossRef]
74. de Mattos Nascimento, D.L.; Mury Nepomuceno, R.; Caiado, R.G.G.; Maqueira, J.M.; Moyano-Fuentes, J.; Garza-Reyes, J.A. A sustainable circular 3D printing model for recycling metal scrap in the automotive industry. *J. Manuf. Technol. Manag.* **2022**, *33*, 876–892. [CrossRef]
75. Khosravani, M.R.; Reinicke, T. On the environmental impacts of 3D printing technology. *Appl. Mater. Today* **2020**, *20*, 100689. [CrossRef]
76. Duda, T.; Raghavan, L.V. 3D metal printing technology: The need to re-invent design practice. *AI Soc.* **2018**, *33*, 241–252. [CrossRef]
77. Duda, T.; Raghavan, L.V. 3D metal printing technology. *IFAC-Pap.* **2016**, *49*, 103–110. [CrossRef]
78. Atzeni, E.; Salmi, A. Economics of additive manufacturing for end-usable metal parts. *Int. J. Adv. Manuf. Technol.* **2012**, *62*, 1147–1155. [CrossRef]
79. Jiménez, M.; Romero, L.; Domínguez, I.A.; Espinosa, M.D.M.; Domínguez, M. Additive Manufacturing Technologies: An Overview about 3D Printing Methods and Future Prospects. *Complexity* **2019**, *2019*, 1–30. [CrossRef]
80. Embia, G.; Moharana, B.R.; Mohamed, A.; Muduli, K.; Muhammad, N.B. 3D Printing Pathways for Sustainable Manufacturing. In *New Horizons for Industry 4.0 in Modern Business*; Nayyar, A., Naved, M., Rameshwar, R., Eds.; Contributions to Environmental Sciences & Innovative Business Technology; Springer International Publishing: Cham, Switzerland, 2023; pp. 253–272, ISBN 978-3-031-20442-5. Available online: https://link.springer.com/10.1007/978-3-031-20443-2_12 (accessed on 5 July 2024).
81. Nguyen, H.D.; Pramanik, A.; Basak, A.K.; Dong, Y.; Prakash, C.; Debnath, S.; Shankar, S.; Jawahir, I.S.; Dixit, S.; Buddhi, D. A critical review on additive manufacturing of Ti-6Al-4V alloy: Microstructure and mechanical properties. *J. Mater. Res. Technol.* **2022**, *18*, 4641–4661. [CrossRef]
82. Carrozza, A.; Aversa, A.; Fino, P.; Lombardi, M. A study on the microstructure and mechanical properties of the Ti-6Al-2Sn-4Zr-6Mo alloy produced via Laser Powder Bed Fusion. *J. Alloys Compd.* **2021**, *870*, 159329. [CrossRef]
83. Gao, P.; Wei, K.; Yu, H.; Yang, J.; Wang, Z.; Zeng, X. Influence of layer thickness on microstructure and mechanical properties of selective laser melted Ti-5Al-2.5 Sn alloy. *Acta Metall. Sin.* **2018**, *54*, 999–1009.
84. Wu, A.S.; Brown, D.W.; Kumar, M.; Gallegos, G.F.; King, W.E. An Experimental Investigation into Additive Manufacturing-Induced Residual Stresses in 316L Stainless Steel. *Metall. Mater. Trans. A* **2014**, *45*, 6260–6270. [CrossRef]
85. Gonzalez-Gutierrez, J.; Arbeiter, F.; Schlauf, T.; Kukla, C.; Holzer, C. Tensile properties of sintered 17-4PH stainless steel fabricated by material extrusion additive manufacturing. *Mater. Lett.* **2019**, *248*, 165–168. [CrossRef]

86. Wang, Z.; Palmer, T.A.; Beese, A.M. Effect of processing parameters on microstructure and tensile properties of austenitic stainless steel 304L made by directed energy deposition additive manufacturing. *Acta Mater.* **2016**, *110*, 226–235. [CrossRef]
87. Nong, X.D.; Zhou, X.L.; Wang, Y.D.; Yu, L.; Li, J.H. Effects of geometry, location, and direction on microstructure and mechanical properties of 15–5PH stainless steel fabricated by directed energy deposition. *Mater. Sci. Eng. A* **2021**, *821*, 141587. [CrossRef]
88. Zhu, B.; Lin, J.; Lei, Y.; Zhang, Y.; Sun, Q.; Cheng, S. Additively manufactured δ-ferrite-free 410 stainless steel with desirable performance. *Mater. Lett.* **2021**, *293*, 129579. [CrossRef]
89. Rosenthal, I.; Stern, A.; Frage, N. Microstructure and Mechanical Properties of AlSi10Mg Parts Produced by the Laser Beam Additive Manufacturing (AM) Technology. *Metallogr. Microstruct. Anal.* **2014**, *3*, 448–453. [CrossRef]
90. Roberts, C.E.; Bourell, D.; Watt, T.; Cohen, J. A novel processing approach for additive manufacturing of commercial aluminum alloys. *Phys. Procedia* **2016**, *83*, 909–917. [CrossRef]
91. Rashid, R.; Masood, S.H.; Ruan, D.; Palanisamy, S.; Rashid, R.R.; Elambasseril, J.; Brandt, M. Effect of energy per layer on the anisotropy of selective laser melted AlSi12 aluminium alloy. *Addit. Manuf.* **2018**, *22*, 426–439. [CrossRef]
92. Muñiz-Lerma, J.A.; Nommeots-Nomm, A.; Waters, K.E.; Brochu, M. A comprehensive approach to powder feedstock characterization for powder bed fusion additive manufacturing: A case study on AlSi7Mg. *Materials* **2018**, *11*, 2386. [CrossRef] [PubMed]
93. Jia, Q.; Gu, D. Selective laser melting additive manufacturing of Inconel 718 superalloy parts: Densification, microstructure and properties. *J. Alloys Compd.* **2014**, *585*, 713–721. [CrossRef]
94. Karmuhilan, M.; Kumanan, S. A Review on Additive Manufacturing Processes of Inconel 625. *J. Mater. Eng. Perform.* **2022**, *31*, 2583–2592. [CrossRef]
95. Han, Q.; Gu, Y.; Setchi, R.; Lacan, F.; Johnston, R.; Evans, S.L.; Yang, S. Additive manufacturing of high-strength crack-free Ni-based Hastelloy X superalloy. *Addit. Manuf.* **2019**, *30*, 100919. [CrossRef]
96. Kannan, A.R.; Kumar, S.M.; Pramod, R.; Shanmugam, N.S.; Vishnukumar, M.; Channabasavanna, S.G. Microstructure and corrosion resistance of Ni-Cu alloy fabricated through wire arc additive manufacturing. *Mater. Lett.* **2022**, *308*, 131262. [CrossRef]
97. Atabay, S.E.; Sanchez-Mata, O.; Muñiz-Lerma, J.A.; Gauvin, R.; Brochu, M. Microstructure and mechanical properties of rene 41 alloy manufactured by laser powder bed fusion. *Mater. Sci. Eng. A* **2020**, *773*, 138849. [CrossRef]
98. Mordas, G.; Jasulaitienė, V.; Steponavičiūtė, A.; Gaspariūnas, M.; Petkevič, R.; Selskienė, A.; Juškėnas, R.; Paul, D.F.; Mann, J.E.; Remeikis, V.; et al. Characterisation of CoCrMo powder for additive manufacturing. *Int. J. Adv. Manuf. Technol.* **2020**, *111*, 3083–3093. [CrossRef]
99. Miyake, M.; Matsuda, T.; Sano, T.; Hirose, A.; Shiomi, Y.; Sasaki, M. Microstructure and mechanical properties of additively manufactured CoCrW alloy using laser metal deposition. *Weld. World* **2020**, *64*, 1397–1407. [CrossRef]
100. Liu, R.; Dang, X.; Peng, Y.; Wu, T. Microstructure and Wear Behavior of Laser Cladded CoCrNiMox Coatings on the Low Carbon Steel. *Crystals* **2022**, *12*, 1229. [CrossRef]
101. Huo, J.; Zhang, G. New process for integrated manufacturing of copper alloy shells by bimetal 3D printing remanufacturing technology. *Energy Rep.* **2022**, *8*, 11052–11063. [CrossRef]
102. Tran, T.Q.; Chinnappan, A.; Lee, J.K.Y.; Loc, N.H.; Tran, L.T.; Wang, G.; Kumar, V.V.; Jayathilaka, W.; Ji, D.; Doddamani, M. 3D printing of highly pure copper. *Metals* **2019**, *9*, 756. [CrossRef]
103. El-Wardany, T.; She, Y.; Jagdale, V.; Garofano, J.K.; Liou, J.; Schmidt, W. Challenges in 3D printing of high conductivity copper. In Proceedings of the International Electronic Packaging Technical Conference and Exhibition, San Francisco, CA, USA, 29 August–1 September 2017; p. V001T01A005. Available online: https://asmedigitalcollection.asme.org/InterPACK/proceedings-abstract/InterPACK2017/58097/266256 (accessed on 2 July 2024).
104. Constantin, L.; Wu, Z.; Li, N.; Fan, L.; Silvain, J.-F.; Lu, Y.F. Laser 3D printing of complex copper structures. *Addit. Manuf.* **2020**, *35*, 101268. [CrossRef]
105. Thijs, L.; Verhaeghe, F.; Craeghs, T.; Van Humbeeck, J.; Kruth, J.-P. A study of the microstructural evolution during selective laser melting of Ti–6Al–4V. *Acta Mater.* **2010**, *58*, 3303–3312. [CrossRef]
106. Vrancken, B.; Thijs, L.; Kruth, J.-P.; Van Humbeeck, J. Heat treatment of Ti6Al4V produced by Selective Laser Melting: Microstructure and mechanical properties. *J. Alloys Compd.* **2012**, *541*, 177–185. [CrossRef]
107. He, B.; Wu, W.; Zhang, L.; Lu, L.; Yang, Q.; Long, Q.; Chang, K. Microstructural characteristic and mechanical property of Ti6Al4V alloy fabricated by selective laser melting. *Vacuum* **2018**, *150*, 79–83. [CrossRef]
108. Singla, A.K.; Banerjee, M.; Sharma, A.; Singh, J.; Bansal, A.; Gupta, M.K.; Khanna, N.; Shahi, A.S.; Goyal, D.K. Selective laser melting of Ti6Al4V alloy: Process parameters, defects and post-treatments. *J. Manuf. Process.* **2021**, *64*, 161–187. [CrossRef]
109. Kolamroudi, M.K.; Asmael, M.; Ilkan, M.; Kordani, N. Developments on Electron Beam Melting (EBM) of Ti–6Al–4V: A Review. *Trans. Indian Inst. Met.* **2021**, *74*, 783–790. [CrossRef]
110. Tamayo, J.A.; Riascos, M.; Vargas, C.A.; Baena, L.M. Additive manufacturing of Ti6Al4V alloy via electron beam melting for the development of implants for the biomedical industry. *Heliyon* **2021**, *7*, e06892. [CrossRef]
111. Ran, J.; Jiang, F.; Sun, X.; Chen, Z.; Tian, C.; Zhao, H. Microstructure and mechanical properties of Ti-6Al-4V fabricated by electron beam melting. *Crystals* **2020**, *10*, 972. [CrossRef]
112. Silvestri, A.T.; Foglia, S.; Borrelli, R.; Franchitti, S.; Pirozzi, C.; Astarita, A. Electron beam melting of Ti6Al4V: Role of the process parameters under the same energy density. *J. Manuf. Process.* **2020**, *60*, 162–179. [CrossRef]

113. Shrestha, S.; Panakarajupally, R.P.; Kannan, M.; Morscher, G.; Gyekenyesi, A.L.; Scott-Emuakpor, O.E. Analysis of microstructure and mechanical properties of additive repaired Ti–6Al–4V by Direct Energy Deposition. *Mater. Sci. Eng. A* **2021**, *806*, 140604. [CrossRef]
114. Lee, Y.; Kim, E.S.; Park, S.; Park, J.M.; Seol, J.B.; Kim, H.S.; Lee, T.; Sung, H.; Kim, J.G. Effects of Laser Power on the Microstructure Evolution and Mechanical Properties of Ti–6Al–4V Alloy Manufactured by Direct Energy Deposition. *Met. Mater. Int.* **2022**, *28*, 197–204. [CrossRef]
115. Gorunov, A.I. Additive manufacturing of Ti6Al4V parts using ultrasonic assisted direct energy deposition. *J. Manuf. Process.* **2020**, *59*, 545–556. [CrossRef]
116. Stevens, E.; Schloder, S.; Bono, E.; Schmidt, D.; Chmielus, M. Density variation in binder jetting 3D-printed and sintered Ti-6Al-4V. *Addit. Manuf.* **2018**, *22*, 746–752. [CrossRef]
117. Simchi, A.; Petzoldt, F.; Hartwig, T.; Hein, S.B.; Barthel, B.; Reineke, L. Microstructural development during additive manufacturing of biomedical grade Ti-6Al-4V alloy by three-dimensional binder jetting: Material aspects and mechanical properties. *Int. J. Adv. Manuf. Technol.* **2023**, *127*, 1541–1558. [CrossRef]
118. Yadav, P.; Fu, Z.; Knorr, M.; Travitzky, N. Binder Jetting 3D Printing of Titanium Aluminides Based Materials: A Feasibility Study. *Adv. Eng. Mater.* **2020**, *22*, 2000408. [CrossRef]
119. Janzen, K.; Kallies, K.J. Fabrication of patient-specific finger joint implants from Ti-6Al-4V using metal binder jetting. *Trans. Addit. Manuf. Meets Med.* **2023**, *5*, 830.
120. Fan, H.; Yang, S. Effects of direct aging on near-alpha Ti–6Al–2Sn–4Zr–2Mo (Ti-6242) titanium alloy fabricated by selective laser melting (SLM). *Mater. Sci. Eng. A* **2020**, *788*, 139533. [CrossRef]
121. Fan, H.; Liu, Y.; Yang, S. Martensite decomposition during post-heat treatments and the aging response of near-α Ti–6Al–2Sn–4Zr–2Mo (Ti-6242) titanium alloy processed by selective laser melting (SLM). *J. Micromech. Mol. Phys.* **2021**, *06*, 2050018. [CrossRef]
122. Roshani, M.; Abedi, H.R.; Saboori, A. Comparing the Cold, Warm, and Hot Deformation Flow Behavior of Selective Laser-Melted and Electron-Beam-Melted Ti–6Al–2Sn–4Zr–2Mo Alloy. *Adv. Eng. Mater.* **2024**, *26*, 2301046. [CrossRef]
123. Chamanfar, A.; Pasang, T.; Ventura, A.; Misiolek, W.Z. Mechanical properties and microstructure of laser welded Ti–6Al–2Sn–4Zr–2Mo (Ti6242) titanium alloy. *Mater. Sci. Eng. A* **2016**, *663*, 213–224. [CrossRef]
124. Galati, M.; Defanti, S.; Saboori, A.; Rizza, G.; Tognoli, E.; Vincenzi, N.; Gatto, A.; Iuliano, L. An investigation on the processing conditions of Ti-6Al-2Sn-4Zr-2Mo by electron beam powder bed fusion: Microstructure, defect distribution, mechanical properties and dimensional accuracy. *Addit. Manuf.* **2022**, *50*, 102564. [CrossRef]
125. Galati, M.; Giordano, M.; Saboori, A.; Defanti, S. Electron beam powder bed fusion of Ti-6Al-2Sn-4Zr-2Mo lattice structures: Morphometrical and mechanical characterisations. *Int. J. Adv. Manuf. Technol.* **2024**, *131*, 1223–1239. [CrossRef]
126. Lopez, M.; Pickett, C.; Arrieta, E.; Murr, L.E.; Wicker, R.B.; Ahlfors, M.; Godfrey, D.; Medina, F. Effects of postprocess hot isostatic pressing treatments on the mechanical performance of EBM fabricated TI-6Al-2Sn-4Zr-2Mo. *Materials* **2020**, *13*, 2604. [CrossRef]
127. Carrozza, A.; Aversa, A.; Fino, P.; Lombardi, M. Towards customized heat treatments and mechanical properties in the LPBF-processed Ti-6Al-2Sn-4Zr-6Mo alloy. *Mater. Des.* **2022**, *215*, 110512. [CrossRef]
128. Hassanin, H.; Zweiri, Y.; Finet, L.; Essa, K.; Qiu, C.; Attallah, M. Laser powder bed fusion of Ti-6Al-2Sn-4Zr-6Mo alloy and properties prediction using deep learning approaches. *Materials* **2021**, *14*, 2056. [CrossRef] [PubMed]
129. Peng, H.; Wu, S.; Kan, W.H.; Lim, S.C.V.; Zhu, Y.; Huang, A. Rapid hardening response of ultra-hard Ti-6Al-2Sn-4Zr-6Mo alloy produced by laser powder bed fusion. *Scr. Mater.* **2023**, *226*, 115209. [CrossRef]
130. Wei, K.; Wang, Z.; Zeng, X. Preliminary investigation on selective laser melting of Ti-5Al-2.5 Sn α-Ti alloy: From single tracks to bulk 3D components. *J. Mater. Process. Technol.* **2017**, *244*, 73–85. [CrossRef]
131. Wei, K.; Wang, Z.; Zeng, X. Effect of heat treatment on microstructure and mechanical properties of the selective laser melting processed Ti-5Al-2.5 Sn α titanium alloy. *Mater. Sci. Eng. A* **2018**, *709*, 301–311. [CrossRef]
132. Wei, K.; Lv, M.; Zeng, X.; Xiao, Z.; Huang, G.; Liu, M.; Deng, J. Effect of laser remelting on deposition quality, residual stress, microstructure, and mechanical property of selective laser melting processed Ti-5Al-2.5 Sn alloy. *Mater. Charact.* **2019**, *150*, 67–77. [CrossRef]
133. Wei, K.; Wang, Z.; Li, F.; Zhang, H.; Zeng, X. Densification behavior, microstructure evolution, and mechanical performances of selective laser melted Ti-5Al-2.5 Sn α titanium alloy: Effect of laser energy input. *J. Alloys Compd.* **2019**, *774*, 1024–1035. [CrossRef]
134. Zhang, G.; Xiong, H.; Yu, H.; Qin, R.; Liu, W.; Yuan, H. Microstructure evolution and mechanical properties of wire-feed electron beam additive manufactured Ti-5Al-2Sn-2Zr-4Mo-4Cr alloy with different subtransus heat treatments. *Mater. Des.* **2020**, *195*, 109063. [CrossRef]
135. Popovski, M.; Qiu, D.; Easton, M.; Barter, S.; Liu, Q.; Das, R. Additively manufactured pearlitic titanium-copper alloys: The effect of copper concentration on the microstructure and hardness. In Proceedings of the AIAC 2023: 20th Australian International Aerospace Congress: 20th Australian International Aerospace Congress, Melbourne, Australia, 27 February–2 March 2023; pp. 133–139. Available online: https://search.informit.org/doi/abs/10.3316/informit.063527078236645 (accessed on 14 June 2024).
136. Brooke, R.; Zhang, D.; Qiu, D.; Gibson, M.A.; Mayes, E.; Moravek, T.; Shankar, N.B.; Chandran, N.; Banerjee, R.; Easton, M. Novel bainitic Ti alloys designed for Additive manufacturing. *Mater. Des.* **2024**, *244*, 113176. [CrossRef]

137. Zhang, D.; Qiu, D.; Gibson, M.A.; Zheng, Y.; Fraser, H.L.; StJohn, D.H.; Easton, M.A. Additive manufacturing of ultrafine-grained high-strength titanium alloys. *Nature* **2019**, *576*, 91–95. [CrossRef]
138. Kang, N.; Lin, X.; Coddet, C.; Wen, X.; Huang, W. Selective laser melting of low modulus Ti-Mo alloy: α/β heterogeneous conchoidal structure. *Mater. Lett.* **2020**, *267*, 127544. [CrossRef]
139. Chen, J.; Liao, X.; Shu, J.; Zhou, L.; Li, C.; Ren, Y.; Niu, Y. Microstructure tailoring of Ti–15Mo alloy fabricated by selective laser melting with high strength and ductility. *Mater. Sci. Eng. A* **2021**, *826*, 141962. [CrossRef]
140. Xu, H.; Li, Z.; Dong, A.; Xing, H.; Zhang, T.; Wang, D.; Zhu, G.; Sun, B. Study of superior strength in Ti15Mo alloy manufactured using selective laser melting. *J. Alloys Compd.* **2021**, *885*, 161186. [CrossRef]
141. Yao, K.; Min, X.; Shi, S.; Tan, Y. Volatilization behavior of β-type Ti-Mo alloy manufactured by electron beam melting. *Metals* **2018**, *8*, 206. [CrossRef]
142. Duport, M.; Lhuisser, P.; Blandin, J.-J.; Dendievel, R.; Veron, M.; Prima, F.; Martin, G. Processing, microstructures and mechanical response of a β-metastable Ti-14Mo alloy fabricated by Electron Beam Powder Bed Fusion. *Addit. Manuf.* **2023**, *61*, 103340. [CrossRef]
143. Bhardwaj, T.; Shukla, M.; Paul, C.P.; Bindra, K.S. Direct energy deposition-laser additive manufacturing of titanium-molybdenum alloy: Parametric studies, microstructure and mechanical properties. *J. Alloys Compd.* **2019**, *787*, 1238–1248. [CrossRef]
144. Kang, N.; Wu, K.; Kang, J.; Li, J.; Lin, X.; Huang, W. Effect of cycling heat treatment on the microstructure, phase, and compression behaviour of directed energy deposited Ti-Mo alloys. *Light Adv. Manuf.* **2021**, *2*, 136. [CrossRef]
145. Tan, H.; Hu, T.; Zhang, F.; Qiu, Y.; Clare, A.T. Direct Metal Deposition of Satellited Ti-15Mo: Microstructure and Mechanical Properties. *Adv. Eng. Mater.* **2019**, *21*, 1900152. [CrossRef]
146. Yu, J. Establishing Novel Titanium-Based Candidate Materials for Selective Laser Melting. Ph.D. Thesis, University of Miami, Miami, FL, USA, 2020. Available online: https://scholarship.miami.edu/view/pdfCoverPage?instCode=01UOML_INST&filePid=13372067130002976&download=true (accessed on 25 July 2024).
147. Zhang, K.; Kan, W.H.; Zhu, Y.; Lim, S.C.V.; Gao, X.; Sit, C.K.; Bai, C.; Huang, A. Achieving ultra-high strength rapidly in Ti-3Al-8V-6Cr-4Mo-4Zr alloy processed by directed energy deposition. *Mater. Des.* **2022**, *224*, 111325. [CrossRef]
148. Carlton, H.D.; Klein, K.D.; Elmer, J.W. Evolution of microstructure and mechanical properties of selective laser melted Ti-5Al-5V-5Mo-3Cr after heat treatments. *Sci. Technol. Weld. Join.* **2019**, *24*, 465–473. [CrossRef]
149. Yuan, W.; Zhao, X.; Li, S.; Zhu, Y. Effect of laser scanning speed on microstructure and mechanical properties of SLM porous Ti-5Al-5V-5Mo-3Cr-1Fe alloy. *Front. Mater.* **2022**, *9*, 973829. [CrossRef]
150. Lee, C.H.; Kühn, U.; Lee, S.C.; Park, S.J.; Schwab, H.; Scudino, S.; Kosiba, K. Optimizing laser powder bed fusion of Ti-5Al-5V-5Mo-3Cr by artificial intelligence. *J. Alloys Compd.* **2021**, *862*, 158018.
151. Chlebus, E.; Kuźnicka, B.; Kurzynowski, T.; Dybała, B. Microstructure and mechanical behaviour of Ti—6Al—7Nb alloy produced by selective laser melting. *Mater. Charact.* **2011**, *62*, 488–495. [CrossRef]
152. Sercombe, T.; Jones, N.; Day, R.; Kop, A. Heat treatment of Ti-6Al-7Nb components produced by selective laser melting. *Rapid Prototyp. J.* **2008**, *14*, 300–304. [CrossRef]
153. Pawlak, A.; Szymczyk, P.; Ziolkowski, G.; Chlebus, E.; Dybala, B. Fabrication of microscaffolds from Ti-6Al-7Nb alloy by SLM. *Rapid Prototyp. J.* **2015**, *21*, 393–401. [CrossRef]
154. Marcu, T.; Todea, M.; Gligor, I.; Berce, P.; Popa, C. Effect of surface conditioning on the flowability of Ti6Al7Nb powder for selective laser melting applications. *Appl. Surf. Sci.* **2012**, *258*, 3276–3282. [CrossRef]
155. Macias-Sifuentes, M.A.; Xu, C.; Sanchez-Mata, O.; Kwon, S.Y.; Atabay, S.E.; Muñiz-Lerma, J.A.; Brochu, M. Microstructure and mechanical properties of β-21S Ti alloy fabricated through laser powder bed fusion. *Prog. Addit. Manuf.* **2021**, *6*, 417–430. [CrossRef]
156. Akmal, M.; Jeong, W.; Ryu, H.J. Ti-Zr-Nb based BCC alloy containing Mo prepared by laser directed energy deposition—Ømega phase and cellular structure. *J. Alloys Compd.* **2023**, *969*, 172306. [CrossRef]
157. Rudolph, S.M. Near-Beta Titanium Alloys Produced Using Laser Powder-Bed Fusion. Master's Thesis, Stellenbosch University, Stellenbosch, South Africa, 2023. Available online: https://scholar.sun.ac.za/bitstream/10019.1/126995/1/rudolph_nearbeta_2023.pdf (accessed on 25 July 2024).
158. Wei, K.; Zeng, X.; Huang, G.; Deng, J.; Liu, M. Selective laser melting of Ti-5Al-2.5 Sn alloy with isotropic tensile properties: The combined effect of densification state, microstructural morphology, and crystallographic orientation characteristics. *J. Mater. Process. Technol.* **2019**, *271*, 368–376. [CrossRef]
159. Chen, Z.; Liu, Y.; Wu, H.; Zhang, W.; Guo, W.; Tang, H.; Liu, N. Microstructures and wear properties of surface treated Ti–36Nb–2Ta–3Zr–0.35 O alloy by electron beam melting (EBM). *Appl. Surf. Sci.* **2015**, *357*, 2347–2354. [CrossRef]
160. Surmeneva, M.; Grubova, I.; Glukhova, N.; Khrapov, D.; Koptyug, A.; Volkova, A.; Ivanov, Y.; Cotrut, C.M.; Vladescu, A.; Teresov, A. New Ti–35Nb–7Zr–5Ta alloy manufacturing by electron beam melting for medical application followed by high current pulsed electron beam treatment. *Metals* **2021**, *11*, 1066. [CrossRef]
161. Narayana, P.L.; Kim, J.H.; Hong, J.-K. Microstructural evolution and tensile properties of direct energy deposited Ti-4Al-5Co-0.25 Si alloy during heat treatment. *J. Alloys Compd.* **2024**, *993*, 174657. [CrossRef]
162. Attar, H.; Calin, M.; Zhang, L.C.; Scudino, S.; Eckert, J. Manufacture by selective laser melting and mechanical behavior of commercially pure titanium. *Mater. Sci. Eng. A* **2014**, *593*, 170–177. [CrossRef]

163. Attar, H.; Ehtemam-Haghighi, S.; Kent, D.; Wu, X.; Dargusch, M.S. Comparative study of commercially pure titanium produced by laser engineered net shaping, selective laser melting and casting processes. *Mater. Sci. Eng. A* **2017**, *705*, 385–393. [CrossRef]
164. Santos, E.C.; Osakada, K.; Shiomi, M.; Kitamura, Y.; Abe, F. Microstructure and mechanical properties of pure titanium models fabricated by selective laser melting. *Proc. Inst. Mech. Eng. Part C J. Mech. Eng. Sci.* **2004**, *218*, 711–719. [CrossRef]
165. Li, X.P.; Van Humbeeck, J.; Kruth, J.P. Selective laser melting of weak-textured commercially pure titanium with high strength and ductility: A study from laser power perspective. *Mater. Des.* **2017**, *116*, 352–358. [CrossRef]
166. Yamanaka, K.; Saito, W.; Mori, M.; Matsumoto, H.; Chiba, A. Preparation of weak-textured commercially pure titanium by electron beam melting. *Addit. Manuf.* **2015**, *8*, 105–109. [CrossRef]
167. Park, H.K.; Ahn, Y.K.; Lee, B.S.; Jung, K.H.; Lee, C.W.; Kim, H.G. Refining effect of electron beam melting on additive manufacturing of pure titanium products. *Mater. Lett.* **2017**, *187*, 98–100. [CrossRef]
168. Yamanaka, K.; Saito, W.; Mori, M.; Matsumoto, H.; Sato, S.; Chiba, A. Abnormal grain growth in commercially pure titanium during additive manufacturing with electron beam melting. *Materialia* **2019**, *6*, 100281. [CrossRef]
169. Gushchina, M.O.; Kuzminova, Y.O.; Dubinin, O.N.; Evlashin, S.A.; Vildanov, A.M.; Klimova-Korsmik, O.G.; Turichin, G.A. Multilayer composite Ti-6Al-4 V/Cp-Ti alloy produced by laser direct energy deposition. *Int. J. Adv. Manuf. Technol.* **2023**, *124*, 907–918. [CrossRef]
170. Barro, O.; Arias-González, F.; Lusquiños, F.; Comesaña, R.; del Val, J.; Riveiro, A.; Badaoui, A.; Gómez-Baño, F.; Pou, J. Improved commercially pure titanium obtained by laser directed energy deposition for dental prosthetic applications. *Metals* **2020**, *11*, 70. [CrossRef]
171. Wheat, E. Process Mapping and Optimization of Titanium Parts Made by Binder Jetting Additive Manufacturing. Master's Thesis, University of Waterloo, Waterloo, ON, Canada, 2018.
172. Wheat, E.; Vlasea, M.; Hinebaugh, J.; Metcalfe, C. Data related to the sinter structure analysis of titanium structures fabricated via binder jetting additive manufacturing. *Data Brief* **2018**, *20*, 1029–1038. [CrossRef]
173. Irgolič, T.; Potočnik, D.; Ficko, M.; Kirbiš, P. Microstructural characterization of laser cladded AISI 316 stainless steel on a carbon steel substrate. *Adv. Technol. Mater.* **2019**, *44*, 1–5. [CrossRef]
174. Rivolta, B.; Gerosa, R.; Crema, L.; Alberti, F. Characterization of Selective Laser Melting materials for micro co-generation solar plant components. In the Proceedings of DIGESPO 2013. Available online: https://www.researchgate.net/profile/Fabrizio-Alberti-2/publication/322315847_Characterization_of_Selective_Laser_Melting_materials_for_micro_co-generation_solar_plant_components/links/5a53a4130f7e9bbc1057003d/Characterization-of-Selective-Laser-Melting-materials-for-micro-co-generation-solar-plant-components.pdf (accessed on 25 July 2024).
175. Abolhasani, D.; Seyedkashi, S.M.H.; Hoseinpour Gollo, M.; Moon, Y.H. Effects of laser beam parameters on bendability and microstructure of stainless steel in three-dimensional laser forming. *Appl. Sci.* **2019**, *9*, 4463. [CrossRef]
176. Ritchie, M.; Lee, P.D.; Mitchell, A.; Cockcroft, S.L.; Wang, T. X-ray-based measurement of composition during electron beam melting of AISI 316 stainless steel: Part II. Evaporative processes and simulation. *Metall. Mater. Trans. A* **2003**, *34*, 863–877. [CrossRef]
177. Shamsaei, N.; Simsiriwong, J. Fatigue behaviour of additively-manufactured metallic parts. *Procedia Struct. Integr.* **2017**, *7*, 3–10. [CrossRef]
178. Krankenhagen, R. Thermographic Investigation of the Anisotropic Behaviour of Additively Manufactured AISI 316 Steel Using DED-arc. 2024. Available online: https://opus4.kobv.de/opus4-bam/frontdoor/index/index/docId/60574 (accessed on 25 July 2024).
179. Wang, C.; Tan, X.; Liu, E.; Tor, S.B. Process parameter optimization and mechanical properties for additively manufactured stainless steel 316L parts by selective electron beam melting. *Mater. Des.* **2018**, *147*, 157–166. [CrossRef]
180. Liu, Y.; Yang, Y.; Mai, S.; Wang, D.; Song, C. Investigation into spatter behavior during selective laser melting of AISI 316L stainless steel powder. *Mater. Des.* **2015**, *87*, 797–806. [CrossRef]
181. D'Andrea, D.; Risitano, G.; Guglielmino, E.; Piperopoulos, E.; Santonocito, D. Correlation between mechanical behaviour and microstructural features of AISI 316L produced by SLM. *Procedia Struct. Integr.* **2022**, *41*, 199–207. [CrossRef]
182. D'Andrea, D. Additive manufacturing of AISI 316L stainless steel: A review. *Metals* **2023**, *13*, 1370. [CrossRef]
183. Saboori, A.; Aversa, A.; Marchese, G.; Biamino, S.; Lombardi, M.; Fino, P. Microstructure and mechanical properties of AISI 316L produced by directed energy deposition-based additive manufacturing: A review. *Appl. Sci.* **2020**, *10*, 3310. [CrossRef]
184. Ostolaza, M.; Arrizubieta, J.I.; Lamikiz, A.; Cortina, M. Functionally graded AISI 316L and AISI H13 manufactured by L-DED for die and mould applications. *Appl. Sci.* **2021**, *11*, 771. [CrossRef]
185. Saboori, A.; Aversa, A.; Bosio, F.; Bassini, E.; Librera, E.; De Chirico, M.; Biamino, S.; Ugues, D.; Fino, P.; Lombardi, M. An investigation on the effect of powder recycling on the microstructure and mechanical properties of AISI 316L produced by Directed Energy Deposition. *Mater. Sci. Eng. A* **2019**, *766*, 138360. [CrossRef]
186. Aversa, A.; Marchese, G.; Bassini, E. Directed energy deposition of aisi 316l stainless steel powder: Effect of process parameters. *Metals* **2021**, *11*, 932. [CrossRef]
187. Atapour, M.; Wang, X.; Persson, M.; Wallinder, I.O.; Hedberg, Y.S. Corrosion of Binder Jetting Additively Manufactured 316L Stainless Steel of Different Surface Finish. *J. Electrochem. Soc.* **2020**, *167*, 131503. [CrossRef]
188. Zago, M.; Lecis, N.; Mariani, M.; Cristofolini, I. Analysis of the causes determining dimensional and geometrical errors in 316L and 17-4PH stainless steel parts fabricated by metal binder jetting. *Int. J. Adv. Manuf. Technol.* **2024**, *132*, 835–851. [CrossRef]

189. Mirzababaei, S.; Pasebani, S. A Review on Binder Jet Additive Manufacturing of 316L Stainless Steel. *J. Manuf. Mater. Process.* **2019**, *3*, 82. [CrossRef]
190. Pazzucconi, G. Properties of Binder Jetting 3D Printed 316L Stainless Steel. Master's Thesis, The Polytechnic University of Milan, Milan, Italy, 2021. Available online: https://www.politesi.polimi.it/handle/10589/177760 (accessed on 25 July 2024).
191. De Moura Filho, O.C.; Pacheco, J.T.; Veiga, M.T.; Teixeira, M.F.; Da Silva, L.J.; Da Costa, C.E.; Milan, J.C.G. Effect of Different Heat Treatment Routes on the Tribological Behavior of the Inconel 718 Alloy Deposited on Aisi 316 L by Laser Cladding. *Lasers Manuf. Mater. Process.* **2022**, *9*, 241–256. [CrossRef]
192. Castanheira, L.C.L. Production of Sustainable Powders for Direct Energy Deposition (DED). Master's Thesis, University of Porto, Porto, Portugal, 2022. Available online: https://repositorio-aberto.up.pt/bitstream/10216/145021/2/590264.pdf (accessed on 25 July 2024).
193. Castanheira, L.; Reis, A.; Vieira, M.; Emadinia, O. Microstructural evolution of a printed AISI 303 upcycled powder on a dissimilar substrate. *J. Mater. Res. Technol.* **2024**, *30*, 2291–2298. [CrossRef]
194. Castanheira, L.; Gil, J.; Amaral, R.; Vieira, T.; Reis, A.; Emadinia, O. Parametrization and characterization of DED printings using recycled AISI 303 powder particles. *Powder Technol.* **2024**, *435*, 119453. [CrossRef]
195. Pasebani, S.; Ghayoor, M.; Badwe, S.; Irrinki, H.; Atre, S.V. Effects of atomizing media and post processing on mechanical properties of 17-4 PH stainless steel manufactured via selective laser melting. *Addit. Manuf.* **2018**, *22*, 127–137. [CrossRef]
196. Vunnam, S.; Saboo, A.; Sudbrack, C.; Starr, T.L. Effect of powder chemical composition on the as-built microstructure of 17-4 PH stainless steel processed by selective laser melting. *Addit. Manuf.* **2019**, *30*, 100876. [CrossRef]
197. Hsu, T.-H.; Huang, P.-C.; Lee, M.-Y.; Chang, K.-C.; Lee, C.-C.; Li, M.-Y.; Chen, C.-P.; Jen, K.-K.; Yeh, A.-C. Effect of processing parameters on the fractions of martensite in 17-4 PH stainless steel fabricated by selective laser melting. *J. Alloys Compd.* **2021**, *859*, 157758. [CrossRef]
198. Merlin, M.; Morales, C.; Ferroni, M.; Fortini, A.; Soffritti, C. Influence of Heat Treatment Parameters on the Microstructure of 17-4 PH Single Tracks Fabricated by Direct Energy Deposition. *Appl. Sci.* **2024**, *14*, 700. [CrossRef]
199. Mathoho, I.; Akinlabi, E.T.; Arthur, N.; Tlotleng, M. Impact of DED process parameters on the metallurgical characteristics of 17-4 PH SS deposited using DED. *CIRP J. Manuf. Sci. Technol.* **2020**, *31*, 450–458. [CrossRef]
200. Forcellese, P. Investigation of Corrosion Resistance of 17-4 PH Stainless Steel Additive-Manufactured by Bound Metal Deposition and Binder Jetting. Ph.D. Thesis, Marche Polytechnic University, Ancona, Italy, 2024. Available online: https://iris.univpm.it/handle/11566/329794 (accessed on 25 July 2024).
201. Nezhadfar, P.D.; Verquin, B.; Lefebvre, F.; Reynaud, C.; Robert, M.; Shamsaei, N. Effect of Heat Treatment on the Tensile Behavior of 17-4 PH Stainless Steel Additively Manufactured by Metal Binder Jetting. In Proceedings of the 2021 International Solid Freeform Fabrication Symposium, Online, 2–4 August 2021. Available online: https://hdl.handle.net/2152/90692 (accessed on 25 July 2024).
202. Emanuelli, L.; Segata, G.; Perina, M.; Regolini, M.; Nicchiotti, V.; Molinari, A. Study of microstructure and mechanical properties of 17-4 PH stainless steel produced via Binder Jetting. *Powder Metall.* **2023**, *66*, 377–386. [CrossRef]
203. Abolhasani, D.; Seyedkashi, S.M.H.; Kang, N.; Kim, Y.J.; Woo, Y.Y.; Moon, Y.H. Analysis of Melt-Pool Behaviors during Selective Laser Melting of AISI 304 Stainless-Steel Composites. *Metals* **2019**, *9*, 876. [CrossRef]
204. Yu, H.; Yang, J.; Yin, J.; Wang, Z.; Zeng, X. Comparison on mechanical anisotropies of selective laser melted Ti-6Al-4V alloy and 304 stainless steel. *Mater. Sci. Eng. A* **2017**, *695*, 92–100. [CrossRef]
205. Miyata, Y.; Okugawa, M.; Koizumi, Y.; Nakano, T. Inverse Columnar-Equiaxed Transition (CET) in 304 and 316L Stainless Steels Melt by Electron Beam for Additive Manufacturing (AM). *Crystals* **2021**, *11*, 856. [CrossRef]
206. Hoosain, S.E.; Tshabalala, L.C.; Skhosana, S.; Freemantle, C.; Mndebele, N. Investigation of the properties of direct energy deposition additive manufactured 304 stainless steel. *S. Afr. J. Ind. Eng.* **2021**, *32*, 258–263. [CrossRef]
207. Shin, S.; Kwon, S.-M.; Kim, C.; Lee, J.; Hwang, J.; Kim, H. Optimization of Direct Energy Deposition of 304L Stainless Steel through Laser Process Parameters. *J. Weld. Join.* **2021**, *39*, 182–188. [CrossRef]
208. Pan, T.; Karnati, S.; Zhang, Y.; Zhang, X.; Hung, C.-H.; Li, L.; Liou, F. Experiment characterization and formulation estimation of tensile properties for selective laser melting manufactured 304L stainless steel. *Mater. Sci. Eng. A* **2020**, *798*, 140086. [CrossRef]
209. Zhu, Z.; Li, W.; Nguyen, Q.B.; An, X.; Lu, W.; Li, Z.; Ng, F.L.; Ling Nai, S.M.; Wei, J. Enhanced strength–ductility synergy and transformation-induced plasticity of the selective laser melting fabricated 304L stainless steel. *Addit. Manuf.* **2020**, *35*, 101300. [CrossRef]
210. Ghayoor, M.; Lee, K.; He, Y.; Chang, C.; Paul, B.K.; Pasebani, S. Selective laser melting of 304L stainless steel: Role of volumetric energy density on the microstructure, texture and mechanical properties. *Addit. Manuf.* **2020**, *32*, 101011. [CrossRef]
211. Burkhardt, C.; Wendler, M.; Lehnert, R.; Hauser, M.; Clausnitzer, P.; Volkova, O.; Biermann, H.; Weidner, A. Fine-grained microstructure without texture obtained by electron beam powder bed fusion for AISI 304 L-based stainless steel. *Addit. Manuf.* **2023**, *69*, 103539. [CrossRef]
212. Nong, X.D.; Zhou, X.L. Effect of scanning strategy on the microstructure, texture, and mechanical properties of 15-5PH stainless steel processed by selective laser melting. *Mater. Charact.* **2021**, *174*, 111012. [CrossRef]
213. Sarkar, S.; Mukherjee, S.; Kumar, C.S.; Kumar Nath, A. Effects of heat treatment on microstructure, mechanical and corrosion properties of 15-5 PH stainless steel parts built by selective laser melting process. *J. Manuf. Process.* **2020**, *50*, 279–294. [CrossRef]

214. Mansoura, A.; Dehghan, S.; Barka, N.; Sattarpanah Karganroudi, S.; Houria, M. Effect of heat treatment parameters on microstructure and microhardness of 15-5PH stainless steel fabricated by selective laser melting. *J. Braz. Soc. Mech. Sci. Eng.* **2024**, *46*, 424. [CrossRef]
215. Tapoglou, N.; Clulow, J.; Patterson, A.; Curtis, D. Characterisation of mechanical properties of 15-5PH stainless steel manufactured through direct energy deposition. *CIRP J. Manuf. Sci. Technol.* **2022**, *38*, 172–185. [CrossRef]
216. Tapoglou, N.; Clulow, J.; Curtis, D. Increased shielding of a Direct Energy Deposition process to enable Deposition of reactive materials; an investigation into Deposition of 15-5 PH Stainless Steel, Inconel 718 and Ti-6Al-4V. *CIRP J. Manuf. Sci. Technol.* **2022**, *36*, 227–235. [CrossRef]
217. Das, T.; Roy, H.; Lohar, A.K.; Samanta, S.K. Mechanical and microstructural properties of laser direct energy deposited 15–5 PH and SS 316L stainless steel. *Mater. Today Proc.* **2022**, *66*, 3809–3813. [CrossRef]
218. Suren, A. Laser Powder Bed Fusion of AISI 310S and Inconel 625 with CW and PW Emissions. Master's Thesis, The Polytechnic University of Milan, Milan, Italy, 2021. Available online: https://www.politesi.polimi.it/handle/10589/177649 (accessed on 14 June 2024).
219. Moskvina, V.; Astafurova, E.; Astafurov, S.; Reunova, K.; Panchenko, M.; Melnikov, E.; Kolubaev, E. Effect of Ion-plasma nitriding on phase composition and tensile properties of AISI 321-type stainless steel produced by wire-feed electron-beam additive manufacturing. *Metals* **2022**, *12*, 176. [CrossRef]
220. Kalashnikov, K.N.; Khoroshko, K.S.; Kalashnikova, T.A.; Chumaevskii, A.V.; Filippov, A.V. Structural evolution of 321 stainless steel in electron beam freeform fabrication. *J. Phys. Conf. Ser.* **2018**, *1115*, 042049. [CrossRef]
221. Yin, Q.; Chen, G.; Cao, H.; Zhang, G.; Zhang, B.; Wei, S. Transformation law of microstructure evolution and mechanical properties of electron beam freeform fabricated 321 austenitic stainless steel. *Vacuum* **2021**, *194*, 110594. [CrossRef]
222. Liverani, E.; Fortunato, A. Additive manufacturing of AISI 420 stainless steel: Process validation, defect analysis and mechanical characterization in different process and post-process conditions. *Int. J. Adv. Manuf. Technol.* **2021**, *117*, 809–821. [CrossRef]
223. Zhao, X.; Wei, Q.; Song, B.; Liu, Y.; Luo, X.; Wen, S.; Shi, Y. Fabrication and Characterization of AISI 420 Stainless Steel Using Selective Laser Melting. *Mater. Manuf. Process.* **2015**, *30*, 1283–1289. [CrossRef]
224. Yang, X.H.; Jiang, C.M.; Ho, J.R.; Tung, P.C.; Lin, C.K. Effects of Laser Spot Size on the Mechanical Properties of AISI 420 Stainless Steel Fabricated by Selective Laser Melting. *Materials* **2021**, *14*, 4593. [CrossRef] [PubMed]
225. Krakhmalev, P.; Yadroitsava, I.; Fredriksson, G.; Yadroitsev, I. In situ heat treatment in selective laser melted martensitic AISI 420 stainless steels. *Mater. Des.* **2015**, *87*, 380–385. [CrossRef]
226. Hassan, M.M.; Radhakrishnan, M.; Otazu, D.; Lienert, T.; Anderoglu, O. Investigation of Microstructure and Mechanical Properties of Additive Manufactured AISI-420 Martensitic Steel Developed by Directed Energy Deposition Method. In Proceedings of the ASME International Mechanical Engineering Congress and Exposition, Online, 1–5 November 2021. [CrossRef]
227. Muthu, S.M.; Veeman, D.; Vijayakumar, A.; Prabu, S.S.; Sujai, S.; Arvind, M.; Gobinath, E. Evaluation of metallurgical and mechanical characteristics of the ferritic stainless steel AISI 430 produced by GTAW-based WAAM. *Mater. Lett.* **2024**, *354*, 135362. [CrossRef]
228. Kim, H.; Liu, Z.; Cong, W.; Zhang, H.C. Tensile Fracture Behavior and Failure Mechanism of Additively-Manufactured AISI 4140 Low Alloy Steel by Laser Engineered Net Shaping. *Materials* **2017**, *10*, 1283. [CrossRef] [PubMed]
229. Damon, J.; Koch, R.; Kaiser, D.; Graf, G.; Dietrich, S.; Schulze, V. Process development and impact of intrinsic heat treatment on the mechanical performance of selective laser melted AISI 4140. *Addit. Manuf.* **2019**, *28*, 275–284. [CrossRef]
230. Haghdadi, N.; Ledermueller, C.; Chen, H.; Chen, Z.; Liu, Q.; Li, X.; Rohrer, G.; Liao, X.; Ringer, S.; Primig, S. Evolution of microstructure and mechanical properties in 2205 duplex stainless steels during additive manufacturing and heat treatment. *Mater. Sci. Eng. A* **2022**, *835*, 142695. [CrossRef]
231. Piras, M.; Hor, A.; Charkaluk, E. Control of the Microstructure and Mechanical Properties of a Super Duplex SAF 2507 Steel Produced by Additive Manufacturing. In *Advances in Additive Manufacturing: Materials, Processes and Applications*; Mabrouki, T., Sahlaoui, H., Sallem, H., Ghanem, F., Benyahya, N., Eds.; Lecture Notes in Mechanical Engineering; Springer Nature: Cham, Switzerland, 2024; pp. 1–9, ISBN 978-3-031-47783-6. Available online: https://link.springer.com/10.1007/978-3-031-47784-3_1 (accessed on 14 June 2024).
232. Vishnukumar, M.; Muthupandi, V.; Jerome, S. Microstructural characteristics, mechanical properties and corrosion performance of super austenitic stainless steel 904L produced by wire arc additive manufacturing. *Mater. Today Commun.* **2023**, *35*, 105801. [CrossRef]
233. Trevisan, F.; Calignano, F.; Lorusso, M.; Pakkanen, J.; Aversa, A.; Ambrosio, E.P.; Lombardi, M.; Fino, P.; Manfredi, D. On the Selective Laser Melting (SLM) of the AlSi10Mg Alloy: Process, Microstructure, and Mechanical Properties. *Materials* **2017**, *10*, 76. [CrossRef]
234. Read, N.; Wang, W.; Essa, K.; Attallah, M.M. Selective laser melting of AlSi10Mg alloy: Process optimisation and mechanical properties development. *Mater. Des.* **2015**, *65*, 417–424. [CrossRef]
235. Kempen, K.; Thijs, L.; Yasa, E.; Badrossamay, M.; Verheecke, W.; Kruth, J.-P. Process Optimization and Microstructural Analysis for Selective Laser Melting of AlSi10Mg. In Proceedings of the 2011 International Solid Freeform Fabrication Symposium, Austin, TX, USA, 8–10 August 2011. Available online: https://hdl.handle.net/2152/88371 (accessed on 25 July 2024).
236. Javidani, M.; Arreguin-Zavala, J.; Danovitch, J.; Tian, Y.; Brochu, M. Additive Manufacturing of AlSi10Mg Alloy Using Direct Energy Deposition: Microstructure and Hardness Characterization. *J. Therm. Spray Tech.* **2017**, *26*, 587–597. [CrossRef]

237. Gong, J.; Wei, K.; Liu, M.; Song, W.; Li, X.; Zeng, X. Microstructure and mechanical properties of AlSi10Mg alloy built by laser powder bed fusion/direct energy deposition hybrid laser additive manufacturing. *Addit. Manuf.* **2022**, *59*, 103160. [CrossRef]
238. Kiani, P.; Dupuy, A.D.; Ma, K.; Schoenung, J.M. Directed energy deposition of AlSi10Mg: Single track nonscalability and bulk properties. *Mater. Des.* **2020**, *194*, 108847. [CrossRef]
239. Baitimerov, R.; Lykov, P.; Zherebtsov, D.; Radionova, L.; Shultc, A.; Prashanth, K.G. Influence of Powder Characteristics on Processability of AlSi12 Alloy Fabricated by Selective Laser Melting. *Materials* **2018**, *11*, 742. [CrossRef] [PubMed]
240. Siddique, S.; Imran, M.; Wycisk, E.; Emmelmann, C.; Walther, F. Influence of process-induced microstructure and imperfections on mechanical properties of AlSi12 processed by selective laser melting. *J. Mater. Process. Technol.* **2015**, *221*, 205–213. [CrossRef]
241. Rahman Rashid, R.A.; Ali, H.; Palanisamy, S.; Masood, S.H. Effect of process parameters on the surface characteristics of AlSi12 samples made via selective laser melting. *Mater. Today Proc.* **2017**, *4*, 8724–8730. [CrossRef]
242. Shanmugam, R.; Chandran, J.; Vinayagam, M.; Fakron, O.; Dennison, S.; Romine, S. Comparative Study of Mechanical Properties of Aluminum Alloy A356 (Al-12Si) Fabricated by Directed Energy. In Proceedings of the 2022 International Solid Freeform Fabrication Symposium, Austin, TX, USA, 25–27 July 2022. Available online: https://hdl.handle.net/2152/117449 (accessed on 25 July 2024).
243. Rodríguez-González, P.; Zapico, P.; Robles-Valero, P.E.; Barreiro, J. Novel post-processing procedure to enhance casting molds manufactured by binder jetting AM. *Addit. Manuf.* **2022**, *59*, 103142. [CrossRef]
244. Lupi, G.; de Menezes, J.T.O.; Belelli, F.; Bruzzo, F.; López, E.; Volpp, J.; Castrodeza, E.M.; Casati, R. Fracture toughness of AlSi10Mg alloy produced by direct energy deposition with different crack plane orientations. *Mater. Today Commun.* **2023**, *37*, 107460. [CrossRef]
245. Kumar, M.; Gibbons, G.J.; Das, A.; Manna, I.; Tanner, D.; Kotadia, H.R. Additive manufacturing of aluminium alloy 2024 by laser powder bed fusion: Microstructural evolution, defects and mechanical properties. *Rapid Prototyp. J.* **2021**, *27*, 1388–1397. [CrossRef]
246. Pekok, M.A.; Setchi, R.; Ryan, M.; Han, Q.; Gu, D. Effect of process parameters on the microstructure and mechanical properties of AA2024 fabricated using selective laser melting. *Int. J. Adv. Manuf. Technol.* **2021**, *112*, 175–192. [CrossRef]
247. Ahmed, M.M.; El-Sayed Seleman, M.M.; Elfishawy, E.; Alzahrani, B.; Touileb, K.; Habba, M.I. The effect of temper condition and feeding speed on the additive manufacturing of AA2011 parts using friction stir deposition. *Materials* **2021**, *14*, 6396. [CrossRef] [PubMed]
248. Zhang, Y.; Gao, M.; Lu, Y.; Du, W. Deposition geometrical characteristics of wire arc additive-manufactured AA2219 aluminium alloy with cold metal transfer pulse advance arc mode. *Int. J. Adv. Manuf. Technol.* **2022**, *123*, 3807–3818. [CrossRef]
249. Sojiphan, K. Effects of Very High Power Ultrasonic Additive Manufacturing Process Parameters on Hardness, Microstructure, and Texture of Aluminum 3003-H18 Alloy. Ph.D. Thesis, The Ohio State University, Columbus, OH, USA, 2015. Available online: https://search.proquest.com/openview/681ee61bf5f75f7df418ae95fcc330c4/1?pq-origsite=gscholar&cbl=18750 (accessed on 14 June 2024).
250. Pan, Q.; Kapoor, M.; Mileski, S.; Li, D.; Yang, J.; Zheng, Y.; Carsley, J.; Lou, X. Phase transformation and microstructural evolution in Al-Mn-Fe-Si 3104 aluminum alloy made by laser directed energy deposition. *Addit. Manuf.* **2023**, *77*, 103797. [CrossRef]
251. Pan, Q.; Kapoor, M.; Mileski, S.; Carsley, J.; Lou, X. Technical basis of using laser direct energy deposition as a high-throughput combinatorial method for DC-cast Al-Mn alloy development. *Mater. Des.* **2021**, *212*, 110290. [CrossRef]
252. Løvøy, M. Microstructural Analysis of Additive Manufactured Walls of AA5083 and AA4020 Alloys Produced by Cold Metal Transfer. Master's Thesis, University of Oslo, Oslo, Norway, 2018. Available online: https://www.duo.uio.no/handle/10852/63568 (accessed on 14 June 2024).
253. Singh, A. Additive Manufacturing of Al 4047 and Al 7050 Alloys Using Direct Laser Metal Deposition Process. Ph.D. Thesis, Wayne State University, Detroit, MI, USA, 2017. Available online: https://search.proquest.com/openview/be626188df4a687883ee1b57a0659f22/1?pq-origsite=gscholar&cbl=18750 (accessed on 14 June 2024).
254. Rousseau, J.-N.; Bois-Brochu, A.; Giguère, N.; Blais, C. Study of ultrasonic additive manufacturing and its utilization for the production of aluminum components made of alloys of the AA5XXX series. *Int. J. Adv. Manuf. Technol.* **2022**, *119*, 7983–8002. [CrossRef]
255. Horgar, A.; Fostervoll, H.; Nyhus, B.; Ren, X.; Eriksson, M.; Akselsen, O.M. Additive manufacturing using WAAM with AA5183 wire. *J. Mater. Process. Technol.* **2018**, *259*, 68–74. [CrossRef]
256. Bock, F.E.; Froend, M.; Herrnring, J.; Enz, J.; Kashaev, N.; Klusemann, B. Thermal analysis of laser additive manufacturing of aluminium alloys: Experiment and simulation. In *AIP Conference Proceedings*; AIP Publishing: College Park, MD, USA, 2018. Available online: https://pubs.aip.org/aip/acp/article-abstract/1960/1/140004/887110 (accessed on 14 June 2024).
257. Froend, M.; Ventzke, V.; Riekehr, S.; Kashaev, N.; Klusemann, B.; Enz, J. Microstructure and hardness evolution of laser metal deposited AA5087 wall-structures. *Procedia CIRP* **2018**, *74*, 131–135. [CrossRef]
258. Svetlizky, D.; Zheng, B.; Buta, T.; Zhou, Y.; Golan, O.; Breiman, U.; Haj-Ali, R.; Schoenung, J.M.; Lavernia, E.J.; Eliaz, N. Directed energy deposition of Al 5xxx alloy using Laser Engineered Net Shaping (LENS®). *Mater. Des.* **2020**, *192*, 108763. [CrossRef]
259. Mehta, A.; Zhou, L.; Huynh, T.; Park, S.; Hyer, H.; Song, S.; Bai, Y.; Imholte, D.D.; Woolstenhulme, N.E.; Wachs, D.M. Additive manufacturing and mechanical properties of the dense and crack free Zr-modified aluminum alloy 6061 fabricated by the laser-powder bed fusion. *Addit. Manuf.* **2021**, *41*, 101966. [CrossRef]

260. Loh, L.-E.; Chua, C.-K.; Yeong, W.-Y.; Song, J.; Mapar, M.; Sing, S.-L.; Liu, Z.-H.; Zhang, D.-Q. Numerical investigation and an effective modelling on the Selective Laser Melting (SLM) process with aluminium alloy 6061. *Int. J. Heat Mass Transf.* **2015**, *80*, 288–300. [CrossRef]
261. Maamoun, A.; Xue, Y.; Elbestawi, M.; Veldhuis, S. The Effect of Selective Laser Melting Process Parameters on the Microstructure and Mechanical Properties of Al6061 and AlSi10Mg Alloys. *Materials* **2019**, *12*, 12. [CrossRef]
262. Dadbakhsh, S.; Mertens, R.; Vanmeensel, K.; Vleugels, J.; Humbeeck, J.V.; Kruth, J.-P. In situ alloying and reinforcing of Al6061 during selective laser melting. *Procedia CIRP* **2018**, *74*, 39–43. [CrossRef]
263. Jeon, S.; Park, S.; Song, Y.; Park, J.; Park, H.; Lee, B.; Choi, H. Combinatorial Experiment for Al-6061 and Al-12Si alloy Based on Directed Energy Deposition (DED) Process. *J. Powder Mater.* **2023**, *30*, 463–469. [CrossRef]
264. de la Vega, F.M. Optimization of Thermal Cycles for a Novel Al 6061 Alloy Produced by Binder Jetting. Master's Thesis, Polytechnic University of Milan, Milan, Italy, 2023. Available online: https://www.politesi.polimi.it/handle/10589/214304 (accessed on 25 July 2024).
265. Patel, M.; Chaudhary, B.; Murugesan, J.; Jain, N.K. Additive Manufacturing of AA6063-ZrO2 Composite Using Friction Stir Surface Additive Manufacturing. *Trans. Indian Inst. Met.* **2023**, *76*, 581–588. [CrossRef]
266. Chen, X.; Duan, X.; Jiang, G. Numerical investigation of Transient Temperature Field on the Selective Laser Melting process with Al6063. *IOP Conf. Ser. Mater. Sci. Eng.* **2019**, *677*, 032070. [CrossRef]
267. Li, F.; Zhang, T.; Wu, Y.; Chen, C.; Zhou, K. Microstructure, mechanical properties, and crack formation of aluminum alloy 6063 produced via laser powder bed fusion. *J. Mater. Sci.* **2022**, *57*, 9631–9645. [CrossRef]
268. Blindheim, J.; Grong, Ø.; Welo, T.; Steinert, M. On the mechanical integrity of AA6082 3D structures deposited by hybrid metal extrusion & bonding additive manufacturing. *J. Mater. Process. Technol.* **2020**, *282*, 116684.
269. Yoder, J.K.; Griffiths, R.J.; Hang, Z.Y. Deformation-based additive manufacturing of 7075 aluminum with wrought-like mechanical properties. *Mater. Des.* **2021**, *198*, 109288. [CrossRef]
270. Montero-Sistiaga, M.L.; Mertens, R.; Vrancken, B.; Wang, X.; Van Hooreweder, B.; Kruth, J.-P.; Van Humbeeck, J. Changing the alloy composition of Al7075 for better processability by selective laser melting. *J. Mater. Process. Technol.* **2016**, *238*, 437–445. [CrossRef]
271. Tan, Q.; Fan, Z.; Tang, X.; Yin, Y.; Li, G.; Huang, D.; Zhang, J.; Liu, Y.; Wang, F.; Wu, T.; et al. A novel strategy to additively manufacture 7075 aluminium alloy with selective laser melting. *Mater. Sci. Eng. A* **2021**, *821*, 141638. [CrossRef]
272. Zhao, Z.; Wang, J.; Du, W.; Bai, P.; Wu, X. Numerical simulation and experimental study of the 7075 aluminum alloy during selective laser melting. *Opt. Laser Technol.* **2023**, *167*, 109814. [CrossRef]
273. Xu, H.; Ren, W.; Ma, C.; Xu, L.; Han, Y.; Zhao, L.; Hao, K. Laser-directed energy deposition of ZrH2 particles reinforced Al7075 alloy: Cracks elimination and strength enhancement. *Addit. Manuf.* **2023**, *78*, 103877. [CrossRef]
274. Qi, T.; Zhu, H.; Zhang, H.; Yin, J.; Ke, L.; Zeng, X. Selective laser melting of Al7050 powder: Melting mode transition and comparison of the characteristics between the keyhole and conduction mode. *Mater. Des.* **2017**, *135*, 257–266. [CrossRef]
275. Singh, A.; Ramakrishnan, A.; Baker, D.; Biswas, A.; Dinda, G.P. Laser metal deposition of nickel coated Al 7050 alloy. *J. Alloys Compd.* **2017**, *719*, 151–158. [CrossRef]
276. Davoren, B.; Sacks, N.; Theron, M. Microstructure characterization of WC-9.2wt%Monel 400 fabricated using laser engineered net shaping. *Prog. Addit. Manuf.* **2021**, *6*, 431–443. [CrossRef]
277. Anderson, R.; Terrell, J.; Schneider, J.; Thompson, S.; Gradl, P. Characteristics of Bi-metallic Interfaces Formed During Direct Energy Deposition Additive Manufacturing Processing. *Met. Mater. Trans. B* **2019**, *50*, 1921–1930. [CrossRef]
278. Mani, M.; Mohanraj, M.; Karthikeyan, A.G.; Kalaiselvan, K. Investigations of performance characteristics on direct metal laser sintered MONEL K-500 superalloy. *Mater. Sci. Technol.* **2023**, *39*, 3111–3122. [CrossRef]
279. Chen, Z.; Wang, C.; Kandukuri, S.Y.; Zhou, K. Additive Manufacturing of Monel K-500 via Directed Energy Deposition for Pressure Vessel Applications. In Proceedings of the Pressure Vessels and Piping Conference, Las Vegas, NV, USA, 17–22 July 2022; Vol. 86175; p. V04AT06A016. Available online: https://asmedigitalcollection.asme.org/PVP/proceedings-abstract/PVP2022/V04AT06A016/1149864 (accessed on 14 June 2024).
280. Mani, H.T.; Savarimuthu, J.; Varma, S.R.; Muraleedharan, M.B.; Suni, N.K.; Nandakumar, Y. Investigation of mechanical and microstructure properties of metal inert gas based wire arc additive manufactured Inconel 600 superalloy. *Int. J. Mater. Res.* **2023**, *114*, 844–854. [CrossRef]
281. Poudel, A.; Gradl, P.R.; Shao, S.; Shamsaei, N. Tensile deformation behavior of laser powder direct energy deposited Inconel 625: Cryogenic to elevated temperatures. *Mater. Sci. Eng. A* **2024**, *889*, 145826. [CrossRef]
282. Yang, Z.; Sun, H.; Shang, S.-L.; Liu, Z.-K.; Beese, A.M. Effect of heat treatment on functionally graded 304L stainless steel to Inconel 625 fabricated by directed energy deposition. *Materialia* **2024**, *34*, 102067. [CrossRef]
283. Marchese, G.; Colera, X.G.; Calignano, F.; Lorusso, M.; Biamino, S.; Minetola, P.; Manfredi, D. Characterization and Comparison of Inconel 625 Processed by Selective Laser Melting and Laser Metal Deposition. *Adv. Eng. Mater.* **2017**, *19*, 1600635. [CrossRef]
284. Li, S.; Wei, Q.; Shi, Y.; Zhu, Z.; Zhang, D. Microstructure Characteristics of Inconel 625 Superalloy Manufactured by Selective Laser Melting. *J. Mater. Sci. Technol.* **2015**, *31*, 946–952. [CrossRef]
285. Murr, L.E.; Martinez, E.; Gaytan, S.M.; Ramirez, D.A.; Machado, B.I.; Shindo, P.W.; Martinez, J.L.; Medina, F.; Wooten, J.; Ciscel, D.; et al. Microstructural Architecture, Microstructures, and Mechanical Properties for a Nickel-Base Superalloy Fabricated by Electron Beam Melting. *Met. Mater. Trans. A* **2011**, *42*, 3491–3508. [CrossRef]

286. Koike, R.; Misawa, T.; Aoyama, T.; Kondo, M. Controlling metal structure with remelting process in direct energy deposition of Inconel 625. *CIRP Ann.* **2018**, *67*, 237–240. [CrossRef]
287. Koike, R.; Misawa, T.; Kakinuma, Y.; Oda, Y. Basic Study on Remelting Process to Enhance Density of Inconel 625 in Direct Energy Deposition. *Int. J. Autom. Technol.* **2018**, *12*, 424–433. [CrossRef]
288. Jiang, R.; Monteil, L.; Kimes, K.; Mostafaei, A.; Chmielus, M. Influence of powder type and binder saturation on binder jet 3D–printed and sintered Inconel 625 samples. *Int. J. Adv. Manuf. Technol.* **2021**, *116*, 3827–3838. [CrossRef]
289. Mostafaei, A.; Neelapu, S.H.V.R.; Kisailus, C.; Nath, L.M.; Jacobs, T.D.B.; Chmielus, M. Characterizing surface finish and fatigue behavior in binder-jet 3D-printed nickel-based superalloy 625. *Addit. Manuf.* **2018**, *24*, 200–209. [CrossRef]
290. Mostafaei, A. Powder Bed Binder Jet 3D Printing of Alloy 625: Microstructural Evolution, Densification Kinetics and Mechanical Properties. Ph.D. Thesis, University of Pittsburgh, Pittsburgh, PA, USA, 2018. Available online: http://d-scholarship.pitt.edu/34920/ (accessed on 25 July 2024).
291. Amato, K.N.; Gaytan, S.M.; Murr, L.E.; Martinez, E.; Shindo, P.W.; Hernandez, J.; Collins, S.; Medina, F. Microstructures and mechanical behavior of Inconel 718 fabricated by selective laser melting. *Acta Mater.* **2012**, *60*, 2229–2239. [CrossRef]
292. Li, X.; Shi, J.J.; Wang, C.H.; Cao, G.H.; Russell, A.M.; Zhou, Z.J.; Li, C.P.; Chen, G.F. Effect of heat treatment on microstructure evolution of Inconel 718 alloy fabricated by selective laser melting. *J. Alloys Compd.* **2018**, *764*, 639–649. [CrossRef]
293. Chlebus, E.; Gruber, K.; Kuźnicka, B.; Kurzac, J.; Kurzynowski, T. Effect of heat treatment on the microstructure and mechanical properties of Inconel 718 processed by selective laser melting. *Mater. Sci. Eng. A* **2015**, *639*, 647–655. [CrossRef]
294. Sames, W.J.; Unocic, K.A.; Dehoff, R.R.; Lolla, T.; Babu, S.S. Thermal effects on microstructural heterogeneity of Inconel 718 materials fabricated by electron beam melting. *J. Mater. Res.* **2014**, *29*, 1920–1930. [CrossRef]
295. Kirka, M.M.; Medina, F.; Dehoff, R.; Okello, A. Mechanical behavior of post-processed Inconel 718 manufactured through the electron beam melting process. *Mater. Sci. Eng. A* **2017**, *680*, 338–346. [CrossRef]
296. Helmer, H.; Bauereiß, A.; Singer, R.F.; Körner, C. Grain structure evolution in Inconel 718 during selective electron beam melting. *Mater. Sci. Eng. A* **2016**, *668*, 180–187. [CrossRef]
297. Wang, Z.; Wang, J.; Xu, S.; Liu, B.; Sui, Q.; Zhao, F.; Gong, L.; Liu, J. Influence of powder characteristics on microstructure and mechanical properties of Inconel 718 superalloy manufactured by direct energy deposition. *Appl. Surf. Sci.* **2022**, *583*, 152545. [CrossRef]
298. Gullipalli, C.; Thawari, N.; Chandak, A.; Gupta, T. Statistical Analysis of Clad Geometry in Direct Energy Deposition of Inconel 718 Single Tracks. *J. Mater. Eng. Perform.* **2022**, *31*, 6922–6932. [CrossRef]
299. Nandwana, P.; Elliott, A.M.; Siddel, D.; Merriman, A.; Peter, W.H.; Babu, S.S. Powder bed binder jet 3D printing of Inconel 718: Densification, microstructural evolution and challenges. *Curr. Opin. Solid State Mater. Sci.* **2017**, *21*, 207–218. [CrossRef]
300. Eriksson, T. Process Optimization and Characterization of Inconel 718 Manufactured by Metal Binder Jetting. Master's Thesis, Luleå University of Technology, Luleå, Sweden, 2021. Available online: https://urn.kb.se/resolve?urn=urn:nbn:se:ltu:diva-87168 (accessed on 25 July 2024).
301. Rajkumar, V.; Vishnukumar, M.; Sowrirajan, M.; Kannan, A.R. Microstructure, mechanical properties and corrosion behaviour of Incoloy 825 manufactured using wire arc additive manufacturing. *Vacuum* **2022**, *203*, 111324. [CrossRef]
302. Yan, D. Effect of Laser Powder Bed Fusion Parameters and Hot Isostatic Pressing on the Microstructure and Mechanical Properties of C22 Alloy. Master's Thesis, Oregon State University, Corvallis, OR, USA, 2021.
303. Montealegre-Meléndez, I.; Pérez-Soriano, E.M.; Ariza, E.; Neubauer, E.; Kitzmantel, M.; Arévalo, C. Manufacturing via Plasma Metal Deposition of Hastelloy C-22 Specimens Made from Particles with Different Granulometries. *Machines* **2024**, *12*, 253. [CrossRef]
304. Madesh, R.; Kumar, K.G. Microstructural and Mechanical Properties of Nickel-Based Superalloy Fabricated by Pulsed-Mode Arc-Based Additive Manufacturing Technology. *Met. Mater. Int.* **2024**. [CrossRef]
305. Obidigbo, C.; Tatman, E.-P.; Gockel, J. Processing parameter and transient effects on melt pool geometry in additive manufacturing of Invar 36. *Int. J. Adv. Manuf. Technol.* **2019**, *104*, 3139–3146. [CrossRef]
306. Qiu, C.; Adkins, N.J.E.; Attallah, M.M. Selective laser melting of Invar 36: Microstructure and properties. *Acta Mater.* **2016**, *103*, 382–395. [CrossRef]
307. Wei, K.; Yang, Q.; Ling, B.; Yang, X.; Xie, H.; Qu, Z.; Fang, D. Mechanical properties of Invar 36 alloy additively manufactured by selective laser melting. *Mater. Sci. Eng. A* **2020**, *772*, 138799. [CrossRef]
308. Wegener, T.; Brenne, F.; Fischer, A.; Möller, T.; Hauck, C.; Auernhammer, S.; Niendorf, T. On the structural integrity of Fe-36Ni Invar alloy processed by selective laser melting. *Addit. Manuf.* **2021**, *37*, 101603. [CrossRef]
309. Park, B.S.; Baik, H.K. Refining of Invar and Permalloy Fe-Ni Alloys by <Ar/Ar-H_2 Plasma and Electron Beam Melting. *J. Korea Foundry Soc.* **1995**, *15*, 175–183.
310. Lores, A.; Azurmendi, N.; Agote, I.; Espinosa, E.; García-Blanco, M.B. A study of parameter and post-processing effects on surface quality improvement of Binder Jet 3D-printed Invar36 alloy parts. *Prog. Addit. Manuf.* **2022**, *7*, 917–930. [CrossRef]
311. Azurmendi, N. Binder Jetting of High Dimensional Stability Alloy for Space Applications. Available online: https://www.infona.pl/resource/bwmeta1.element.ID-e6a5a9d2-a2db-4f12-b165-d5438a3e1491 (accessed on 25 July 2024).
312. Huang, G.; He, G.; Gong, X.; He, Y.; Liu, Y.; Huang, K. Additive manufacturing of Invar 36 alloy. *J. Mater. Res. Technol.* **2024**, *30*, 1241–1268. [CrossRef]

313. Walker, J.; Andani, M.T.; Haberland, C.; Elahinia, M. Additive manufacturing of Nitinol shape memory alloys to overcome challenges in conventional Nitinol fabrication. In Proceedings of the ASME International Mechanical Engineering Congress and Exposition, Montreal, QC, Canada, 14–20 November 2014; Volume 46438, p. V02AT02A037. Available online: https://asmedigitalcollection.asme.org/IMECE/proceedings-abstract/IMECE2014/262362 (accessed on 14 June 2024).
314. Shishkovsky, I.; Yadroitsev, I.; Smurov, I. Direct Selective Laser Melting of Nitinol Powder. *Phys. Procedia* **2012**, *39*, 447–454. [CrossRef]
315. Chekotu, J.C.; Groarke, R.; O'Toole, K.; Brabazon, D. Advances in Selective Laser Melting of Nitinol Shape Memory Alloy Part Production. *Materials* **2019**, *12*, 809. [CrossRef]
316. Walker, J.; Elahinia, M.; Haberland, C. An Investigation of Process Parameters on Selective Laser Melting of Nitinol. In Proceedings of the ASME 2013 Conference on Smart Materials, Adaptive Structures and Intelligent Systems, Snowbird, UT, USA, 16–18 September 2013. [CrossRef]
317. Hayat, M.D.; Chen, G.; Liu, N.; Khan, S.; Tang, H.P.; Cao, P. Physical and Tensile Properties of NiTi Alloy by Selective Electron Beam Melting. *Key Eng. Mater.* **2018**, *770*, 148–154. [CrossRef]
318. Fink, A.; Fu, Z.; Körner, C. Functional properties and shape memory effect of Nitinol manufactured via electron beam powder bed fusion. *Materialia* **2023**, *30*, 101823. [CrossRef]
319. Zhou, Q.; Hayat, M.D.; Chen, G.; Cai, S.; Qu, X.; Tang, H.; Cao, P. Selective electron beam melting of NiTi: Microstructure, phase transformation and mechanical properties. *Mater. Sci. Eng. A* **2019**, *744*, 290–298. [CrossRef]
320. Bagheri, A.; Yadollahi, A.; Mahtabi, M.J.; Paudel, Y.; Vance, E.; Shamsaei, N.; Horstemeyer, M.F. Microstructure-Based MultiStage Fatigue Modeling of NiTi Alloy Fabricated via Direct Energy Deposition (DED). *J. Mater. Eng. Perform.* **2022**, *31*, 4761–4775. [CrossRef]
321. Sathishkumar, M.; Kumar, C.P.; Ganesh, S.S.S.; Venkatesh, M.; Radhika, N.; Vignesh, M.; Pazhani, A. Possibilities, performance and challenges of nitinol alloy fabricated by Directed Energy Deposition and Powder Bed Fusion for biomedical implants. *J. Manuf. Process.* **2023**, *102*, 885–909. [CrossRef]
322. Sharma, V.M.; Svetlizky, D.; Das, M.; Tevet, O.; Krämer, M.; Kim, S.; Gault, B.; Eliaz, N. Microstructure and mechanical properties of bulk NiTi shape memory alloy fabricated using directed energy deposition. *Addit. Manuf.* **2024**, *86*, 104224. [CrossRef]
323. Sazerat, M.; Nait-Ali, A.; Cervellon, A.; Lopez-Galilea, I.; Burlot, G.; Gillet, S.; Eyidi, D.; Joulain, A.; Villechaise, P.; Weber, S. High temperature microstructure stability of Waspaloy produced by Wire Arc Additive Manufacturing. *J. Alloys Compd.* **2023**, *966*, 171626. [CrossRef]
324. Mumtaz, K.A.; Erasenthiran, P.; Hopkinson, N. High density selective laser melting of Waspaloy®. *J. Mater. Process. Technol.* **2008**, *195*, 77–87. [CrossRef]
325. Jedynak, A.; Sviridov, A.; Bambach, M.; Beckers, D.; Graf, G. On the Potential of Using Selective Laser Melting for the Fast Development of Forging Alloys at the Example of Waspaloy. *Procedia Manuf.* **2020**, *47*, 1149–1153. [CrossRef]
326. Mumtaz, K.A.; Hopkinson, N. Laser melting functionally graded composition of Waspaloy® and Zirconia powders. *J. Mater. Sci.* **2007**, *42*, 7647–7656. [CrossRef]
327. Lövhall, J. Process Parameter Optimisation for Waspaloy Using Laser-Directed Energy Deposition with Powder. Bachelor's Thesis, University West, Trollhättan, Sweden, 2024. Available online: https://urn.kb.se/resolve?urn=urn:nbn:se:hv:diva-21294 (accessed on 25 July 2024).
328. Zhou, X.; Li, K.; Zhang, D.; Liu, X.; Ma, J.; Liu, W.; Shen, Z. Textures formed in a CoCrMo alloy by selective laser melting. *J. Alloys Compd.* **2015**, *631*, 153–164. [CrossRef]
329. Song, C.; Zhang, M.; Yang, Y.; Wang, D.; Jia-kuo, Y. Morphology and properties of CoCrMo parts fabricated by selective laser melting. *Mater. Sci. Eng. A* **2018**, *713*, 206–213. [CrossRef]
330. Monroy, K.; Delgado, J.; Ciurana, J. Study of the Pore Formation on CoCrMo Alloys by Selective Laser Melting Manufacturing Process. *Procedia Eng.* **2013**, *63*, 361–369. [CrossRef]
331. Zhang, M.; Yang, Y.; Song, C.; Bai, Y.; Xiao, Z. An investigation into the aging behavior of CoCrMo alloys fabricated by selective laser melting. *J. Alloys Compd.* **2018**, *750*, 878–886. [CrossRef]
332. Gong, X.; Li, Y.; Nie, Y.; Huang, Z.; Liu, F.; Huang, L.; Jiang, L.; Mei, H. Corrosion behaviour of CoCrMo alloy fabricated by electron beam melting. *Corros. Sci.* **2018**, *139*, 68–75. [CrossRef]
333. Vutova, K.; Stefanova, V.; Markov, M.; Vassileva, V. Study on Hardness of Heat-Treated CoCrMo Alloy Recycled by Electron Beam Melting. *Materials* **2023**, *16*, 2634. [CrossRef]
334. Petit, C.; Maire, E.; Meille, S.; Adrien, J.; Kurosu, S.; Chiba, A. CoCrMo cellular structures made by Electron Beam Melting studied by local tomography and finite element modelling. *Mater. Charact.* **2016**, *116*, 48–54. [CrossRef]
335. Vutova, K.; Stefanova, V.; Vassileva, V.; Atanasova-Vladimirova, S. Recycling of Technogenic CoCrMo Alloy by Electron Beam Melting. *Materials* **2022**, *15*, 4168. [CrossRef]
336. Liu, M.; Kuttolamadom, M. Characterization of Co-Cr-Mo Alloys Manufacturing via Directed Energy Deposition. In Proceedings of the ASME 2021 16th International Manufacturing Science and Engineering Conference, Online, 21–25 June 2021. [CrossRef]
337. Khademitab, M.; de Vecchis, P.R.; Staszel, P.; Vaicik, M.K.; Chmielus, M.; Mostafaei, A. Structure-property relationships of differently heat-treated binder jet printed Co-Cr-Mo biomaterial. *Mater. Today Commun.* **2024**, *38*, 107716. [CrossRef]
338. Onler, R.; Koca, A.S.; Kirim, B.; Soylemez, E. Multi-objective optimization of binder jet additive manufacturing of Co-Cr-Mo using machine learning. *Int. J. Adv. Manuf. Technol.* **2022**, *119*, 1091–1108. [CrossRef]

339. Lee, H.W.; Jung, K.-H.; Hwang, S.-K.; Kang, S.-H.; Kim, D.-K. Microstructure and mechanical anisotropy of CoCrW alloy processed by selective laser melting. *Mater. Sci. Eng. A* **2019**, *749*, 65–73. [CrossRef]
340. Zou, S.; Zhao, Z.; Xu, W.; Ni, X.; Zhang, L.; Wu, W.; Kong, D.; He, X.; Wang, L.; Dong, C. Effects of scanning speeds on the wear behavior of CoCrW alloy fabricated by selective laser melting. *Opt. Laser Technol.* **2022**, *147*, 107652. [CrossRef]
341. Lu, Y.; Wu, S.; Gan, Y.; Li, J.; Zhao, C.; Zhuo, D.; Lin, J. Investigation on the microstructure, mechanical property and corrosion behavior of the selective laser melted CoCrW alloy for dental application. *Mater. Sci. Eng. C* **2015**, *49*, 517–525. [CrossRef]
342. Jo, Y.-K.; Song, D.-B.; Choi, J.-S.; Suh, J.; Kahhal, P.; Park, S.-H. Higher wear-resistant surfacing at high temperatures using a hybrid cladding process. *Mater. Des.* **2023**, *225*, 111553. [CrossRef]
343. Moradi, M.; Ashoori, A.; Hasani, A. Additive manufacturing of stellite 6 superalloy by direct laser metal deposition–Part 1: Effects of laser power and focal plane position. *Opt. Laser Technol.* **2020**, *131*, 106328. [CrossRef]
344. Bakhshayesh, M.M.; Khodabakhshi, F.; Farshidianfar, M.H.; Nagy, Š.; Mohammadi, M.; Wilde, G. Additive manufacturing of Stellite 6 alloy by laser-directed energy deposition: Engineering the crystallographic texture. *Mater. Charact.* **2024**, *207*, 113511. [CrossRef]
345. Mariani, M.; Lecis, N.; Mostafaei, A. Binder Jetting-based Metal Printing. In *Solid-State Metal Additive Manufacturing*; John Wiley & Sons, Ltd.: Hoboken, NJ, USA, 2024; pp. 339–359, ISBN 978-3-527-83935-3. Available online: https://onlinelibrary.wiley.com/doi/abs/10.1002/9783527839353.ch15 (accessed on 25 July 2024).
346. Mostafaei, A.; Rodriguez De Vecchis, P.; Buckenmeyer, M.J.; Wasule, S.R.; Brown, B.N.; Chmielus, M. Microstructural evolution and resulting properties of differently sintered and heat-treated binder-jet 3D-printed Stellite 6. *Mater. Sci. Eng. C* **2019**, *102*, 276–288. [CrossRef]
347. Freiße, H.; Khazan, P.; Stroth, M.; Köhler, H. Properties of large 3D parts made From Stellite 21 through direct powder deposition. In Proceedings of the Laser in Manufacturing Conference, München, Germany, 22–25 June 2015. Available online: https://www.wlt.de/lim/Proceedings/Stick/PDF/Contribution310_final.pdf (accessed on 14 June 2024).
348. Smoqi, Z.; Toddy, J.; Halliday, H.; Shield, J.E.; Rao, P. Process-structure relationship in the directed energy deposition of cobalt-chromium alloy (Stellite 21) coatings. *Mater. Des.* **2021**, *197*, 109229. [CrossRef]
349. Ren, B.; Zhang, M.; Chen, C.; Wang, X.; Zou, T.; Hu, Z. Effect of Heat Treatment on Microstructure and Mechanical Properties of Stellite 12 Fabricated by Laser Additive Manufacturing. *J. Mater. Eng. Perform.* **2017**, *26*, 5404–5413. [CrossRef]
350. Liu, Y.; Huang, Z.; Zhang, C.; Lu, J.; Ouyang, N.; Shen, Q.; Huang, A.; Chen, F. Microstructure and mechanical properties of Haynes 188 alloy manufactured by laser powder bed fusion. *Mater. Charact.* **2024**, *211*, 113880. [CrossRef]
351. Liu, Y.; Huang, Z.; Zhang, C.; Lu, J.; Ouyang, N.; Shen, Q.; Zhu, Y.; Huang, A.; Chen, F. Tailoring microstructure and twin-induced work hardening of a laser powder bed fusion manufactured Haynes 188 alloy. *Mater. Sci. Eng. A* **2024**, *891*, 145925. [CrossRef]
352. Liu, Y.; Huang, Z.; Zhang, C.; Lu, J.; Ouyang, N.; Shen, Q.; Chen, F. Twin-Induced Tensile Strengthening in a Laser Powder Bed Fusion Manufactured Haynes 188 Alloy by Heat Treatment. 2022. Available online: https://papers.ssrn.com/abstract=4299736 (accessed on 25 July 2024).
353. Yang, B.; Shang, Z.; Ding, J.; Lopez, J.; Jarosinski, W.; Sun, T.; Richter, N.; Zhang, Y.; Wang, H.; Zhang, X. Investigation of strengthening mechanisms in an additively manufactured Haynes 230 alloy. *Acta Mater.* **2022**, *222*, 117404. [CrossRef]
354. He, J.; Wang, R.; Li, N.; Xiao, Z.; Gu, J.; Yu, H.; Bi, Z.; Liu, W.; Song, M. Unravelling the origin of multiple cracking in an additively manufactured Haynes 230. *Mater. Res. Lett.* **2023**, *11*, 281–288. [CrossRef]
355. Paul, M.; Ghiaasiaan, R.; Gradl, P.; Caron, J.; Wang, P.; Shao, S.; Shamsaei, N. Tensile and fatigue behaviors of newly developed HAYNES® 233 alloy: Additively manufactured vs. wrought. *Mater. Des.* **2024**, *244*, 113165. [CrossRef]
356. Magnin, C.; Islam, Z.; Elbakhshwan, M.; Brittan, A.; Thoma, D.J.; Anderson, M.H. The performance of additively manufactured Haynes 282 in supercritical CO2. *Mater. Sci. Eng. A* **2022**, *841*, 143007. [CrossRef]
357. Otto, R.; Brøtan, V.; Carvalho, P.A.; Reiersen, M.; Graff, J.S.; Sunding, M.F.; Berg, O.Å.; Diplas, S.; Azar, A.S. Roadmap for additive manufacturing of HAYNES® 282® superalloy by laser beam powder bed fusion (PBF-LB) technology. *Mater. Des.* **2021**, *204*, 109656. [CrossRef]
358. Boswell, J.; Jones, J.; Barnard, N.; Clark, D.; Whittaker, M.; Lancaster, R. The effects of energy density and heat treatment on the microstructure and mechanical properties of laser additive manufactured Haynes 282. *Mater. Des.* **2021**, *205*, 109725. [CrossRef]
359. Unocic, K.A.; Kirka, M.M.; Cakmak, E.; Greeley, D.; Okello, A.O.; Dryepondt, S. Evaluation of additive electron beam melting of haynes 282 alloy. *Mater. Sci. Eng. A* **2020**, *772*, 138607. [CrossRef]
360. Fernandez-Zelaia, P.; Rojas, J.O.; Ferguson, J.; Dryepondt, S.; Kirka, M.M. Fatigue crack growth resistance of a mesoscale composite microstructure Haynes 282 fabricated via electron beam melting additive manufacturing. *J. Mater. Sci.* **2022**, *57*, 9866–9884. [CrossRef]
361. Cloots, M.; Kunze, K.; Uggowitzer, P.J.; Wegener, K. Microstructural characteristics of the nickel-based alloy IN738LC and the cobalt-based alloy Mar-M509 produced by selective laser melting. *Mater. Sci. Eng. A* **2016**, *658*, 68–76. [CrossRef]
362. Wang, X.; Chen, C.; Zhao, R.; Liu, L.; Shuai, S.; Hu, T.; Wang, J.; Ren, Z. Selective Laser Melting of Carbon-Free Mar-M509 Co-Based Superalloy: Microstructure, Micro-Cracks, and Mechanical Anisotropy. *Acta Metall. Sin. (Engl. Lett.)* **2022**, *35*, 501–516. [CrossRef]
363. Ferreri, N.C.; Ghorbanpour, S.; Bhowmik, S.; Lussier, R.; Bicknell, J.; Patterson, B.M.; Knezevic, M. Effects of build orientation and heat treatment on the evolution of microstructure and mechanical properties of alloy Mar-M-509 fabricated via laser powder bed fusion. *Int. J. Plast.* **2019**, *121*, 116–133. [CrossRef]

364. Ghorbanpour, S.; Bicknell, J.; Knezevic, M. Fatigue strength of additive manufactured Mar-M-509 superalloy. *Mater. Sci. Eng. A* **2022**, *840*, 142913. [CrossRef]
365. Ikeshoji, T.T.; Nakamura, K.; Yonehara, M.; Imai, K.; Kyogoku, H. Selective Laser Melting of Pure Copper. *JOM* **2018**, *70*, 396–400. [CrossRef]
366. Jadhav, S.D.; Dadbakhsh, S.; Goossens, L.; Kruth, J.-P.; Van Humbeeck, J.; Vanmeensel, K. Influence of selective laser melting process parameters on texture evolution in pure copper. *J. Mater. Process. Technol.* **2019**, *270*, 47–58. [CrossRef]
367. Lykov, P.A.; Safonov, E.V.; Akhmedianov, A.M. Selective Laser Melting of Copper. *Mater. Sci. Forum* **2016**, *843*, 284–288. [CrossRef]
368. Ramirez, D.A.; Murr, L.E.; Li, S.J.; Tian, Y.X.; Martinez, E.; Martinez, J.L.; Machado, B.I.; Gaytan, S.M.; Medina, F.; Wicker, R.B. Open-cellular copper structures fabricated by additive manufacturing using electron beam melting. *Mater. Sci. Eng. A* **2011**, *528*, 5379–5386. [CrossRef]
369. Guschlbauer, R.; Momeni, S.; Osmanlic, F.; Körner, C. Process development of 99.95% pure copper processed via selective electron beam melting and its mechanical and physical properties. *Mater. Charact.* **2018**, *143*, 163–170. [CrossRef]
370. Megahed, S.; Fischer, F.; Nell, M.; Forsmark, J.; Leonardi, F.; Zhu, L.; Hameyer, K.; Schleifenbaum, J.H. Manufacturing of Pure Copper with Electron Beam Melting and the Effect of Thermal and Abrasive Post-Processing on Microstructure and Electric Conductivity. *Materials* **2023**, *16*, 73. [CrossRef] [PubMed]
371. Kumar, A.; Bai, Y.; Eklund, A.; Williams, C.B. Effects of Hot Isostatic Pressing on Copper Parts Fabricated via Binder Jetting. *Procedia Manuf.* **2017**, *10*, 935–944. [CrossRef]
372. Yegyan Kumar, A.; Wang, J.; Bai, Y.; Huxtable, S.T.; Williams, C.B. Impacts of process-induced porosity on material properties of copper made by binder jetting additive manufacturing. *Mater. Des.* **2019**, *182*, 108001. [CrossRef]
373. Li, M.; Huang, J.; Fang, A.; Mansoor, B.; Pei, Z.; Ma, C. Binder jetting additive manufacturing of copper/diamond composites: An experimental study. *J. Manuf. Process.* **2021**, *70*, 205–213. [CrossRef]
374. Zhang, X.; Lei, Q.; Andani, M.T.; Liu, X.; Zhang, H.; Wang, W.; Li, Y.; Yang, Y. Effects of build orientation and heat treatment on microstructure and properties of Cu–Cr–Zr alloy manufactured by laser powder bed fusion. *Mater. Chem. Phys.* **2023**, *298*, 127477. [CrossRef]
375. Hu, Z.; Du, Z.; Yang, Z.; Yu, L.; Ma, Z. Preparation of Cu–Cr–Zr alloy by selective laser melting: Role of scanning parameters on densification, microstructure and mechanical properties. *Mater. Sci. Eng. A* **2022**, *836*, 142740. [CrossRef]
376. Sun, F.; Liu, P.; Chen, X.; Zhou, H.; Guan, P.; Zhu, B. Materials Mechanical Properties of High-Strength Cu–Cr–Zr Alloy Fabricated by Selective Laser Melting. *Materials* **2020**, *13*, 5028. [CrossRef] [PubMed]
377. Ma, Z.; Zhang, D.Z.; Liu, F.; Jiang, J.; Zhao, M.; Zhang, T. Lattice structures of Cu-Cr-Zr copper alloy by selective laser melting: Microstructures, mechanical properties and energy absorption. *Mater. Des.* **2020**, *187*, 108406. [CrossRef]
378. Ordás, N.; Portolés, L.; Azpeleta, M.; Gómez, A.; Blasco, J.R.; Martinez, M.; Ureña, J.; Iturriza, I. Development of CuCrZr via Electron Beam Powder Bed Fusion (EB-PBF). *J. Nucl. Mater.* **2021**, *548*, 152841. [CrossRef]
379. Li, X.; Xu, X.; Hu, X.; Shi, H.; Li, X.; Liu, W.; Gan, W.; Xu, C.; Wang, X. Microstructure and mechanical properties of Cu-Cr-Zr alloy prepared by electron beam additive manufacturing and laser-MIG hybrid welding. *J. Manuf. Process.* **2024**, *117*, 24–39. [CrossRef]
380. Zardoshtian, A.; Ansari, M.; Esmaeilzadeh, R.; Keshavarzkermani, A.; Jahed, H.; Toyserkani, E. Laser-directed energy deposition of CuCrZr alloy: From statistical process parameter optimization to microstructural analysis. *Int. J. Adv. Manuf. Technol.* **2023**, *126*, 4407–4418. [CrossRef]
381. Zardoshtian, A.; Ansari, M.; Esmaeilzadeh, R.; Keshavarzkermai, A.; Jahed, H.; Toyserkani, E. On the Process Optimization, Microstructure Evolution, and Mechanical Properties of Cucrzr Produced by Laser Directed Energy Deposition. 2022. Available online: https://papers.ssrn.com/abstract=4265285 (accessed on 25 July 2024).
382. Jeyaprakash, N.; Kumar, M.S.; Yang, C.-H. Enhanced nano-level mechanical responses on additively manufactured Cu-Cr-Zr copper alloy containing Cu2O nano precipitates. *J. Alloys Compd.* **2023**, *930*, 167425. [CrossRef]
383. Ma, Z.; Zhang, K.; Ren, Z.; Zhang, D.Z.; Tao, G.; Xu, H. Selective laser melting of Cu–Cr–Zr copper alloy: Parameter optimization, microstructure and mechanical properties. *J. Alloys Compd.* **2020**, *828*, 154350. [CrossRef]
384. Ren, Z.; Zhang, D.Z.; Fu, G.; Jiang, J.; Zhao, M. High-fidelity modelling of selective laser melting copper alloy: Laser reflection behavior and thermal-fluid dynamics. *Mater. Des.* **2021**, *207*, 109857. [CrossRef]
385. Zhang, S.; Zhu, H.; Zhang, L.; Zhang, W.; Yang, H.; Zeng, X. Microstructure and properties of high strength and high conductivity Cu-Cr alloy components fabricated by high power selective laser melting. *Mater. Lett.* **2019**, *237*, 306–309. [CrossRef]
386. Uchida, S.; Kimura, T.; Nakamoto, T.; Ozaki, T.; Miki, T.; Takemura, M.; Oka, Y.; Tsubota, R. Microstructures and electrical and mechanical properties of Cu-Cr alloys fabricated by selective laser melting. *Mater. Des.* **2019**, *175*, 107815. [CrossRef]
387. Chen, Y.; Ren, S.; Zhao, Y.; Qu, X. Microstructure and properties of CuCr alloy manufactured by selective laser melting. *J. Alloys Compd.* **2019**, *786*, 189–197. [CrossRef]
388. Momeni, S.; Guschlbauer, R.; Osmanlic, F.; Körner, C. Selective electron beam melting of a copper-chrome powder mixture. *Mater. Lett.* **2018**, *223*, 250–252. [CrossRef]
389. Li, J.; Liu, Z.; Zhou, H.; Ye, S.; Zhang, Y.; Liu, T.; Jiang, D.; Chen, L.; Zhou, R. Effect of Process Parameters on the Microstructure and Properties of Cu–Cr–Nb–Ti Alloy Manufactured by Selective Laser Melting. *Materials* **2023**, *16*, 2912. [CrossRef] [PubMed]
390. Dai, Z.; Liu, X.; Xie, H.; Guan, W.; Gao, M.; Li, S.; Wu, Y.; Xiao, X.; Ling, G.; Bao, G.; et al. Laser additive manufacturing of Cu–Cr–Nb alloys by using elemental powder. *J. Mater. Sci.* **2024**, *59*, 6965–6985. [CrossRef]

391. Wilms, M.B.; Rittinghaus, S.-K. Laser additive manufacturing of oxide dispersion-strengthened copper–chromium–niobium alloys. *J. Manuf. Mater. Process.* **2022**, *6*, 102. [CrossRef]
392. Kini, A.R. Laser Additive Manufacturing of Oxide Dispersion Strengthened Steels and Cu-Cr-Nb Alloys. Ph.D. Thesis, RWTH Aachen University, Aachen, Germany, 2019. Available online: http://publications.rwth-aachen.de/record/765327/files/765327.pdf (accessed on 25 July 2024).
393. Demeneghi, G.; Barnes, B.; Gradl, P.; Ellis, D.; Mayeur, J.R.; Hazeli, K. Directed energy deposition GRCop-42 copper alloy: Characterization and size effects. *Mater. Des.* **2022**, *222*, 111035. [CrossRef]
394. Bai, Y.; Zhang, J.; Zhao, C.; Li, C.; Wang, H. Dual interfacial characterization and property in multi-material selective laser melting of 316L stainless steel and C52400 copper alloy. *Mater. Charact.* **2020**, *167*, 110489. [CrossRef]
395. Mao, Z.; Zhang, D.Z.; Jiang, J.; Fu, G.; Zhang, P. Processing optimisation, mechanical properties and microstructural evolution during selective laser melting of Cu-15Sn high-tin bronze. *Mater. Sci. Eng. A* **2018**, *721*, 125–134. [CrossRef]
396. Mao, Z.; Zhang, D.Z.; Wei, P.; Zhang, K. Manufacturing Feasibility and Forming Properties of Cu-4Sn in Selective Laser Melting. *Materials* **2017**, *10*, 333. [CrossRef] [PubMed]
397. Raghavendra, S.; Jayashree, P.; Rita, D.A.; Piras, G.; Scheider, D.; Chemello, M.; Benedetti, M. Wear and material characterization of CuSn10 additively manufactured using directed energy deposition. *Addit. Manuf. Lett.* **2023**, *6*, 100136. [CrossRef]
398. Jin, K.; Li, G.; Wei, B.; Chen, R.; Chen, P.; Cheng, J. Preparation of Bronze (CuSn10) Parts by Material Extrusion Process Using Paraffin-Based Binder. *J. Mater. Eng. Perform.* **2024**. [CrossRef]
399. Zhang, G.; Chen, C.; Wang, X.; Wang, P.; Zhang, X.; Gan, X.; Zhou, K. Additive manufacturing of fine-structured copper alloy by selective laser melting of pre-alloyed Cu-15Ni-8Sn powder. *Int. J. Adv. Manuf. Technol.* **2018**, *96*, 4223–4230. [CrossRef]
400. Zhao, C.; Wang, Z.; Li, D.; Kollo, L.; Luo, Z.; Zhang, W.; Prashanth, K.G. Selective laser melting of Cu–Ni–Sn: A comprehensive study on the microstructure, mechanical properties, and deformation behavior. *Int. J. Plast.* **2021**, *138*, 102926. [CrossRef]
401. Kim, Y.-K.; Park, S.-H.; Lee, K.-A. Effect of post-heat treatment on the thermophysical and compressive mechanical properties of Cu-Ni-Sn alloy manufactured by selective laser melting. *Mater. Charact.* **2020**, *162*, 110194. [CrossRef]
402. Mussatto, A.; Groarke, R.; O'Neill, A.; Obeidi, M.A.; Delaure, Y.; Brabazon, D. Influences of powder morphology and spreading parameters on the powder bed topography uniformity in powder bed fusion metal additive manufacturing. *Addit. Manuf.* **2021**, *38*, 101807. [CrossRef]
403. Mostafaei, A.; De Vecchis, P.R.; Nettleship, I.; Chmielus, M. Effect of powder size distribution on densification and microstructural evolution of binder-jet 3D-printed alloy 625. *Mater. Des.* **2019**, *162*, 375–383. [CrossRef]
404. Kassym, K.; Perveen, A. Atomization processes of metal powders for 3D printing. *Mater. Today Proc.* **2020**, *26*, 1727–1733. [CrossRef]
405. Strondl, A.; Lyckfeldt, O.; Brodin, H.; Ackelid, U. Characterization and Control of Powder Properties for Additive Manufacturing. *JOM* **2015**, *67*, 549–554. [CrossRef]
406. Wei, L.K.; Abd Rahim, S.Z.; Al Bakri Abdullah, M.M.; Yin, A.T.M.; Ghazali, M.F.; Omar, M.F.; Nemeș, O.; Sandu, A.V.; Vizureanu, P.; Abdellah, A.E. Producing metal powder from machining chips using ball milling process: A review. *Materials* **2023**, *16*, 4635. [CrossRef] [PubMed]
407. Lou, D.; Cao, J.; Huang, Y.; Lin, C.; He, C.; Bennett, P.; Liu, D. Effect of ball milling on the microstructure and performances of laser clad forming Cr3C2-NiCr composites. *Rapid Prototyp. J.* **2019**, *25*, 448–453. [CrossRef]
408. Sarwat, S.G. Contamination in wet-ball milling. *Powder Metall.* **2017**, *60*, 267–272. [CrossRef]
409. Cacace, S.; Furlan, V.; Sorci, R.; Semeraro, Q.; Boccadoro, M. Using recycled material to produce gas-atomized metal powders for additive manufacturing processes. *J. Clean. Prod.* **2020**, *268*, 122218. [CrossRef]
410. Asgarian, A.; Tang, Z.; Bussmann, M.; Chattopadhyay, K. Water atomisation of metal powders: Effect of water spray configuration. *Powder Metall.* **2020**, *63*, 288–299. [CrossRef]
411. Yin, Z.; Yu, D.; Zhang, Q.; Yang, S.; Yang, T. Experimental and Numerical Analysis of a Reverse-polarity Plasma Torch for Plasma Atomization. *Plasma Chem. Plasma Process.* **2021**, *41*, 1471–1495. [CrossRef]
412. Tang, J.; Nie, Y.; Lei, Q.; Li, Y. Characteristics and atomization behavior of Ti-6Al-4V powder produced by plasma rotating electrode process. *Adv. Powder Technol.* **2019**, *30*, 2330–2337. [CrossRef]
413. Cui, Y.; Zhao, Y.; Numata, H.; Bian, H.; Wako, K.; Yamanaka, K.; Aoyagi, K.; Zhang, C.; Chiba, A. Effects of plasma rotating electrode process parameters on the particle size distribution and microstructure of Ti-6Al-4 V alloy powder. *Powder Technol.* **2020**, *376*, 363–372. [CrossRef]
414. Yin, J.G.; Chen, G.; Zhao, S.Y.; Tan, P.; Li, Z.F.; Wang, J.; Tang, H.P. Titanium-Tantalum Alloy Powder Produced by the Plasma Rotating Electrode Process (PREP). *Key Eng. Mater.* **2018**, *770*, 18–22. [CrossRef]
415. Airoldi, L.; Brucculeri, R.; Baldini, P.; Pini, F.; Vigani, B.; Rossi, S.; Auricchio, F.; Anselmi-Tamburini, U.; Morganti, S. 3D Printing of Copper Using Water-Based Colloids and Reductive Sintering. *3d Print. Addit. Manuf.* **2023**, *10*, 559–568. [CrossRef]
416. Pavlovic, M.G.; Popov, K.I. Metal Powder Production by Electrolysis. Electrochemistry Encyclopedia. 2005. Available online: https://knowledge.electrochem.org/encycl/art-p04-metalpowder.htm (accessed on 2 July 2024).
417. Frink, S.; Connor, P. Precious Metal Powder Precipitation and Processing. *Int. J. Powder Metall.* **2009**, *45*.
418. Hryha, E.; Shvab, R.; Gruber, H.; Leicht, A.; Nyborg, L. Surface oxide state on metal powder and its changes during additive manufacturing: An overview. *Metall. Ital.* **2018**, *3*, 34–39.

419. Sanaei, N.; Fatemi, A.; Phan, N. Defect characteristics and analysis of their variability in metal L-PBF additive manufacturing. *Mater. Des.* **2019**, *182*, 108091. [CrossRef]
420. Gunenthiram, V.; Peyre, P.; Schneider, M.; Dal, M.; Coste, F.; Fabbro, R. Analysis of laser–melt pool–powder bed interaction during the selective laser melting of a stainless steel. *J. Laser Appl.* **2017**, *29*. [CrossRef]
421. Li, E.; Zhou, Z.; Wang, L.; Zou, R.; Yu, A. Particle scale modelling of powder recoating and melt pool dynamics in laser powder bed fusion additive manufacturing: A review. *Powder Technol.* **2022**, *409*, 117789. [CrossRef]
422. Li, E.L.; Wang, L.; Yu, A.B.; Zhou, Z.Y. A three-phase model for simulation of heat transfer and melt pool behaviour in laser powder bed fusion process. *Powder Technol.* **2021**, *381*, 298–312. [CrossRef]
423. Wang, Z.; Liu, M.; Luo, Z.; Yan, Z. Simultaneous modeling of powder rigid motion and molten pool evolution for powder-based additive manufacturing. *Powder Technol.* **2023**, *415*, 118118. [CrossRef]
424. Zapico, P.; Giganto, S.; Barreiro, J.; Martinez-Pellitero, S. Characterisation of 17-4PH metallic powder recycling to optimise the performance of the selective laser melting process. *J. Mater. Res. Technol.* **2020**, *9*, 1273–1285. [CrossRef]
425. Li, K.; Zhao, Z.; Zhou, H.; Zhou, H.; Yin, J.; Zhang, W.; Zhou, G. Numerical Simulation of effect of different initial morphologies on melt hydrodynamics in Laser polishing of Ti6Al4V. *Micromachines* **2021**, *12*, 581. [CrossRef]
426. Alnajjar, M.; Christien, F.; Wolski, K.; Bosch, C. Evidence of austenite by-passing in a stainless steel obtained from laser melting additive manufacturing. *Addit. Manuf.* **2019**, *25*, 187–195. [CrossRef]
427. Sanaei, N.; Fatemi, A. Defects in additive manufactured metals and their effect on fatigue performance: A state-of-the-art review. *Prog. Mater. Sci.* **2021**, *117*, 100724. [CrossRef]
428. Raza, A.; Hryha, E. Characterization of spatter and sublimation in alloy 718 during electron beam melting. *Materials* **2021**, *14*, 5953. [CrossRef]
429. Liu, J.; Wen, P. Metal vaporization and its influence during laser powder bed fusion process. *Mater. Des.* **2022**, *215*, 110505. [CrossRef]
430. Soundarapandiyan, G.; Leung, C.L.A.; Johnston, C.; Chen, B.; Khan, R.H.; McNutt, P.; Bhatt, A.; Atwood, R.C.; Lee, P.D.; Fitzpatrick, M.E. In situ monitoring the effects of Ti6Al4V powder oxidation during laser powder bed fusion additive manufacturing. *Int. J. Mach. Tools Manuf.* **2023**, *190*, 104049. [CrossRef]
431. Ding, W.; Wang, Z.; Chen, G.; Cai, W.; Zhang, C.; Tao, Q.; Qu, X.; Qin, M. Oxidation behavior of low-cost CP-Ti powders for additive manufacturing via fluidization. *Corros. Sci.* **2021**, *178*, 109080. [CrossRef]
432. Galicki, D.; List, F.; Babu, S.S.; Plotkowski, A.; Meyer, H.M.; Seals, R.; Hayes, C. Localized Changes of Stainless Steel Powder Characteristics During Selective Laser Melting Additive Manufacturing. *Met. Mater. Trans. A* **2019**, *50*, 1582–1605. [CrossRef]
433. Caiazzo, F.; Alfieri, V.; Argenio, P.; Sergi, V. Additive manufacturing by means of laser-aided directed metal deposition of 2024 aluminium powder: Investigation and optimization. *Adv. Mech. Eng.* **2017**, *9*, 168781401771498. [CrossRef]
434. Liu, M.; Chiu, L.N.; Shen, H.; Fang, X.; Tao, Z.; Huang, A.; Davies, C.; Wu, X.; Yan, W. Effective thermal conductivities of metal powders for additive manufacturing. *Powder Technol.* **2022**, *401*, 117323. [CrossRef]
435. Nandy, J.; Sarangi, H.; Sahoo, S. A Review on Direct Metal Laser Sintering: Process Features and Microstructure Modeling. *Lasers Manuf. Mater. Process.* **2019**, *6*, 280–316. [CrossRef]
436. Montufar, E.B.; Tkachenko, S.; Casas-Luna, M.; Škarvada, P.; Slámečka, K.; Diaz-de-la-Torre, S.; Koutnỳ, D.; Paloušek, D.; Koledova, Z.; Hernández-Tapia, L. Benchmarking of additive manufacturing technologies for commercially-pure-titanium bone-tissue-engineering scaffolds: Processing-microstructure-property relationship. *Addit. Manuf.* **2020**, *36*, 101516. [CrossRef]
437. DeWitte, L.; Saldana, C.; Kurfess, T.; Fu, K. Effect of coaxial nozzle wear on catchment efficiency in direct energy deposition built components. *J. Manuf. Syst.* **2022**, *63*, 524–538. [CrossRef]
438. Burke, P.; Kipouros, Y.G.; Judge, W.D.; Kipouros, G.J. Surprises and Pitfalls in the Development of Magnesium Powder Metallurgy Alloys. In *Magnesium and Its Alloys*; CRC Press: Boca Raton, FL, USA, 2019; pp. 337–373. Available online: https://www.taylorfrancis.com/chapters/edit/10.1201/9781351045476-12/surprises-pitfalls-development-magnesium-powder-metallurgy-alloys-paul-burke-yiannis-kipouros-william-judge-georges-kipouros (accessed on 3 July 2024).
439. Gouge, M.; Michaleris, P. *Thermo-Mechanical Modeling of Additive Manufacturing*; Butterworth-Heinemann: Oxford, UK, 2017. Available online: https://books.google.com/books?hl=en&lr=&id=MuxGDgAAQBAJ&oi=fnd&pg=PP1&dq=mechanical+forces+in+additive+manufacturing&ots=UFyVDs3erd&sig=On2mEKuF9irlLzdzMZA1RU8sp4 (accessed on 3 July 2024).
440. Xie, D.; Lv, F.; Liang, H.; Shen, L.; Tian, Z.; Zhao, J.; Song, Y.; Shuai, C. Towards a comprehensive understanding of distortion in additive manufacturing based on assumption of constraining force. *Virtual Phys. Prototyp.* **2021**, *16* (Suppl. S1), S85–S97. [CrossRef]
441. Xie, D.; Zhao, J.; Liang, H.; Tian, Z.; Shen, L.; Xiao, M.; Ahsan, M.N.; Wang, C. Assumption of constraining force to explain distortion in laser additive manufacturing. *Materials* **2018**, *11*, 2327. [CrossRef]
442. Hyslop, R.L. Surface Contamination from the Use of Metal Powders at Two Additive Manufacturing Facilities. Ph.D. Thesis, North-West University, Potchefstroom, South Africa, 2018. Available online: https://repository.nwu.ac.za/handle/10394/31145 (accessed on 3 July 2024).
443. Gorji, N.E.; O'Connor, R.; Brabazon, D. XPS, XRD, and SEM characterization of the virgin and recycled metallic powders for 3D printing applications. *IOP Conf. Ser. Mater. Sci. Eng.* **2019**, *591*, 012016. [CrossRef]

444. Horn, M.; Langer, L.; Schafnitzel, M.; Dietrich, S.; Schlick, G.; Seidel, C.; Reinhart, G. Influence of metal powder cross-contaminations on part quality in laser powder bed fusion: Copper alloy particles in maraging steel feedstock. *Procedia CIRP* **2020**, *94*, 167–172. [CrossRef]
445. Ahsan, F.; Ladani, L. Temperature Profile, Bead Geometry, and Elemental Evaporation in Laser Powder Bed Fusion Additive Manufacturing Process. *JOM* **2020**, *72*, 429–439. [CrossRef]
446. Klassen, A.; Scharowsky, T.; Körner, C. Evaporation model for beam based additive manufacturing using free surface lattice Boltzmann methods. *J. Phys. D Appl. Phys.* **2014**, *47*, 275303. [CrossRef]
447. Wang, L.; Zhang, Y.; Yan, W. Evaporation Model for Keyhole Dynamics During Additive Manufacturing of Metal. *Phys. Rev. Appl.* **2020**, *14*, 064039. [CrossRef]
448. Klassen, A.; Forster, V.E.; Körner, C. A multi-component evaporation model for beam melting processes. *Model. Simul. Mater. Sci. Eng.* **2016**, *25*, 025003. [CrossRef]
449. Mirzababaei, S.; Paul, B.K.; Pasebani, S. Metal Powder Recyclability in Binder Jet Additive Manufacturing. *JOM* **2020**, *72*, 3070–3079. [CrossRef]
450. Brennan, M.C.; Keist, J.S.; Palmer, T.A. Defects in Metal Additive Manufacturing Processes. *J. Mater. Eng. Perform.* **2021**, *30*, 4808–4818. [CrossRef]
451. Averardi, A.; Cola, C.; Zeltmann, S.E.; Gupta, N. Effect of particle size distribution on the packing of powder beds: A critical discussion relevant to additive manufacturing. *Mater. Today Commun.* **2020**, *24*, 100964. [CrossRef]
452. Landauer, J.; Kuhn, M.; Nasato, D.S.; Foerst, P.; Briesen, H. Particle shape matters–using 3D printed particles to investigate fundamental particle and packing properties. *Powder Technol.* **2020**, *361*, 711–718. [CrossRef]
453. Yun, H.; Dong, L.; Wang, W.; Bing, Z.; Xiangyun, L. Study on the flowability of TC4 Alloy Powder for 3D Printing. *IOP Conf. Ser. Mater. Sci. Eng.* **2018**, *439*, 042006. [CrossRef]
454. Bellini, C.; Berto, F.; Di Cocco, V.; Franchitti, S.; Iacoviello, F.; Mocanu, L.P.; Razavi, N. Effect of recycling on internal and external defects of Ti-6Al-4V powder particles for electron beam melting process. *Procedia Struct. Integr.* **2022**, *41*, 175–182. [CrossRef]
455. Lu, C.; Zhang, R.; Xiao, M.; Wei, X.; Yin, Y.; Qu, Y.; Li, H.; Liu, P.; Qiu, X.; Guo, T. A comprehensive characterization of virgin and recycled 316L powders during laser powder bed fusion. *J. Mater. Res. Technol.* **2022**, *18*, 2292–2309. [CrossRef]
456. Ahmed, F.; Ali, U.; Sarker, D.; Marzbanrad, E.; Choi, K.; Mahmoodkhani, Y.; Toyserkani, E. Study of powder recycling and its effect on printed parts during laser powder-bed fusion of 17-4 PH stainless steel. *J. Mater. Process. Technol.* **2020**, *278*, 116522. [CrossRef]
457. Delacroix, T.; Lomello, F.; Schuster, F.; Maskrot, H.; Garandet, J.-P. Influence of powder recycling on 316L stainless steel feedstocks and printed parts in laser powder bed fusion. *Addit. Manuf.* **2022**, *50*, 102553. [CrossRef]
458. Asgari, H.; Baxter, C.; Hosseinkhani, K.; Mohammadi, M. On microstructure and mechanical properties of additively manufactured AlSi10Mg_200C using recycled powder. *Mater. Sci. Eng. A* **2017**, *707*, 148–158. [CrossRef]
459. Bajt Leban, M.; Hren, M.; Kosec, T. The microstructure, mechanical and electrochemical properties of 3D printed alloys with reusing powders. *Sci. Rep.* **2023**, *13*, 3245. [CrossRef]
460. Jacob, G.; Jacob, G.; Brown, C.U.; Donmez, M.A.; Watson, S.S.; Slotwinski, J. *Effects of Powder Recycling on Stainless Steel Powder and Built Material Properties in Metal Powder Bed Fusion Processes*; US Department of Commerce, National Institute of Standards and Technology: Gaithersburg, MD, USA, 2017. Available online: https://nvlpubs.nist.gov/nistpubs/ams/NIST.AMS.100-6.pdf (accessed on 3 July 2024).
461. Paccou, E.; Mokhtari, M.; Keller, C.; Nguejio, J.; Lefebvre, W.; Sauvage, X.; Boileau, S.; Babillot, P.; Bernard, P.; Bauster, E. Investigations of powder reusing on microstructure and mechanical properties of Inconel 718 obtained by additive manufacturing. *Mater. Sci. Eng. A* **2021**, *828*, 142113. [CrossRef]
462. Contaldi, V.; Del Re, F.; Palumbo, B.; Squillace, A.; Corrado, P.; Di Petta, P. Mechanical characterisation of stainless steel parts produced by direct metal laser sintering with virgin and reused powder. *Int. J. Adv. Manuf. Technol.* **2019**, *105*, 3337–3351. [CrossRef]
463. Emminghaus, N.; Bernhard, R.; Hermsdorf, J.; Kaierle, S. Residual oxygen content and powder recycling: Effects on microstructure and mechanical properties of additively manufactured Ti-6Al-4V parts. *Int. J. Adv. Manuf. Technol.* **2022**, *121*, 3685–3701. [CrossRef]
464. Del Re, F.; Contaldi, V.; Astarita, A.; Palumbo, B.; Squillace, A.; Corrado, P.; Di Petta, P. Statistical approach for assessing the effect of powder reuse on the final quality of AlSi10Mg parts produced by laser powder bed fusion additive manufacturing. *Int. J. Adv. Manuf. Technol.* **2018**, *97*, 2231–2240. [CrossRef]
465. Weiss, C.; Haefner, C.L.; Munk, J. On the Influence of AlSi10Mg Powder Recycling Behavior in the LPBF Process and Consequences for Mechanical Properties. *JOM* **2022**, *74*, 1188–1199. [CrossRef]
466. Rayan, O.; Brousseau, J.; Belzile, C.; Ouafi, A.E. Maraging steel powder recycling effect on the tensile and fatigue behavior of parts produced through the laser powder bed fusion (L-PBF) process. *Int. J. Adv. Manuf. Technol.* **2023**, *127*, 1737–1754. [CrossRef]
467. Foti, P.; Mocanu, L.P.; Razavi, N.; Bellini, C.; Borrelli, R.; Di Cocco, V.; Franchitti, S.; Iacoviello, F.; Berto, F. Effect of recycling powder on the fatigue properties of AM Ti6Al4V. *Procedia Struct. Integr.* **2022**, *42*, 1436–1441. [CrossRef]
468. Soltani-Tehrani, A.; Pegues, J.; Shamsaei, N. Fatigue behavior of additively manufactured 17-4 PH stainless steel: The effects of part location and powder re-use. *Addit. Manuf.* **2020**, *36*, 101398. [CrossRef]

469. Moghimian, P.; Poirié, T.; Habibnejad-Korayem, M.; Zavala, J.A.; Kroeger, J.; Marion, F.; Larouche, F. Metal powders in additive manufacturing: A review on reusability and recyclability of common titanium, nickel and aluminum alloys. *Addit. Manuf.* **2021**, *43*, 102017. [CrossRef]
470. Koushik, T.; Shen, H.; Kan, W.H.; Gao, M.; Yi, J.; Ma, C.; Lim, S.C.V.; Chiu, L.N.S.; Huang, A. Effective Ti-6Al-4V Powder Recycling in LPBF Additive Manufacturing Considering Powder History. *Sustainability* **2023**, *15*, 15582. [CrossRef]
471. Warner, J.H.; Ringer, S.P.; Proust, G. Strategies for metallic powder reuse in powder bed fusion: A review. *J. Manuf. Process.* **2024**, *110*, 263–290. [CrossRef]
472. Smolina, I.; Gruber, K.; Pawlak, A.; Ziółkowski, G.; Grochowska, E.; Schob, D.; Kobiela, K.; Roszak, R.; Ziegenhorn, M.; Kurzynowski, T. Influence of the AlSi7Mg0. 6 aluminium alloy powder reuse on the quality and mechanical properties of LPBF samples. *Materials* **2022**, *15*, 5019. [CrossRef] [PubMed]
473. Okello, A.; Samper, V. Effective Powder Reuse Strategies. GE Additive. Available online: https://3dprint.com/wp-content/uploads/2022/03/GE-Additive_Powder-Reuse_WP.pdf (accessed on 16 July 2024).
474. Lutter-Günther, M.; Gebbe, C.; Kamps, T.; Seidel, C.; Reinhart, G. Powder recycling in laser beam melting: Strategies, consumption modeling and influence on resource efficiency. *Prod. Eng. Res. Devel.* **2018**, *12*, 377–389. [CrossRef]
475. Diener, S.; Zocca, A.; Günster, J. Literature review: Methods for achieving high powder bed densities in ceramic powder bed based additive manufacturing. *Open Ceram.* **2021**, *8*, 100191. [CrossRef]
476. Popov, V.V.; Grilli, M.L.; Koptyug, A.; Jaworska, L.; Katz-Demyanetz, A.; Klobčar, D.; Balos, S.; Postolnyi, B.O.; Goel, S. Powder bed fusion additive manufacturing using critical raw materials: A review. *Materials* **2021**, *14*, 909. [CrossRef] [PubMed]
477. Solexis, S. Centrifugal separator provides high capacity screening of resin powders. *Filtr. Sep.* **2004**, *41*, 18–19. [CrossRef]
478. Gruber, H.; Henriksson, M.; Hryha, E.; Nyborg, L. Effect of Powder Recycling in Electron Beam Melting on the Surface Chemistry of Alloy 718 Powder. *Met. Mater. Trans. A* **2019**, *50*, 4410–4422. [CrossRef]
479. Keaton, A.I. Assessing the Recyclability of Stainless-Steel Powder Used in Selective Laser Melting-3D Printing. Master's Thesis, North Carolina Agricultural and Technical State University, Greensboro, NC, USA, 2019. Available online: https://digital.library.ncat.edu/theses/386/ (accessed on 4 July 2024).
480. Cherkezova-Zheleva, Z.; Burada, M.; Sobetkii, A.E.; Paneva, D.; Fironda, S.A.; Piticescu, R.-R. Green and Sustainable Rare Earth Element Recycling and Reuse from End-of-Life Permanent Magnets. *Metals* **2024**, *14*, 658. [CrossRef]
481. Wang, Y.Q.; Shen, J.X.; Wu, H.Q. Application and research status of alternative materials for 3D-printing technology. *J. Aeronaut. Mater.* **2016**, *36*, 89–98.
482. Batistão, B.F.; Pinotti, V.E.; de Lima, M.L.; Rodrigues, A.D.G.; de Traglia Amancio-Filho, S.; Gargarella, P. Wet chemical surface functionalization of AA2017 powders for additive manufacturing. *Powder Technol.* **2024**, *443*, 119938. [CrossRef]
483. Qian, J.; Dong, D.; Wei, G.; Shi, M.; Tang, S. A method for the preparation of spherical titanium powder for additive manufacturing. *Powder Technol.* **2022**, *411*, 117927. [CrossRef]
484. Shaikh, A.S. Development of a γ'precipitation hardening Ni-base superalloy for additive manufacturing. Master's Thesis, Chalmers University of Technology, Gothenburg, Sweden, 2018. Available online: https://odr.chalmers.se/handle/20.500.12380/255645 (accessed on 4 July 2024).
485. Anderson, A.; Gallegos, S.; Rezaie, B.; Azarmi, F. Present and Future Sustainability Development of 3D Metal Printing. *Eur. J. Sustain. Dev. Res.* **2021**, *5*, em0168.
486. Kim, D.; Hirayama, Y.; Takagi, K.; Kwon, H. Surface cleaning effect of bare aluminum micro-sized powder by low oxygen induction thermal plasma. *Materials* **2022**, *15*, 1553. [CrossRef] [PubMed]
487. Wei, W.-H.; Wang, L.-Z.; Chen, T.; Duan, X.-M.; Li, W. Study on the flow properties of Ti-6Al-4V powders prepared by radio-frequency plasma spheroidization. *Adv. Powder Technol.* **2017**, *28*, 2431–2437. [CrossRef]